



evropský  
sociální  
fond v ČR



EVROPSKÁ UNIE



MINISTERSTVO ŠKOLSTVÍ,  
MLÁDEŽE A TĚLOVÝCHOVY



OP Vzdělávání  
pro konkurenceschopnost

INVESTICE DO ROZVOJE VZDĚLÁVÁNÍ

**Vysoká škola báňská – Technická univerzita Ostrava**



# **Phase Transformations**

**Didactic Text**

**Vlastimil Vodárek**

**Ostrava 2013**

Review: Prof. Dr. Ing. Jaroslav Sojka

Description: Phase Transformations

Author: Vlastimil Vodárek

Edition: first, 2013

Pages: 123

Published by:

Academic materials for the Material engineering study programme at the Faculty of Metallurgy and Materials Engineering.

Proofreading: none.

**Project designation:**

Operation Programme of Education towards Competitive Strength

Description: ModIn - Modular innovation of bachelor and subsequent master programmes at the Faculty of Metallurgy and Materials Engineering of VŠB - TU Ostrava

Ref. No.: CZ.1.07/2.2.00/28.0304

Realisation: VŠB – Technical University in Ostrava

This pro and the national budget of Czech Republic

© Vlastimil Vodárek

© VŠB – Technical University in Ostrava

# INSTRUCTIONS FOR STUDENTS

## Phase Transformations

The study materials package containing an integrated university textbook for combined study programmes, including the instructions for students, is intended for a specific subject within 1st term of the Advanced Engineering Materials field of study.

### 1. Prerequisites

Completion of subjects as Material Sciences, Structure and Properties of Solids and Heat Treatment Essentials is the vital prerequisite for enrolling in this subject.

### 2. Objectives and Learning Outputs

The objective of this subject is to introduce students to the basic thermodynamic, crystallographic and kinetic laws of phase transformations in engineering materials. Transformations considered vital from the engineering point of view have been demonstrated by means of practical examples.

Thorough study of the text should enable the student to:

- differentiate between basic types of transformations in engineering materials based on their thermodynamic, crystallographic and kinetic characteristics,
- define a plausible mechanism of phase transformations occurring under given conditions during technological processing of metallic materials,
- identify the basic transformation products in engineering materials.

As the scope of agenda, dealing with phase transformations is very large; this textbook does not discuss all the issues defined within the syllabus profile of the subject. Any additional information can be obtained from books listed in the bibliography at the end of this textbook as needed.

### Subject designation:

This subject has been included within the master's programme in the field of Progressive Engineering Materials, the study programme of Material Engineering but it is also suitable for any students from various fields of study provided they comply with the set prerequisites.

### Procedure recommended approaching each chapter:

Read through the text section carefully and solve the exercises provided (for correct solving procedures refer to details shown below each exercise). Try to answer questions listed at the end of each chapter. For more details on the particular agenda please refer to the link [1],

publications [2 - 4] contain various specific examples - see the bibliography at the end of textbook.

**Communication with tutors:**

Any problems can be addressed by means of personal consulting per individual arrangements with the tutor. This subject involves completion of a term project and passing the academic test to obtain the credit required. Project topics and detailed instructions for completion of projects will be notified to students at the beginning of direct full-time tuition. The period for assessment of term projects by the tutor is 14 days following their submission.

Phone: +596 994 432 (prof. Ing. Vlastimil Vodárek, CSc. subject guarantor)

E-mail: [vlastimil.vodarek@vsb.cz](mailto:vlastimil.vodarek@vsb.cz)

## Contents

1. Introduction	1
2. Thermodynamics of Phase Transformations	4
2.1 Gibbs Phase Rule	4
2.2 Ideal Solutions	6
2.3 Chemical Potential	8
2.4 Regular Solutions	10
2.5 Activity	12
2.6 Real Solutions	14
2.7 Equilibrium in Heterogeneous Systems	15
2.8 Binary Phase Diagrams	19
2.9 Interface Effect on Phase Equilibrium	21
3. Classification of Phase Transformations	26
3.1 Thermodynamic and Kinetic Classification	26
4. Interface in Solids and Their Migration	31
4.1 Coherent Interface	31
4.2 Semicoherent Interface	33
4.3 Incoherent Interface	34
4.4 Interface Migration	35
4.4.1 Migration of Non-Glissile Interface	35
4.4.2 Migration of Glissile Interface	37
5. Solidification	43
5.1 Nucleation in Pure Metals	43
5.1.1 Homogeneous Nucleation	43
5.1.2 Rate of Homogeneous Nucleation	48
5.1.3 Heterogeneous Nucleation	49
5.2 Solid Phase Growth in Single-Component System	53
5.2.1 Continuous Growth	54
5.2.2 Lateral Growth	54
5.2.3 Heat Flow and Interface Stability	57
5.3 Solidification of Binary Alloys	59
5.3.1 Solidification of Single-Phase Alloys	59

---

5.3.1.1	Equilibrium Solidification	61
5.3.1.2	No Diffusion in Solid Phase, Complete Mixing in Melt	61
5.3.1.3	No Diffusion in Solid Phase, No Mixing in Melt	63
5.3.2	Cellular and Dendritic Solidification	65
5.3.3	Eutectic Solidification	69
5.4	Crystallisation Example – Ingot	71
6.	Diffusional Transformations	77
6.1	Precipitation	78
6.1.1	Homogeneous Nucleation	78
6.1.2	Heterogeneous Nucleation	84
6.1.3	Growth of Precipitates	87
6.1.4	Coarsening of Precipitates	89
6.1.5	Precipitation Sequence	92
6.2	Kinetics of Diffusional Transformations	93
6.3	Spinodal Decomposition	96
6.4	Discontinuous Transformation	98
6.5	Massive Transformation	101
7.	Diffusionless Transformations	108
7.1	Martensite in Iron Alloys	108
7.1.1	Shape Deformation during Martensitic Transformation	112
7.1.2	Crystallography of Martensitic Transformation in Steels	114
7.1.3	Morphology of Martensite in Iron Alloys	117
7.1.4	Nucleation and Martensite Growth	120
7.2	Shape Memory Effect and Superelasticity	122
7.2.1	Transformation Sequence in NiTi Alloy	128
7.2.2	Temperature-Actuated Switch	130

## 1. Introduction

Phase transformations are associated with changes of state or crystal structure in solids towards the equilibrium state under specific ambient conditions. The resultant microstructure enables division of phase transformations in solids into two categories:

- a) The original phase disappears in full and it is replaced with another one,
- b) The original phase develops a small fraction of one or more new phases (minor phases).

As far as the technology is concerned, phase transformations represent a very significant tool to enable a controlled process for changing of structural characteristics of materials as well as their end-use properties.

When studying phase transformations, we look deeper into the conditions, at which one phase transforms into another or even a mix of several phases. Phase transformations are driven by the fact that the initial structural condition of material is unstable when compared to the new condition. How do we measure the stability of phases? This question is addressed by *thermodynamics*. For transformations occurring at constant temperature and pressure, the Gibbs free energy defines the relative system stability:

$$G = H - TS \quad (1.1)$$

Where H is enthalpy, T is the absolute temperature and S is the system entropy. Enthalpy is a measure of the heat content of the system defined by the following formula:

$$H = E + pV \quad (1.2)$$

Where E is the internal energy of the system (the sum of potential and kinetic energy of atoms in the system), p is the pressure and V refers to the system volume.

The system is in equilibrium when in the most-stable condition, i.e. there is no driving force towards changes. With constant temperature and pressure, the closed system (its weight and composition remain constant) will remain in stable equilibrium provided it reaches the minimum value of Gibbs free energy:

$$dG = 0 \quad (1.3)$$

For graphic depiction of the equilibrium state see Fig. 1.1. Various atomic configurations of the system are shown along the x-axis. The A configuration represents the *stable equilibrium state*. Nevertheless, the system could feature a few more configurations, e.g. B, located within the area of local minimum of the Gibbs free energy. Such configuration is defined as the

**metastable equilibrium state.** With respect to principles of thermodynamics, any reaction is possible when associated with a reduction of Gibbs free energy:

$$\Delta G = G_2 - G_1 \quad (1.4)$$

where  $G_1$  refers to Gibbs energy in the initial state and  $G_2$  is Gibbs energy found in the resultant state. Transformations can occur throughout a whole range of metastable conditions until the system reaches its stable equilibrium.

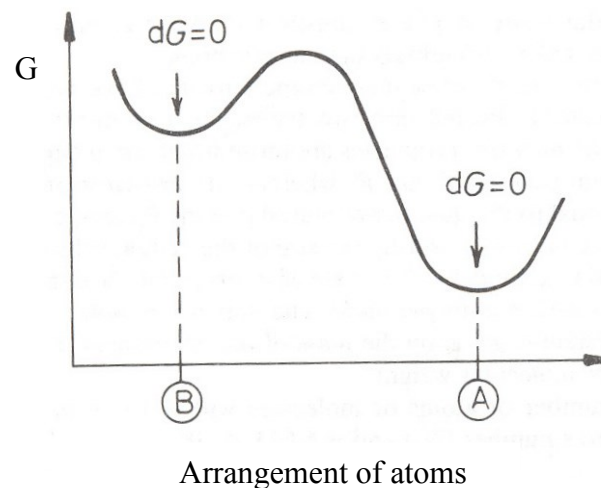


*Fig. 1.1 Change of Gibbs free energy provoked by different arrangements of atoms. The A configuration represents a stable equilibrium (the lowest  $G$ ), whereas the B configuration matches the metastable condition*

As far as technology is concerned, the vital factor here is the rate of phase transformations. This issue is addressed by **kinetics**. Some life cycles of metastable conditions may be very short; other cases might show these periods as almost infinite. These differences are due to the maximum of Gibbs energy located between the metastable and stable conditions, respectively. The maximum represents an energy barrier reducing the rate of transformation. Fig. 1.2 shows the change of free energy per atom throughout the phase transformation, starting at the initial metastable condition towards the condition with reduced free energy. The driving force of transformation is then defined as follows:  $\Delta G = G_2 - G_1$ . Before the amount of free energy per atom drops from the level of  $G_1$  to  $G_2$ , the relevant atom must undergo its activated condition matched by the amount of Gibbs energy expressed as  $G_1 + \Delta G^a$ . The energy shown in Fig. 1.2 represents energy averages related to a great number of atoms. A random thermal shift of atoms will induce change of energy per atom over time and it may be sometimes sufficient to enable the atom to achieve its activated state. This process is called the **thermal activation**.

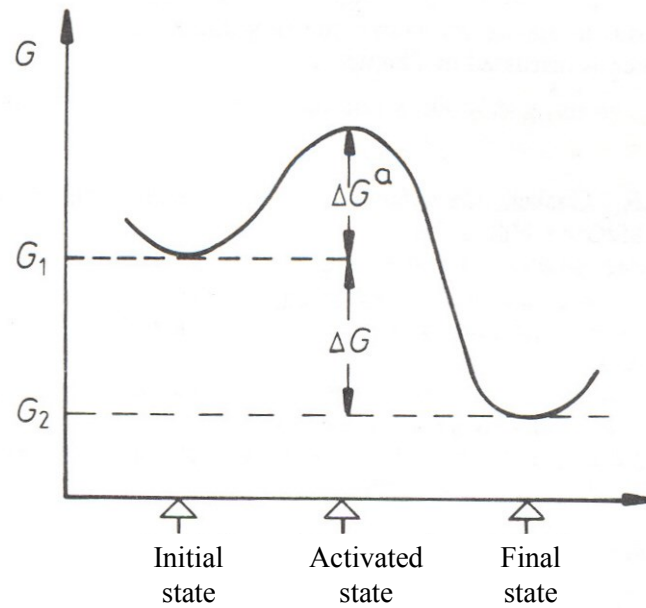


Fig. 1.2 Transfer from the initial state to the final state via the activated state having a greater energy

The theory of kinetics implies the apparent stage, when the atom reaches its activated stage, it is defined by the formula  $\exp\left(-\frac{\Delta G^a}{kT}\right)$ , where  $k$  refers to the Boltzmann's constant ( $k = 1.38 \cdot 10^{-23} \text{ J} \cdot \text{K}^{-1}$ ) and  $\Delta G^a$  is the activation energy barrier. The rate of transformation will depend on frequency of atoms when reaching the activated state:

$$velocity \propto \exp\left(-\frac{\Delta G^a}{kT}\right) \quad (1.5)$$

This formula is called the *Arrhenius rate equation*. It was initially determined on empirical basis using the observed temperature dependence of chemical reaction rate.

## 2. Thermodynamics of Phase Transformations



**Study time:** 5 hours



**Objective:** Completion of this chapter will enable you:

- Define the equilibrium in heterogeneous systems
- Use chemical potential and activity of components in alloys,
- Describe the differences between the ideal and regular solid solutions,
- Describe the relevance between the binary diagram and curves showing Gibbs free energy of phases,
- Characterise the impact of curved interface on the phase equilibrium.



### EXPLANATION

Single-component systems contain all phases with the same composition and their equilibrium is dependent on two variables - temperature and pressure - only. The composition of multi-component systems also plays the role of a variable and, when studying the phase transformations, it is necessary to know, how the Gibbs free energy depends on temperature, pressure and the system compositions.

#### 2.1 Gibbs Phase Rule

Gibbs free energy in binary solution can be calculated using the values of free energy of pure components A and B. The initial assumption is that pure components have identical crystalline structure and they can be mixed at any ratio, i.e. these can form a continuous solid solution with the same crystalline structure. Let us assume that 1 mole of homogeneous solid solution has been produced by mixing  $X_A$  moles of component A with  $X_B$  moles of component B:

$$X_A + X_B = 1 \quad (2.1)$$

where  $X_A$  and  $X_B$  represent molar fractions of A and B components in alloy. To calculate the Gibbs free energy, the process of components mixing can be divided into two steps:

1. Create a system with  $X_A$  moles of pure component A and  $X_B$  moles of pure component B,

2. Mix atoms A and B to develop a homogeneous solid solution.

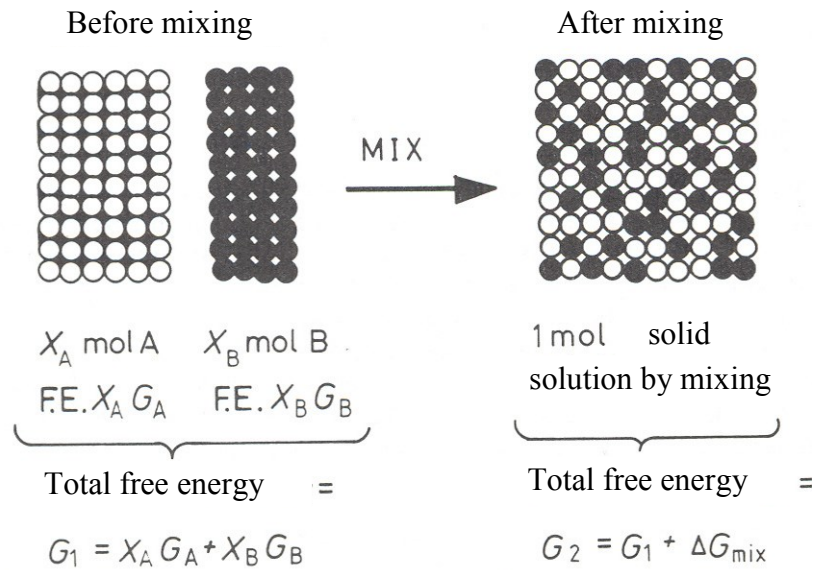


Fig. 2.1 Gibbs free energy of a homogeneous solid solution

Following step 1, the free energy within system will be:

$$G_1 = X_A G_A + X_B G_B \quad (\text{J}\cdot\text{mol}^{-1}) \quad (2.2)$$

where  $G_A$  and  $G_B$  refer to molar Gibbs free energy of pure components A and B under the experimental temperature and pressure.

The value of  $G_1$  may be depicted by means of a diagram, where the molar Gibbs free energy is shown as a function of molar fractions  $X_A$  and  $X_B$ . For any compositions of binary alloys, the values of  $G_1$  lie on the line between  $G_A$  and  $G_B$ .

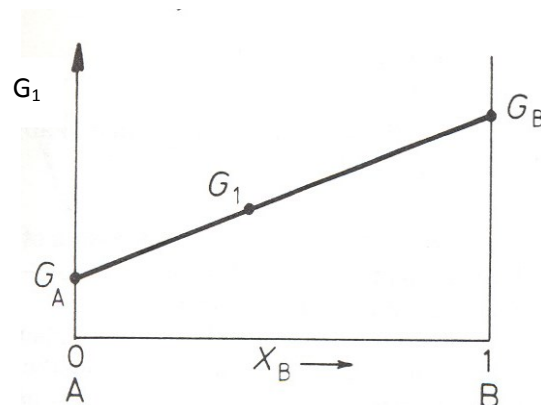


Fig. 2.2 Change of  $G_1$  (Gibbs energy before mixing) with alloy composition ( $X_A$ ,  $X_B$ )

Mixing of atoms A and B will result in change to the Gibbs free energy in the system; the free energy of solid solution present after step 2 can be expressed using the formula:

$$G_2 = G_1 + \Delta G_{mix} \quad (2.3)$$

where  $\Delta G_{mix}$  refers to the change of Gibbs free energy induced by mixing of atoms.

Since  $G_1 = H_1 - TS_1$  and  $G_2 = H_2 - TS_2$ , the formula can be broken to  $\Delta H_{mix} = H_2 - H_1$  and  $\Delta S_{mix} = S_2 - S_1$  and subsequently:

$$\Delta G_{mix} = \Delta H_{mix} - T\Delta S_{mix} \quad (2.4)$$

where  $\Delta H_{mix}$  refers to the heat absorbed or released during the step 2. Disregarding the change in volume during the process,  $\Delta H_{mix}$  represents the difference of internal energy (E) before and after mixing of atoms.  $\Delta S_{mix}$  is the difference in entropy in the mixed condition and the condition before mixing.

## 2.2 Ideal Solutions

The simplest case of atom mixing is represented by the condition, where  $\Delta H_{mix} = 0$ . The resultant solution in this case is defined as ideal and the change of Gibbs energy relevant to the mixing of atoms is expressed as:

$$\Delta G_{mix} = -T\Delta S_{mix} \quad (2.5)$$

Statistical thermodynamics deals with entropy in quantitative relevance to the randomness by means of the Boltzmann's equation:

$$S = k \ln \omega \quad (2.6)$$

where  $k$  is the Boltzmann's constant and  $\omega$  is a measure of randomness. There are two contributions to the entropy of solid solution: thermal contribution  $S_{th}$  and the configuration contribution  $S_{config}$ .

As far as the thermal entropy is concerned,  $\omega$  represents the number of ways how to distribute the thermal energy within a solid substance among atoms, i.e. the total number of ways how to arrange vibrations within a solid substance. In solutions additional randomness exists due to different ways in which atoms can be arranged. That leads to another entropy contribution  $S_{config}$ , for which the  $\omega$  represents a number of identifiable ways for configuration of atoms within a solid solution.

Unless there is a change of volume or temperature during mixing of the atoms, then the only contribution associated with  $\Delta S_{mix}$  is the change of configuration entropy. Before mixing,

atoms of both A and B were kept separately inside the system and there was only one identifiable way of their arrangement. For this reason  $S_1 = k \ln 1 = 0$ , therefore  $\Delta S_{\text{mix}} = S_2$ .

Assuming that mixing of A and B atoms will develop a substitutional solid solution and that all arrangements of atoms occur with the same probability, the number of distinguishable ways of arranging the atoms on the atom sites will be:

$$\omega_{\text{config}} = \frac{(N_A + N_B)!}{N_A! N_B!} \quad (2.7)$$

where  $N_A$  is the number of atoms of component A and  $N_B$  is the number of atoms of component B.

Since we are dealing with a system comprising 1 mole of solution, i.e.  $N_a$  atoms (Avogadro's number):

$$N_A = X_A N_a \quad \text{and} \quad N_B = X_B N_a \quad (2.8)$$

Solving the equations above and using the Stirling's approximation and the formula  $kN_a = R$  ( $R = 8,314 \text{ JK}^{-1} \text{ mol}^{-1}$ , the universal gas constant) produces the following:

$$\Delta S_{\text{mix}} = -R(X_A \ln X_A + X_B \ln X_B) \quad (2.9)$$

As the values of  $X_A$  and  $X_B$  are less than one,  $\Delta S_{\text{mix}}$  is a positive number, i.e. mixing of atoms is associated with an increase of entropy. The change of Gibbs free energy relevant to mixing of atoms is therefore equal to:

$$\Delta G_{\text{mix}} = RT(X_A \ln X_A + X_B \ln X_B) \quad (2.10)$$

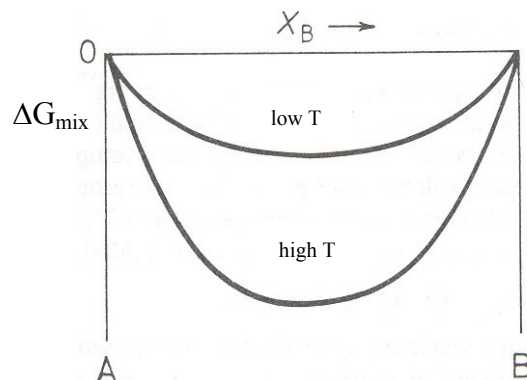


Fig. 2.3 Change of Gibbs free energy induced by mixing of atoms, ideal solution

Fig. 2.3 shows  $\Delta G_{\text{mix}}$  as a function of system composition and temperature. The actual Gibbs free energy in solution  $G$  will be also dependent on values of  $G_A$  and  $G_B$ . Combination of equations (2.2), (2.3) and (2.10) hence produces:

$$G = G_2 = X_A G_A + X_B G_B + RT(X_A \ln X_A + X_B \ln X_B) \quad (2.11)$$

This is shown in the diagram in Fig. 2.4. Rising temperature results in decrease of values  $G_A$  and  $G_B$  and the curve depicting Gibbs free energy will reflect a greater curvature. The drop of values  $G_A$  and  $G_B$  relates to heat entropy of both components,  $G$  is decreasing while the temperature rises at the rate given by  $-S$ .

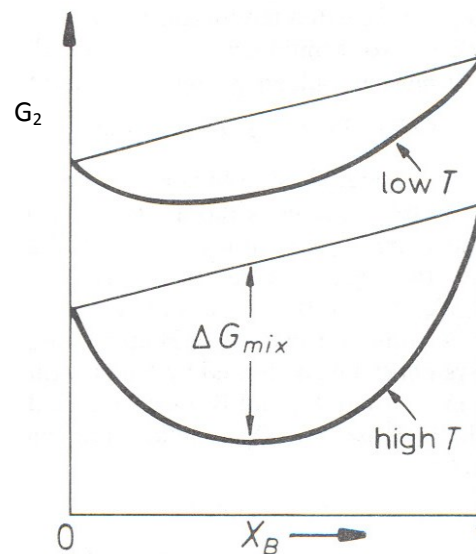


Fig. 2.4 Molar Gibbs free energy for an ideal solid solution

### 2.3 Chemical Potential

The point of interest pursued in solid solutions (alloys) is the change of free energy within particular phase in the case when the number of atoms in the system is increased or reduced. Adding a small quantity of atoms of A, i.e.  $dn_A$  moles, to a large volume of phase at a constant temperature and pressure, the size of system will increase by  $dn_A$ , therefore even the Gibbs free energy within the system will grow by a small value of  $dG'$ . In case  $dn_A$  is sufficiently low,  $dG'$  will represent the proportional quantity of extra atoms of A:

$$dG' = \mu_A dn_A (T, p, n_B \text{ constant}) \quad (2.12)$$

The constant of proportionality  $\mu_A$  is called the **partial molar free energy** of component A or the **chemical potential** of component A within the particular phase.  $\mu_A$  depends on composition of the phase; therefore  $dn_A$  must be low enough to prevent a substantial change

to the composition of the solution. The chemical potential of component A is defined as follows:

$$\mu_A = \left( \frac{\partial G'}{\partial n_A} \right)_{T,p,n_B} \quad (2.13)$$

The Gibbs free energy  $G'$  is related towards the entire system. The regular symbol  $G$  is used to mark the molar Gibbs free energy, it is therefore independent on the system size. A similar equation can be written for the chemical potential of component B.

Separate contributions can be added up for a binary solution at constant temperature and pressure as follows:

$$dG' = \mu_A dn_A + \mu_B dn_B \quad (2.14)$$

This equation could be further expanded for solutions containing more than two components. If changes of temperature and pressure are permitted, the general equation will be in this form:

$$dG' = -SdT + Vdp + \mu_A dn_A + \mu_B dn_B + \dots \quad (2.15)$$

If 1 mole of the initial phase contained  $X_A$  moles of component A and  $X_B$  moles of component B, the system size may increase without any change of the phase compositions provided the components A and B have been added at the correct ratio:  $dn_A : dn_B = X_A : X_B$ . Example: if the phase contains double the amount of A atoms compared to the quantity of B atoms ( $X_A = 2/3$  and  $X_B = 1/3$ ), the composition can be preserved even after addition of two atoms of A per one atom of B ( $dn_A : dn_B = 2$ ). This method enables enlarging the system by 1 mole without any change of  $\mu_A$  or  $\mu_B$ . Adding  $X_A$  moles of the component A and  $X_B$  moles of the component B will increase the free energy within the system by the amount of molar Gibbs free energy  $G$  accordingly.

$$G = \mu_A X_A + \mu_B X_B \quad (\text{Jmol}^{-1}) \quad (2.16)$$

Knowledge of the dependency of molar Gibbs free energy on  $X_A$  and  $X_B$  helps determination of  $\mu_A$  and  $\mu_B$  by extrapolation of tangent to the curve  $G$  on the axis for pure components A and B, Fig. 2.5. It is evident that the values of  $\mu_A$  and  $\mu_B$  are going through systematic changes with respect to the phase composition.

Comparison of equations (2.11) and (2.16) will produce an expression of chemical potential of  $\mu_A$  and  $\mu_B$  for an ideal solution in the following form:

$$\mu_A = G_A + RT \ln X_A \quad (2.17)$$

$$\mu_B = G_B + RT \ln X_B \quad (2.18)$$

For graphic depiction of these equations refer to the Fig. 2.6. The distance  $ac$  matches the expression  $-RT \ln X_A$  and the distance  $bd$  is equal to  $-RT \ln X_B$ .

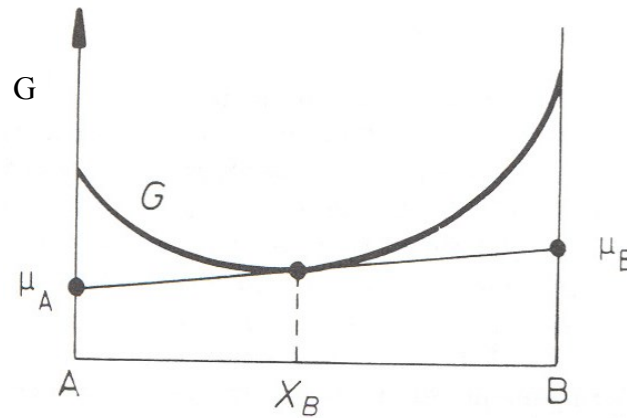


Fig. 2.5 Relation between the curve of Gibbs free energy for a solid solution and chemical potentials of components

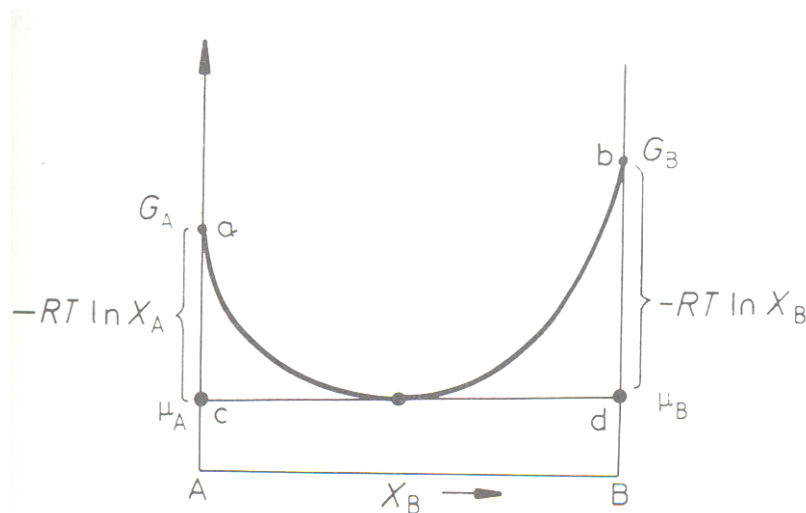


Fig. 2.6 Relations between the curve of Gibbs free energy and chemical potentials for an ideal solution

## 2.4 Regular Solutions

The development of a solid solution (mixing of atoms) is usually based on an endothermic or exothermic reaction in practice. The above mentioned model applicable to an ideal solution can therefore be extended with  $\Delta H_{\text{mix}}$  using the so called "quasi-chemical approach". This model assumes that the heat for mixing ( $\Delta H_{\text{mix}}$ ) is associated with the bonding energy between adjacent atoms only. Volumes of pure components A and B must be necessarily

identical and unchangeable during mixing, so the interatomic distances and bonding energies are independent on the composition.

The structure of a binary solid solution may contain three different types of interatomic bonds between atoms belonging to components A or B:

1. A – A bonds, the energy per bond is equal to  $\varepsilon_{AA}$ ,
2. B – B bonds, the energy per bond is equal to  $\varepsilon_{BB}$ ,
3. A – B bonds, the energy per bond is equal to  $\varepsilon_{AB}$ .

Assuming that zero energy matches the condition, when atoms are mutually distant almost to infinity, the values of  $\varepsilon_{AA}$ ,  $\varepsilon_{BB}$  and  $\varepsilon_{AB}$  are negative, whereas the stronger their bonds, the greater their negativity will become. The internal energy of solid solution will depend on the number of bonds of the specific type  $P_{AA}$ ,  $P_{BB}$  and  $P_{AB}$ :

$$E = P_{AA}\varepsilon_{AA} + P_{BB}\varepsilon_{BB} + P_{AB}\varepsilon_{AB} \quad (2.19)$$

Before mixing atoms of A and B, the system contains bonds A – A and B – B. Bearing in mind the relations between  $P_{AA}$ ,  $P_{BB}$  and  $P_{AB}$  in the solid solution, the change of internal energy induced by mixing of atoms is given by:

$$\Delta H_{mix} = P_{AB}\varepsilon \quad (2.20)$$

Where:

$$\varepsilon = \varepsilon_{AB} - \frac{1}{2}(\varepsilon_{AA} + \varepsilon_{BB}) \quad (2.21)$$

If  $\varepsilon = 0$ ,  $\Delta H_{mix} = 0$  and the solution is ideal. Atoms will be arranged in a random configuration in this case and the mixing entropy is defined by the following equation:

$$\Delta S_{mix} = -R(X_A \ln X_A + X_B \ln X_B) \quad (2.22)$$

Number of A-B bonds can be expressed:

$$P_{AB} = N_a z X_A X_B \quad (\text{number of bonds per 1 mole}) \quad (2.23)$$

where  $N_a$  is the Avogadro's number and  $z$  is the number of bonds per atom.

If  $\varepsilon < 0$ , the atoms within solution will prefer being surrounded by atoms of the opposite type and this even will increase the value  $P_{AB}$ .

If  $\varepsilon > 0$ , the number of bonds  $P_{AB}$  will tend to remain lower than in a solution with random configuration. Nevertheless, if the values of  $\varepsilon$  are not so far from zero, the equation (2.23) still represents a fair approximation:

$$\Delta H_{mix} = \Omega X_A X_B \quad (2.24)$$

where:  $\Omega = N_a z \varepsilon$ .

Real solutions behaving in compliance with the equation (2.24) are defined as regular solutions. The change of  $\Delta H_{mix}$  depending on composition is parabolic and it is depicted in Fig. 2.7, which clearly implies graphic determination of  $\Omega$ .

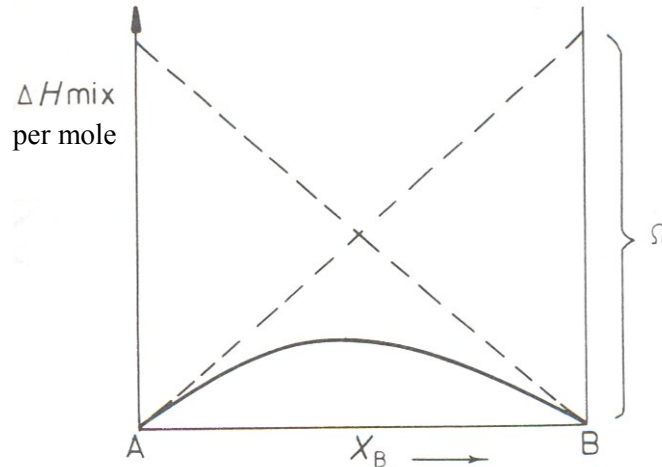


Fig. 2.7 Change of  $\Delta H_{mix}$  with the composition of regular solutions

### 2.5 Activity

The equation (2.17) applied to chemical potential within an ideal solution is simple; it is therefore desirable to define a similar equation for any solution. That can be achieved by defining the activity of component in such manner that the Fig. 2.8 shows the distance  $ac$  equal to the value of  $-RT \ln a_A$  and the distance  $bd$  matches the value of  $-RT \ln a_B$ . In this case:

$$\mu_A = G_A + RT \ln a_A \quad \text{a} \quad \mu_B = G_B + RT \ln a_B \quad (2.25)$$

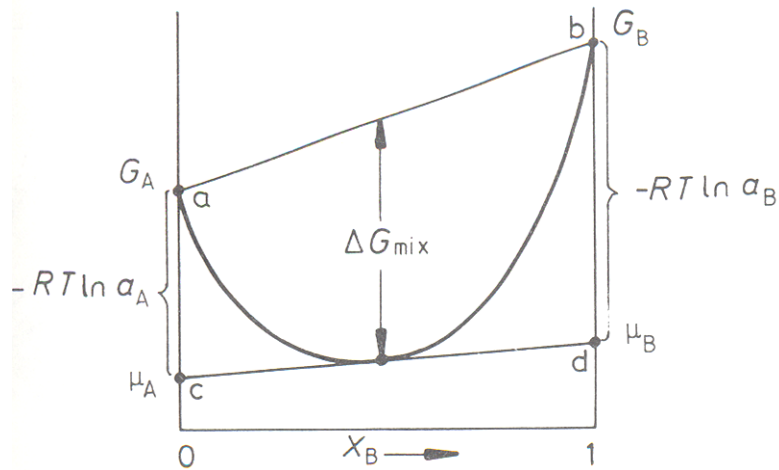


Fig. 2.8 Mutual relationship between the molar Gibbs free energy and activity

The values  $a_A$  and  $a_B$  will be generally different from values of  $X_A$  and  $X_B$  and the relation between these parameters will be changed with composition of the solution. Assuming that the crystal structures of pure components A and B are identical, the relationship between activity and molar fraction for any solid solution may be expressed graphically, as shown in the Fig. 2.9. Line 1 represents an ideal solid solution, where  $a_A = X_A$  and  $a_B = X_B$ . If  $\Delta H_{\text{mix}} < 0$ , the activity of components of the solid solution will be lower compared to an ideal solid solution (curve 2) and vice versa; if  $\Delta H_{\text{mix}} > 0$ , the activity of components in a solid solution will be greater compared to an ideal solid solution (curve 3).

The ratio of activity and molar fraction is usually defined as the **coefficient of activity** of the particular component:

$$\gamma_A = \frac{a_A}{X_A} \quad (2.26)$$

A diluted solution of component B in component A can be defined as:

$$\gamma_B = \frac{a_B}{X_B} \cong \text{constant (Henry's law)} \quad (2.27)$$

And

$$\gamma_A = \frac{a_A}{X_A} \cong 1 \quad \text{(Raoult's law)} \quad (2.28)$$

These equations can be applied to any solutions if diluted sufficiently. The component activity is just another way to describe the condition of a particular component of solid solution besides its chemical potential. Both the activity and chemical potential represent a measure of tendency of an atom towards leaving the solid solution. If the value of activity or of chemical

potential is low, atoms will be reluctant to leave the solid solution, which means that e.g. component vapour pressure in equilibrium with the solid solution will be relatively low.

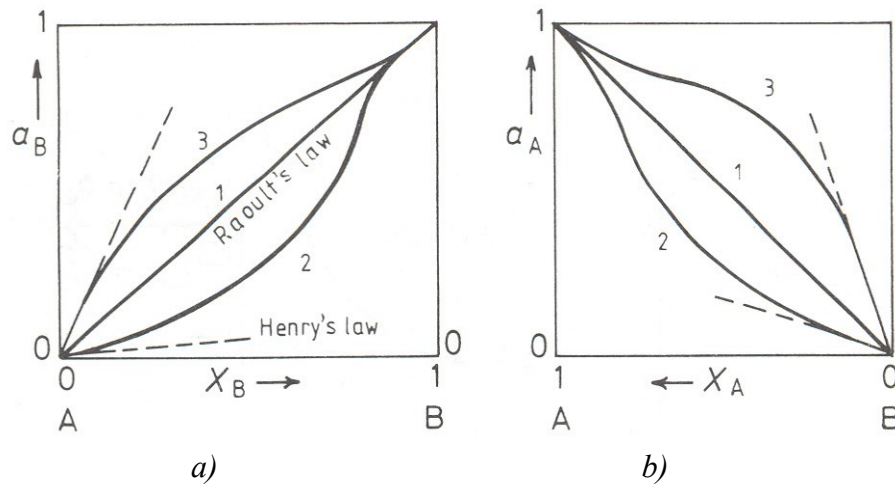


Fig. 2.9 Change of activity depending on composition, a)  $a_B$  b)  $a_A$ . Line 1: ideal solid solution (Raoult's law), curve 2:  $\Delta H_{mix} < 0$ , curve 3:  $\Delta H_{mix} > 0$ .

## 2.6 Real Solutions

The model mentioned above represents a useful description of the effect of configuration entropy and interatomic bond on the free energy in binary solutions but its use in practice is limited. This model is a way too great simplification of reality for many systems and it is unable to predict correct dependency of  $\Delta G_{mix}$  on composition and temperature.

As far as alloys with mixing enthalpy different from zero ( $\epsilon$  and  $\Omega \neq 0$ ) are concerned, it may be assumed that the random configuration of atoms represents an equilibrium or the most stable configuration of atoms, which is not true and the calculated values of  $\Delta G_{mix}$  will not correspond with the minimum of Gibbs free energy. The actual configuration of atoms will be a compromise that enables achievement of the lowest value of the internal energy with sufficient level of entropy to achieve the minimum value of Gibbs free energy. The internal energy in systems, where  $\epsilon < 0$ , is reduced by increasing number of bonds type A – B, i.e. the configuration of atoms, as shown in the Fig. 2.10a. If  $\epsilon > 0$ , the internal energy can be reduced by increasing the number of bonds type A – A and B – B, i.e. clustering of atoms in areas abundant with atoms of either A or B, Fig. 2.10b. The level of ordering or clustering of atoms will be reduced with rising temperature due to the increasing importance of entropy.

Systems with differences in atom size are associated with quasi-chemical models underestimating the change of internal energy during mixing of atoms, as these disregard the elastic distortion fields. If the difference in atom size is significant, this effect may prevail

over the chemical term. If the difference in atom size is great, the interstitial solid solutions should be selected as more convenient from the energetic prospective, see Fig. 2.10c. Systems with strong chemical bond between atoms show tendencies towards development of intermetallic phases.

The rules associated with events of atom ordering (short- or long-range) in solids and basic characteristics of individual types of intermediary phases have been defined in the textbook of the course *Structure and Properties of Solids*.

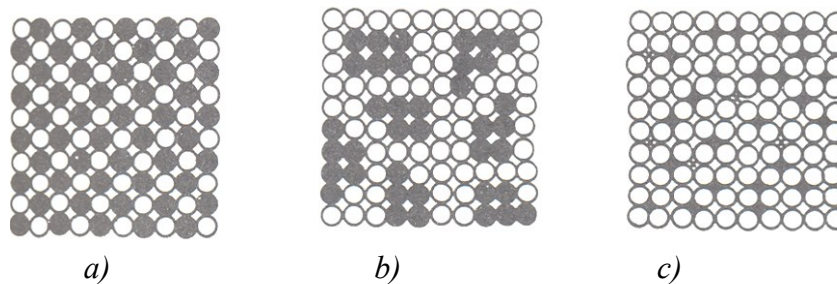


Fig. 2.10 Diagram showing the real solid solutions, a) Substitutional solid solution with long-range ordering, b) Clustering of atoms of the same type, c) Interstitial solid solution.

### 2.7 Equilibrium in Heterogeneous Systems

It is fairly common that pure components A and B do not feature an identical crystal-structure at the temperature level considered. Such cases must be documented by two curves Gibbs free energy – one for each structure. Stable forms of pure components A and B at the particular temperature (and pressure) will be marked  $\alpha$  and  $\beta$ . Let us assume that  $\alpha$  features the FCC structure and the  $\beta$  will form the BCC structure. The molar free energy of pure component A with FCC structure shown in Fig. 2.11 is marked with the letter *a*, whereas the molar free energy of pure component B with BCC structure is marked with the letter *b*. The first step in drafting of the curve showing Gibbs free energy for the phase  $\alpha$  with FCC structure lies in transforming the atoms of B from the stable BCC structure into an unstable configuration of FCC lattice. This step requires an increase of Gibbs free energy from point *b* to point *c*. This stage therefore allows drafting the curve showing Gibbs free energy for the phase  $\alpha$  by mixing of atoms of pure components A and B with FCC structure – see Fig. 2.11a. The value of  $\Delta G_{\text{mix}}$  for phase  $\alpha$  with composition X is defined by the abscissa *de*. A similar procedure can be adopted for drafting the molar Gibbs free energy for phase  $\beta$ . The abscissa *af* in Fig. 2.11b reflects the transformation of atoms of pure component A from FCC into the BCC lattice. The Fig. 2.11b clearly shows that the lowest Gibbs free energy of binary alloys rich in

component A will be identical to that of homogeneous  $\alpha$  phase and the lowest Gibbs free energy of binary alloys rich in component B will be identical to that of homogeneous  $\beta$  phase. The situation is more complicated for alloys located near intersection formed by free energy curves. These cases can serve as evidence, that the total Gibbs energy can be minimised when allocating atoms into two phases.

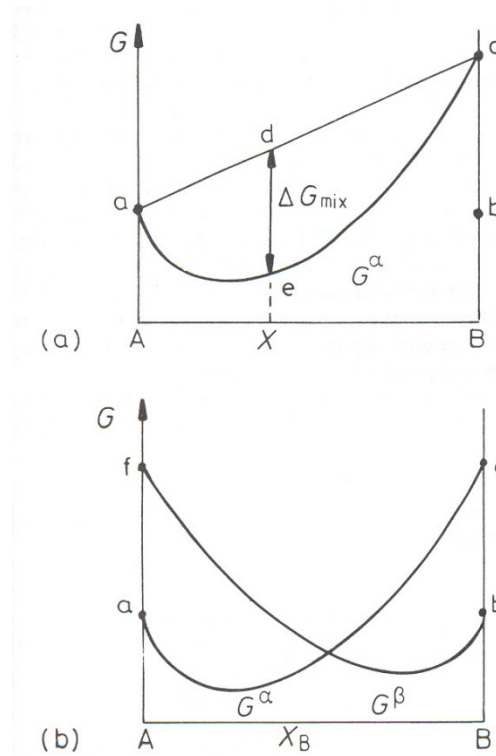
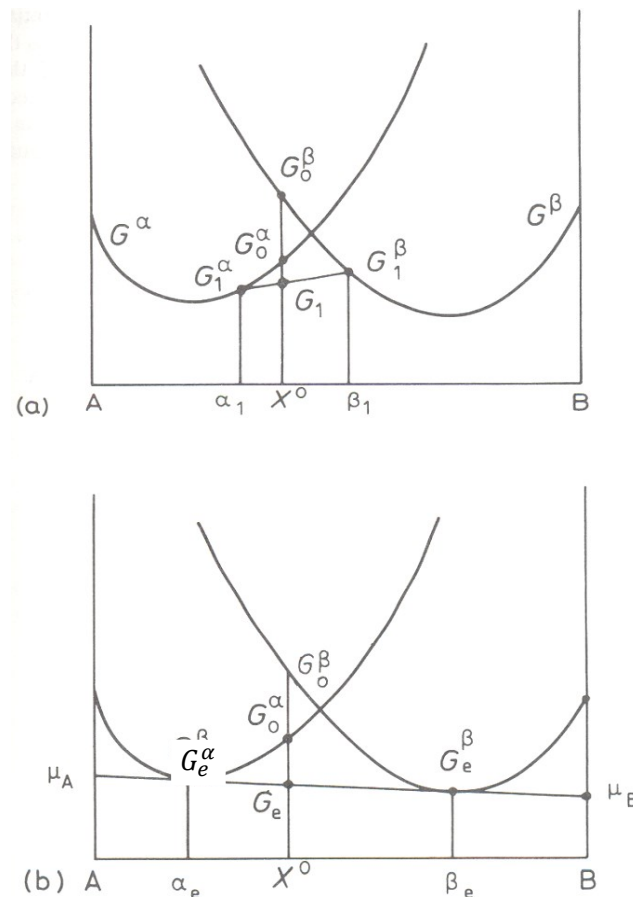


Fig. 2.11 a) Curve of molar Gibbs free energy for phase  $\alpha$ , b) Curves of molar Gibbs free energy for phases  $\alpha$  and  $\beta$

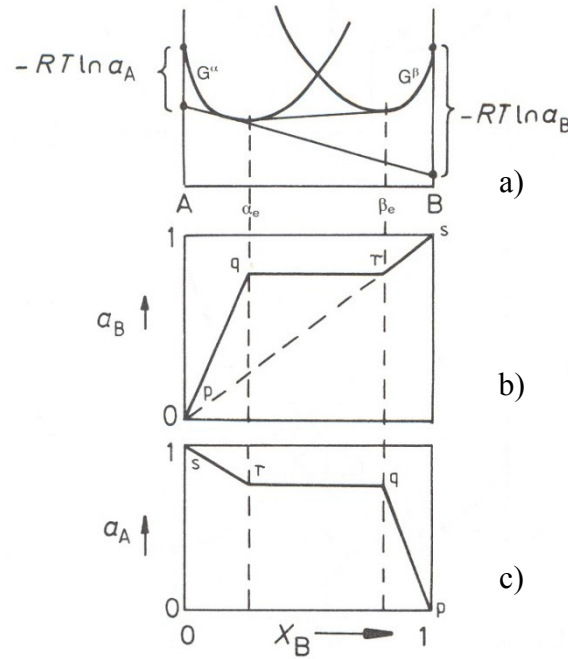
The first aspect to be considered is the general characteristics of diagrams showing the molar Gibbs free energy in presence of phase mixtures. Let us assume we have an alloy comprising phases  $\alpha$  and  $\beta$  with the molar Gibbs free energy of  $G^\alpha$  and  $G^\beta$  respectively, Fig. 2.12. If the total composition of phase mixtures is equal to  $X_B^0$ , the relative number of moles of phases  $\alpha$  and  $\beta$  is defined by the lever rule. The molar Gibbs free energy  $G$  in mixture of phases is defined by the point located on a straight line linking points  $\alpha$  and  $\beta$ . That can be verified by means of geometric analysis, see Fig. 2.12. Vectors  $ad$  and  $cf$  represent the molar Gibbs free energy of phases present within an alloy. Point  $g$  lies in the intersection of vectors  $be$  and  $dc$ , so  $bcg$  and  $acd$  as well as  $deg$  and  $dfc$  represent similar triangles. The above implies that  $bg/ad = bc/ac$  and  $ge/cf = ab/ac$ . The lever rule states that 1 mole of alloy contains  $bc/ac$  moles of phase  $\alpha$  and  $ab/ac$  moles of phase  $\beta$ . That implies both  $bg$  and  $ge$  represent separate



The prerequisite for equilibrium within a heterogeneous system comprising two phases can be also expressed using the activity concept. A heterogeneous system comprising more than one phase can contain pure components of various crystalline structures. The most stable conditions with the lowest Gibbs free energy are usually defined as a state, where pure components adopt unit activity. As far as the discussed case is concerned, this is the situation, when the activity of component A in phase  $\alpha$  composed by A (pure component) equals to 1, i.e.  $X_A = 1$ ,  $a_A^\alpha = 1$  and similarly  $X_B = 1$ ,  $a_B^\beta = 1$ . This definition of activity is depicted in Fig. 2.14a. Figs. 2.14b and 2.14c show changes to activity of components A and B with composition of phases  $\alpha$  and  $\beta$ . The areas with a single stable phase, i.e. A -  $\alpha_e$  and  $\beta_e$  - B are associated with changing values of activity (or chemical potential) and ideal solutions should be considered to simplify the example, as these feature linear dependencies between the activity and composition.



Figs. 2.13 a) The Gibbs free energy in an alloy with composition  $X^0$  is equal to  $G_1$  for a mixture of phases with composition including  $\alpha_1$  and  $\beta_1$ , b) with regards to the equilibrium, the minimum of Gibbs free energy of the alloy  $X^0$  is equal to  $G_e$  and this alloy comprises a mixture of phases including  $\alpha_e$  and  $\beta_e$



Figs. 2.14a – c Changes of activities  $a_A$  and  $a_B$  with composition for a system comprising ideal solutions  $\alpha$  and  $\beta$

The composition of equilibrium phase between  $\alpha_e$  and  $\beta_e$  remains unchanged and activities remain unchanged. In other words, if there are two phases in equilibrium, activities of components within these phases must be identical:

$$a_A^\alpha = a_A^\beta \quad \text{and} \quad a_B^\alpha = a_B^\beta \quad (2.30)$$

## 2.8 Binary Phase Diagrams

The simplest type of a binary diagram identifies a system with full solubility of components A and B both in liquid and solid state (ideal solutions in both cases). The changes of Gibbs free energy will depend on temperature changes, as shown in the Fig. 2.15. Melting temperatures of pure components match the situation when  $G^S = G^L$ , i.e. at temperatures  $T_m(A)$  and  $T_m(B)$ . The Gibbs free energy in both phases will be reduced as the temperature rises. These trends are important, as they define the relative positions of  $G_A^S$ ,  $G_A^L$ ,  $G_B^S$  and  $G_B^L$  in diagrams showing the molar Gibbs free energy at various temperature levels. When the temperature is high, where  $T_1 > T_m(A) > T_m(B)$ , the stable phase will be the liquid phase of pure components A and B. To simplify the example, let us assume that the liquid phase comes with a lower value of Gibbs free energy compared to the solid phase; this is applicable to any composition feasible within an A – B system. Reduction of temperature will produce two effects: the

values of  $G_A^L$  and  $G_B^L$  will be rising faster than values of  $G_A^S$  and  $G_B^S$  and the G curves will flatten out due to lower contribution of the term  $T\Delta S_{\text{mix}}$  towards the value of Gibbs free energy.

The rule at temperature level  $T_m(A)$  will be:  $G_A^S = G_B^S$  and that represents a single point within the binary diagram. When the temperature  $T_2$  is lower, curves of free energy will intersect and the common tangent means that the equilibrium state between points  $A$  and  $b$  is matched by a solid phase, while the interval between points  $c$  and  $B$  is associated with a liquid phase and the section between points  $b$  and  $c$  is matched by a mixture of two phases (S + L) with composition including  $b$  and  $c$ , Fig. 2.15c. These points are also marked in the phase diagram, Fig. 2.15f.

The interval between temperature levels  $T_2$  and  $T_m(B)$  shows the value  $G^L$  rising faster than  $G^S$ , therefore the points  $b$  and  $c$  in Fig. 2.15c will shift to the right in the phase diagram, alongside the curves of solid and liquid. When the temperature reaches final level of  $T_m(B)$ , points  $b$  and  $c$  will converge in a single spot, which is the point  $d$  in Fig. 2.15f. When below the temperature level  $T_m(B)$ , the Gibbs free energy of solid phase will be always below the value of free energy of melt and solid phase will be the stable one for any composition.

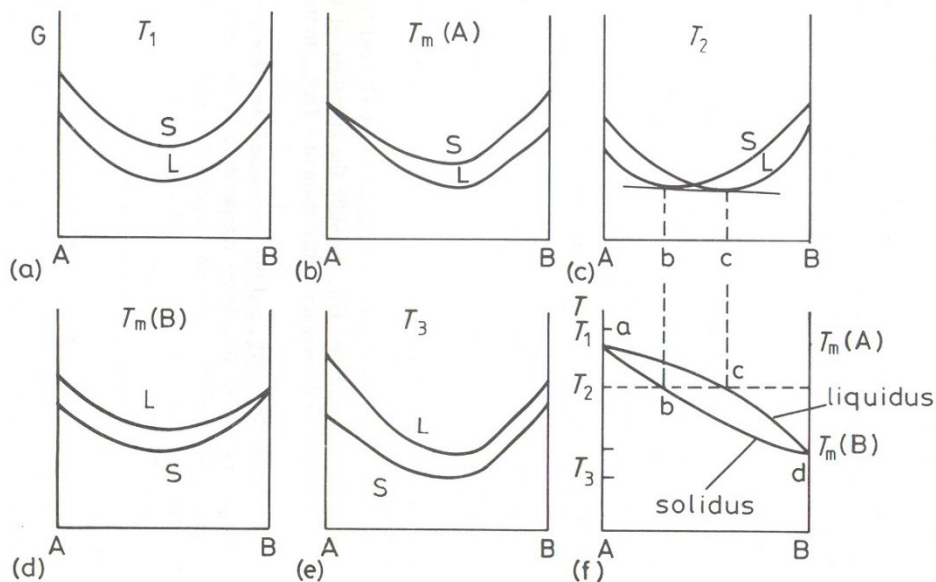


Fig. 2.15 Derivation of binary diagram for full solubility in both liquid and solid state using curves of the Gibbs free energy for the liquid (L) and solid (S) state respectively

## 2.9 The Interface Effect on Phase Equilibrium

The previous chapter shows curves of Gibbs free energy applicable to molar Gibbs free energy contained within an indefinite quantity of material in form of a perfect crystal. Surfaces (grain boundaries, interphase interfaces) have been ignored. However, these defects, while associated with other defects as dislocations or vacancies under real conditions, increase the Gibbs free energy of phases. The minimum Gibbs free energy of alloy, i.e. the equilibrium, is not achieved until all the dislocations and interfaces have been eliminated. Such condition is basically unachievable under practical circumstances.

Interphase interfaces may be extremely important at initial stages of phase transformations, where one phase, e.g.  $\beta$ , is present in form of very small particles in the matrix of  $\alpha$  phase, Fig. 2.16a. If the phase  $\alpha$  is exposed to the pressure of 1atm, the phase  $\beta$  is exposed to extra pressure  $\Delta p$  due to curvature of the  $\alpha/\beta$  interface. If the energy contained within the interphase  $\alpha/\beta$  interface is  $\gamma$  and the particles are spherical objects with the radius  $r$ , the value of  $\Delta p$  is then approximately defined by the following formula:

$$\Delta p = \frac{2\gamma}{r} \quad (2.31)$$

The expression for Gibbs free energy contains the term  $p \cdot V$ , therefore increasing the pressure must induce a rise of Gibbs free energy. For constant temperature:

$$\Delta G = \Delta p \cdot V \quad (2.32)$$

The contribution of curvature of particles within the phase  $\beta$  shown in the diagram of Gibbs free energy versus composition, see Fig. 2.16b, can be expressed as follows:

$$\Delta G_{\gamma} = \frac{2\gamma V_m}{r} \quad (2.33)$$

where  $V_m$  refers to the molar volume of phase  $\beta$ .

This increment of Gibbs free energy due to interfacial energy is defined as the *capillary effect* or *Gibbs – Thomson effect*. Composition of the phase  $\alpha$ , which is in equilibrium with particles with the radius  $r$ , corresponds with the value of  $X_r$ .

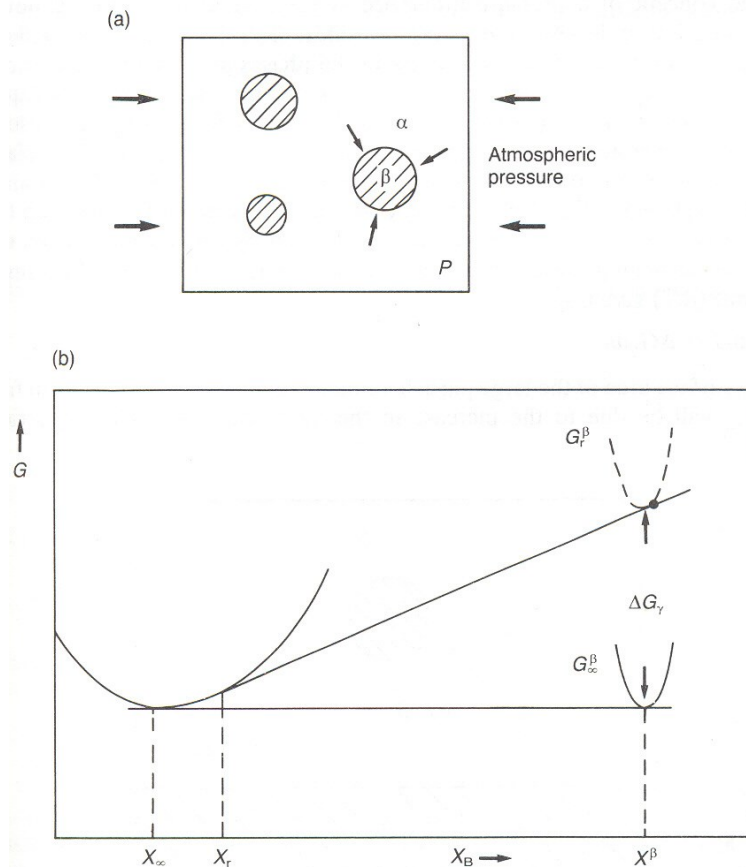


Fig. 2.16 Effect of interfacial energy on solubility of small particles



### Summary of terms in this chapter

**Ideal Solid Solution:** mixing of atoms of A and B does not release or absorb any heat ( $\Delta H_{\text{mix}} = 0$ )

**Chemical Potential:** defines the change of Gibbs free energy of the system after a small change to chemical composition of the system

**Regular Solid Solution:** mixing of atoms of A and B releases or absorbs heat ( $\Delta H_{\text{mix}} \neq 0$ )

**Coefficient of Activity:** the ratio of activity and molar fraction of particular component ( $\gamma_A = \frac{a_A}{X_A}$ ), it is  $\gamma_A = 1$  for ideal solutions.

**Gibbs – Thomson Effect:** increment of free energy of the phase, induced by curvature of interface it is also defined as the **capillary effect**. It is very significant for initial stages of transformations.



### Questions addressing the content covered

1. What is the difference between an ideal and a regular solution?

2. Draw a diagram showing Gibbs free energy versus composition including two phases and define the equilibrium.
3. How would you define activity?
4. What characteristics are carried by chemical potential of components within a system comprising two phases in equilibrium?
5. Draw a diagram showing full solubility in liquid state and limited solubility in solid state and choose three temperature levels to be supplemented with drawings of mutual location of curves representing the Gibbs free energy for phases present within.
6. What impact does the radius of curvature of particles interface of the precipitating phase have on its free energy and what is its impact on the equilibrium solubility of a dissolved component in the master phase?



## Exercises

### Exercise 1

The specific heat coefficient of solid copper exceeding 300 K can be calculated using the formula below:

$$c_p = 22,64 + 6,28 \times 10^{-3} T \quad (\text{Jmol}^{-1}\text{K}^{-1})$$

What is the increase of entropy of copper when heated from 300K to 1358K?

*Solution:*

$$c_p = 22,64 + 6,28 \times 10^{-3} T$$

$$\Delta S = \int_{T_1}^{T_2} \frac{c_p}{T} dT$$

$$\begin{aligned} \Delta S_{300-1358} &= \int_{300}^{1358} \frac{22,64 + 6,28 \times 10^{-3} T}{T} dT = \\ &= 40.83 \text{ Jmol}^{-1}\text{K}^{-1} \end{aligned}$$

### Exercise 2

An ideal solid solution has been formed using 15g of gold and 25g of silver.

- a) How many moles of solid solution have been produced?
- b) What are the molar fractions of gold and silver?
- c) What is the molar mixing entropy?
- d) What is the total mixing entropy?
- e) What is the change of molar free energy at 500°C?
- f) What is the chemical potential of gold and silver at 500°C, assuming that free energies of pure gold and silver are zero?

g) What would be the change of free energy in a solid solution at 500°C, after addition of one atom of gold? State your result in eV·atom<sup>-1</sup>.

*Solution:*

a) atomic weight of Au = 197

atomic weight of Ag = 108

number of moles of Au = 15/197 = 0.076

number of moles of Ag = 25/108 = 0.231

number of moles of solution = 0.307

b) molar fraction of Au = 0,076/0.307 = 0.248

molar fraction of Ag = 0,231/0.307 = 0.752

c) Molar mixing entropy,  $\Delta S_{mix} = -R(X_A \ln X_A + X_B \ln X_B)$

$$\Delta S_{mix} = -8.314 (0.248 \ln 0.248 + 0.752 \ln 0.752) = 4.66 \text{ JK}^{-1} \text{ mol}^{-1}$$

d) Total mixing entropy = molar mixing entropy x number of moles in solution =

$$4.66 \times 0.307 = 1.43 \text{ JK}^{-1}$$

e) change of molar free energy at 500°C:  $\Delta G_{mix} = RT(X_A \ln X_A + X_B \ln X_B)$

$$\Delta G_{mix} = -T\Delta S_{mix} = -733 \times 4.66 = -3.60 \text{ kJmol}^{-1}$$

f)  $\mu_{Au} = G_{Au} + RT \ln X_{Au}$

$$\mu_{Au} = 0 + (8.314 \times 773 \times \ln 0.248) = -8.96 \text{ kJmol}^{-1}$$

$$\mu_{Ag} = G_{Ag} + RT \ln X_{Ag}$$

$$\mu_{Ag} = 0 + (8.314 \times 773 \times \ln 0.752) = -1.83 \text{ kJmol}^{-1}$$

g) with a very low gold addition:  $dG' = \mu_{Au} dn_{Au} (T, p, n_B = \text{constant})$

at 500°C,  $\mu_{Au} = -8.96 \text{ kJmol}^{-1}$

$$1 \text{ eV} = 1.6 \times 10^{-19} \text{ J}$$

$$-8.96 \text{ kJmol}^{-1} = \frac{-8.96 \times 10^3}{1.6 \times 10^{-19} \times 6.023 \times 10^{23}} \text{ eV} \cdot \text{atom}^{-1} = -0.1 \text{ eV} \cdot \text{atom}^{-1}$$

Adding one atom of gold will change the free energy of solid solution by  $-0.1 \text{ eV} \cdot \text{atom}^{-1}$ .

### Exercise 3

The solubility ratio of silicon in aluminium is 1.25 at.% at the temperature of 550°C and 0.46 at.% at the temperature of 450°C. What solubility can be expected at 200°C?

*Solution:*

$$X_{Si} = A \exp - \frac{Q}{RT}$$

$$\ln X_{Si} = \ln A - \frac{Q}{RT}$$

at 550°C:  $\ln 1.25 = \ln A - Q/(8.314 \times 823)$

at 450°C:  $\ln 0.46 = \ln A - Q/(8.314 \times 723)$

*Solution to these equations:*

$$Q = 49.45 \text{ kJmol}^{-1}$$

$$A = 1721$$

*At the temperature of 200°C:*

$$X_{Si} = 1721 \exp \left( \frac{-49450}{8.314 \times 473} \right) = 0,006 \text{ at. \%}$$

### 3. Classification of Phase Transformations



**Study time:** 2.5 hours



**Objective:** Completion of this chapter will enable you:

- differentiate between phase transformations based on the thermodynamic or kinetic approach,
- define basic types of phase transformations,
- differentiate between the first or second order transformations,
- define differences between continuous and discontinuous transformations.



#### EXPLANATION

##### 3.1 Thermodynamic and Kinetic Classification

Most phase transformations belong to the *first order transformations*, where at the equilibrium transformation temperature the first derivations of Gibbs free energy  $\partial G/\partial T$  and  $\partial G/\partial p$  are discontinuous. These transformations include for example melting of solid substance, Fig. 3.1a. As  $\partial G/\partial T = -S$  and  $\partial G/\partial p = V$ , the first rate transformations are associated with discontinuous changes of volume and entropy. There is also a discontinuous change of heat content (enthalpy, H) relevant to the development of latent heat of transformation. The scope of specific heat coefficient is indefinite at the transformation temperature level, as adding a small amount of heat will convert more of the solid substance into melt without any temperature increase. These transformations enable achievement of the metastable state.

Fig. 3.1b characterises *the second order transformations*. These transformations are associated with discontinuous second derivatives of the Gibbs free energy  $\partial^2 G/\partial T^2$  and  $\partial^2 G/\partial p^2$ . Nevertheless, the first derivatives are continuous, which means the course of enthalpy H is also continuous. There is no development of latent heat at the transformation temperature, just a rapid increase of the coefficient of specific heat. These transformations

cannot reach any metastable states. The second order transformations include, for example, the magnetic ordering in metal-based alloys.

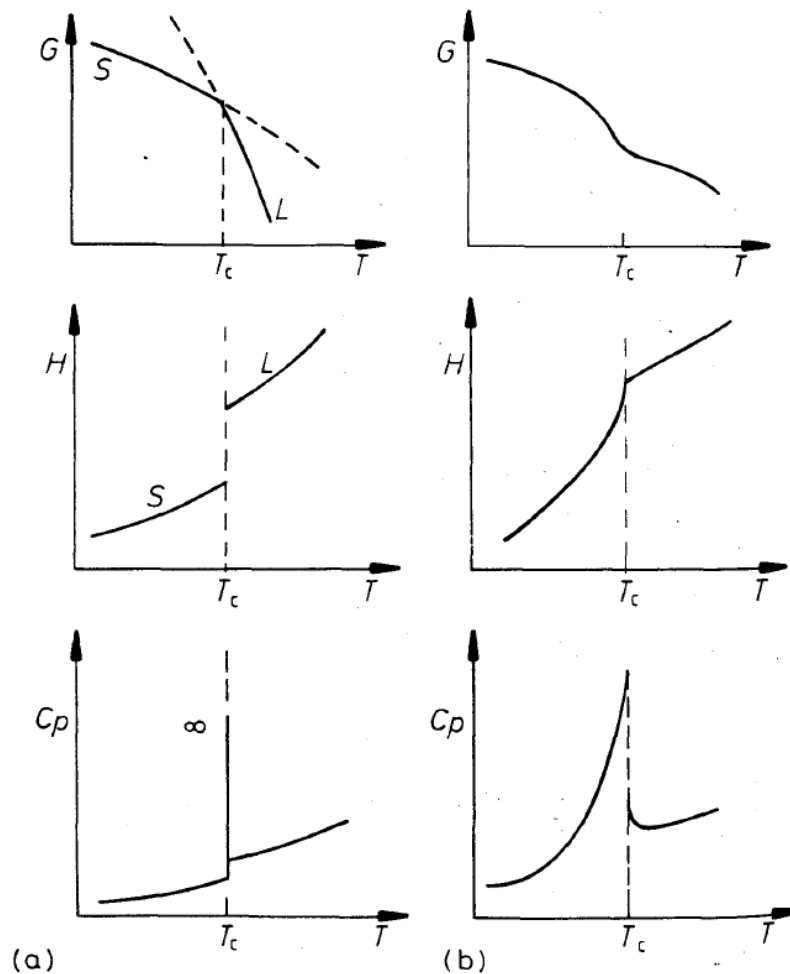


Fig. 3.1 Thermodynamic classification of phase transformations, a) first order transformation b) second order transformation,  $c_p$  is the isobaric coefficient of specific heat

Phase transformations can be characterised with respect to both nucleation and the growth process. As far as nucleation is concerned, phase transformations are divided to homogeneous and heterogeneous. The conditions for decomposition of an unstable phase in case of homogeneous transformations are identical at any point within the old phase. Homogeneous transformations can be typically represented by the spinodal decomposition. On the other hand, regarding heterogeneous transformations developed by formation of nuclei of the new phase, such nuclei start evolving at preferential spots within the old phase already. Heterogeneous transformations can be divided into three groups depending on the effect controlling the growth of the new phase, see Fig. 3.2. Referring to the thermally activated growth, phase transformations can be divided pursuant to the distance migrated by particular atoms: either short or long distance. The short distance migration is typical for single-

component systems exhibiting allotropy. For basic classification of diffusion transformations associated with relocation of atoms over long distances see also the Fig. 3.2.

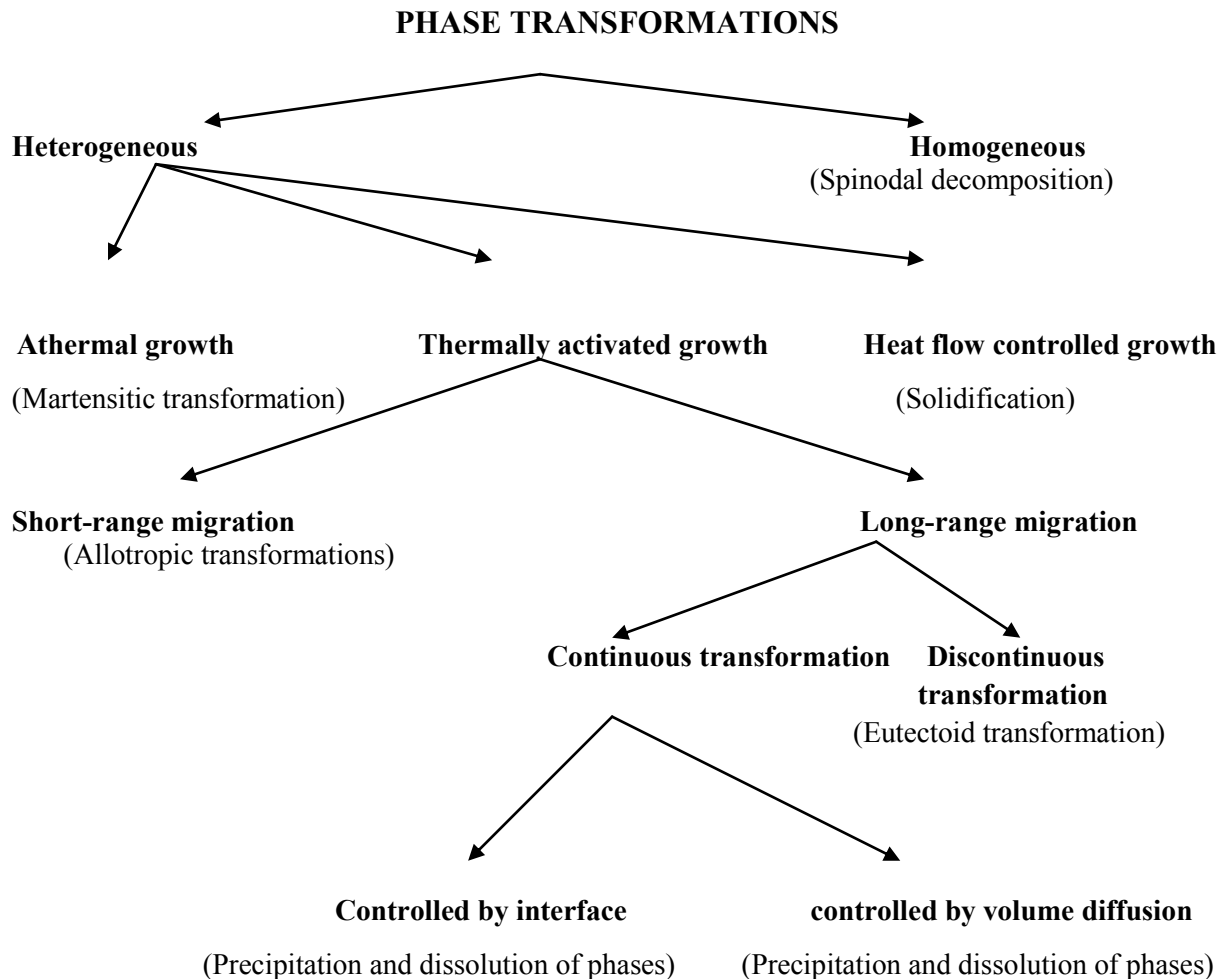


Fig. 3.2 Kinetic classification of phase transformations

**Heterogeneous transformations:** significant changes in atomic configurations within very small volumes, which are initially associated with the increase of Gibbs free energy in the system (at  $T = \text{const.}$ ,  $p = \text{const.}$ ). Overcoming of the energetic barrier is followed by nucleation of a stable nucleus with subsequent growth of transformed areas.

**Homogeneous transformations:** fluctuations associated with minor changes to configuration of atoms within large volumes. Nucleation takes place throughout the entire system volume simultaneously and it is followed by a gradual decrease of Gibbs free energy.

Another option to divide transformations is represented by the **growth mechanism** (kinetic aspect):

**Athermal growth:** the rate of growth is not dependent on temperature; there is a certain similarity with plastic deformation.

**Thermally activated growth:** the interface movement is driven by means of repeated overcoming of energetic barriers; this growth mechanism is strongly dependent on temperature.

**Growth controlled by heat flow:** the interface movement speed depends on the intensity of supply or dissipation of heat in the area of interphase interface.

There are two different cases of thermally activated growth:

**Migration of atoms over a short distance:** the phases on both sides of interface do not differ in terms of chemical composition.

**Migration of atoms over a long distance:** the phases on both sides of interface differ in terms of chemical composition.

Migration of atoms over a long distance can be further divided into two different cases:

**Continuous reaction:** development of areas with a new phase results in changes of chemical composition within the whole remaining volume of the initial phase.

**Discontinuous reaction:** chemical composition of the initial phase is identical to the average composition of product resulting from a discontinuous reaction; however, the product of discontinuous reaction is composed of two phases of different compositions.



### Questions addressing the content covered

1. What are the basic characteristics of the first order transformations?
2. What are the basic characteristics of the second order transformations?
3. What is the division of transformations with respect to the growth mechanism?
4. What is the difference between continuous and discontinuous phase transformations?
5. Why do certain phase transformations require a diffusion over a long distance?
6. What is the meaning of "athermal growth"?
7. What is a thermally activated process?



### Exercises

#### Exercise 1

Based on this resource material, use the classification of phase transformations above to perform detailed categorisation of:

- a) Martensitic transformations,
- b) Massive transformations,
- c) Bainitic transformations.

## 4. Interfaces in Solids and Their Migration



**Study time:** 4 hours



**Objective:** Completion of this chapter will enable you:

- Define basic types of interfaces in solids,
- Characterise of contributions of interphase surface energy and the elastic strain energy to particular types of interfaces,
- Explain the effect of interfaces on the rate of interface movement,
- Define the principle of movement of a glissile and non-glissile interfaces



### EXPLANATION

Interfaces in solids may be divided into the following three groups pursuant to their atomic structure:

- Coherent,
- Semicoherent,
- Incoherent.

#### *4.1 Coherent Interface*

For this type of interface, the perfect match at the interfacial plane is typical, i.e. the atomic configuration of an interface is identical in both phases, Fig. 4.1. That requires a specific mutual alignment of adjacent crystals, which can be expressed by means of the so called ***crystallographic orientation relationship*** defined by two parallel crystallographic planes (hkl) with low Miller indices in these crystals (phases) and two parallel directions [uvw] lying in these parallel planes. Adjacent crystals may have an identical or different crystal structure and their chemical compositions may differ.

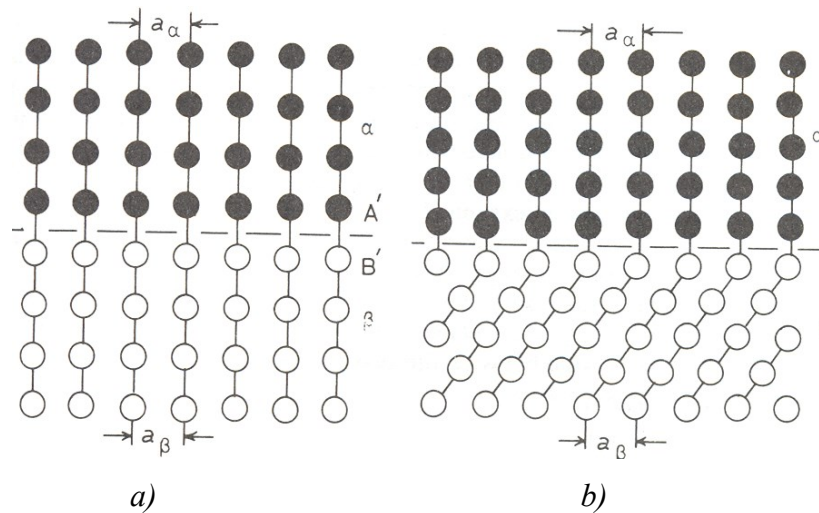


Fig. 4.1 Non-deformed coherent interfaces, a) The structures of adjacent crystals are identical, their chemical compositions differ, b) The structures of adjacent phases  $\alpha$  and  $\beta$  are different.

The arrangement of adjacent atoms within each phase is optimal to achieve a low level of the total system energy. However, the interface is usually affected by a change in composition, so each atom has partially improper neighbours over the interface. That increases the energy of atoms at the interface to produce a chemical contribution to the interfacial energy. That is the only contribution to interfacial energy in case of coherent interface:

$$\gamma_{\text{coh}} = \gamma_{\text{chem}} \quad (4.1)$$

If the crystal structure of adjacent phases is identical, while their lattice parameters differ, coherence of interface can be maintained by distortion of one or both crystal lattices, Fig. 4.2. The resultant elastic distortions of crystalline lattices in the interface area are defined as **coherence strains**.

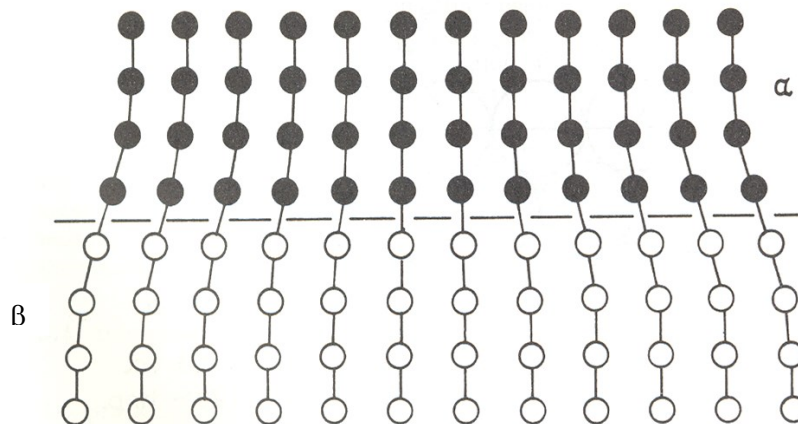


Fig. 4.2 Coherent interface with a minor misfit of crystal lattices resulting in development of coherence elastic strains.

A substantial contribution to the total energy of coherent interfaces is usually represented by the coherent elastic deformation; the contribution of interphase surface energy is low.

#### 4.2 Semicoherent Interface

Deformations associated with the coherent interface increase the total system energy, if there is a truly high misfit of crystal lattices or if the surface of interface is large, the coherent interface should be conveniently replaced with a semi-coherent one to gain energetic benefit, as the semi-coherent interface is subject to periodical reduction of misfit in the interface by means of dislocations ("misfit dislocations"), Fig. 4.3.

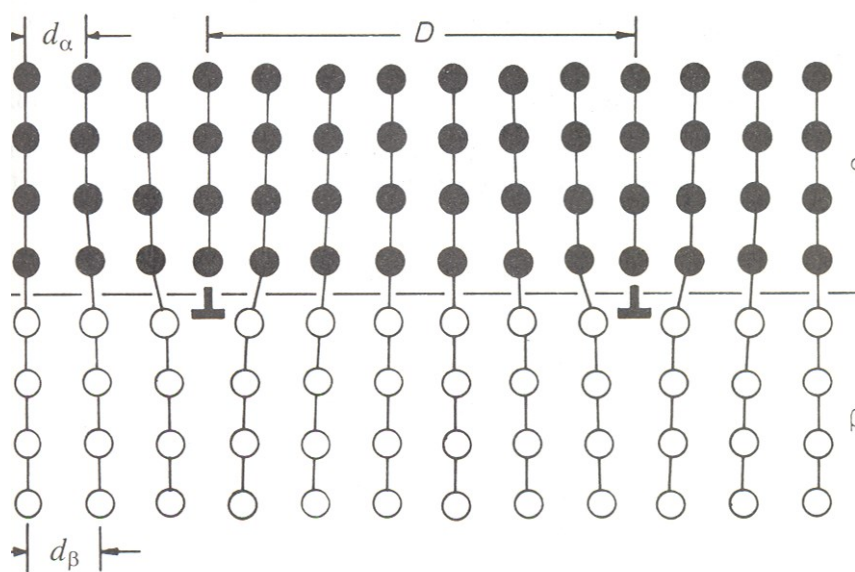


Fig. 4.3 Semicoherent interface, misfit of lattices along the direction parallel with interface is accommodated by a series of edge dislocations

If  $d_\alpha$  and  $d_\beta$  are non-deformed interplanar distances between planes of phases  $\alpha$  and  $\beta$  in the area of interface, the misfit between both lattices is defined by the formula:

$$\delta = \frac{d_\beta - d_\alpha}{d_\alpha} \quad (4.2)$$

**Lattice misfit** in an interface can be eliminated almost perfectly using a suitable configuration of dislocations within the interface, except for areas around the dislocation cores, where the structure is distorted to a high extent.

The interphase surface energy of a semi-coherent interface is formed by two contributions: the chemical contribution  $\gamma_{\text{chem}}$  (similar to the coherent interface) and the structural interface  $\gamma_{\text{str}}$ ,

that represent sufficient energy induced by distortions around the cores of "misfit" dislocations:

$$\gamma_{\text{semi-coh}} = \gamma_{\text{chem}} + \gamma_{\text{str}} \quad (4.3)$$

The structural contribution  $\gamma_{\text{str}}$  to interfacial energy for low values of the lattice misfit will be approximately proportional to the density of dislocations within the interface. If  $\delta > 0.25$ , i.e. there is one dislocation per every fourth interplanar distance, distorted areas around dislocation cores will overlap and the interface is considered incoherent.

### 4.3 Incoherent Interface

If there is a significant difference in atomic configurations within the interfacial plane of adjacent crystals, there is no chance of fine match between atomic configurations over the interface. Atomic configurations in either phase may be very different; or even if similar, the interatomic spacing may differ by more than 25 %. Generally speaking, an incoherent interface develops, when two randomly aligned crystals are bonded alongside any interfacial plane, Fig. 4.4. This interface may exist even in case there are two phases with an orientation relationship, if the atomic configurations in the interfacial plane of both phases are very different.

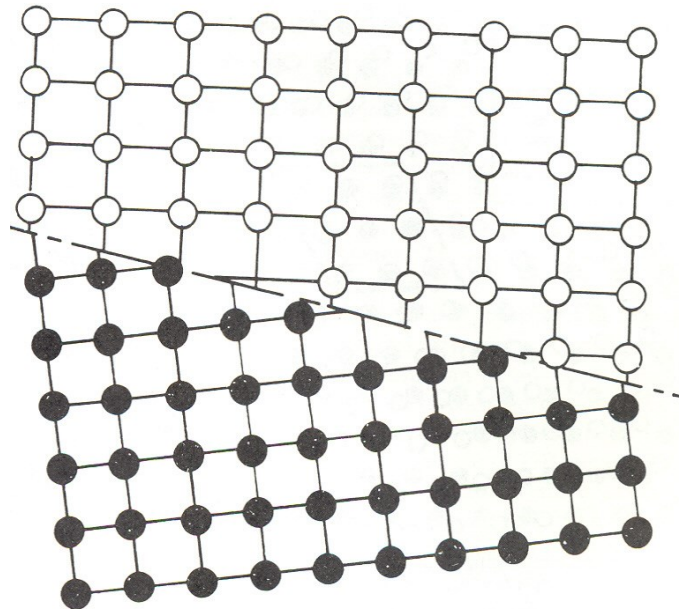


Fig. 4.4 Incoherent Interface

As far as incoherent interfaces are concerned, the dominant role is played by the interfacial surface energy. The coherent strain energy will be zero. Nevertheless, even an incoherent interface may be associated with the energy supplemented by the elastic deformation energy.

That happens in cases with significant differences between the volume of old and new phases, respectively.

#### 4.4 Interface Migration

Most phase transformations in metal systems are conducted by means of nucleation and growth processes. An interface is created at the nucleation stage and it subsequently migrates into a metastable matrix during the growth stage. Growth brings relocation of atoms via the moving interface. This is the heterogeneous type of transformation: the system can be split into the master and resultant phases at any moment during the transformation process.

There are two types of interfaces: glissile and non-glissile. A *glissile interface* migrates in terms of a coordinated sliding movement of dislocations, which induces shear transformation (deformation) of the source phase into a new phase. The movement of a glissile interface is relatively independent from temperature; it is therefore called an athermal growth. However, most of the interfaces are of non-glissile type and these migrate with more or less random atom jumps across interfaces. The additional energy required by atoms to execute a free jump from an old phase and join a new phase is supplied by means of thermal activation. That makes migration of any *non-glissile interface* strongly dependent on temperature.

##### 4.4.1 Migration of Non-Glissile Interface

If there is any difference between chemical composition of matrix and the new phase, the growth of such new phase will require diffusion over a long distance. Fig. 4.5 shows a situation, when the precipitating phase  $\beta$  consisting of the almost pure component B grows with the planar interface into the phase  $\alpha$  (rich in component A) with the initial composition  $X_0$ , Fig. 4.5c. The growth of precipitate causes depletion of the matrix  $\alpha$  in the vicinity of the  $\alpha/\beta$  interface in component B, so the concentration  $X_i$  of component B in phase  $\alpha$  in the vicinity of the interface drops below the average concentration present in the phase  $\alpha$ , Fig. 4.5a. As the growth of precipitate requires flow of atoms of B from the phase  $\alpha$  into the phase  $\beta$ , there must be a driving force across the interface  $\Delta\mu_i$ , Fig. 4.5b. The origin of this difference in chemical potentials is evident from Fig. 4.5c. To enable growth, the concentration of component dissolved within the interface must exceed the equilibrium concentration  $X_e$ . In case the interface mobility is very high, e.g. incoherent interface,  $\Delta\mu_B^i$  can be very low and  $X_i \cong X_e$ . These conditions create a local equilibrium at the interface. The interface then moves as fast as allowed by diffusion and growth occurs under conditions controlled *by the volume diffusion*. Examples of this mechanism may include solidification and diffuse transformations in solids.

In case the interface mobility is low, the reaction within requires a larger differential of the chemical potential ( $\Delta\mu_B^i$ ) and here will be a deviation from the local equilibrium within the interface. The value of  $X_i$  complies with the prerequisite concerning equal flow of atoms of B via the interface and phase  $\alpha$  ( $J_B^i = J_B^\alpha$ ) and the interface will be moving under combined control conditions. As far as the limiting case of very low mobility is concerned,  $X_i \cong X_0$  and  $(\partial c/\partial x)$  interface is almost equal to zero. These conditions imply the **growth controlled by interface** and there is the maximum driving power possible  $\Delta\mu_B^i$  across the interface.

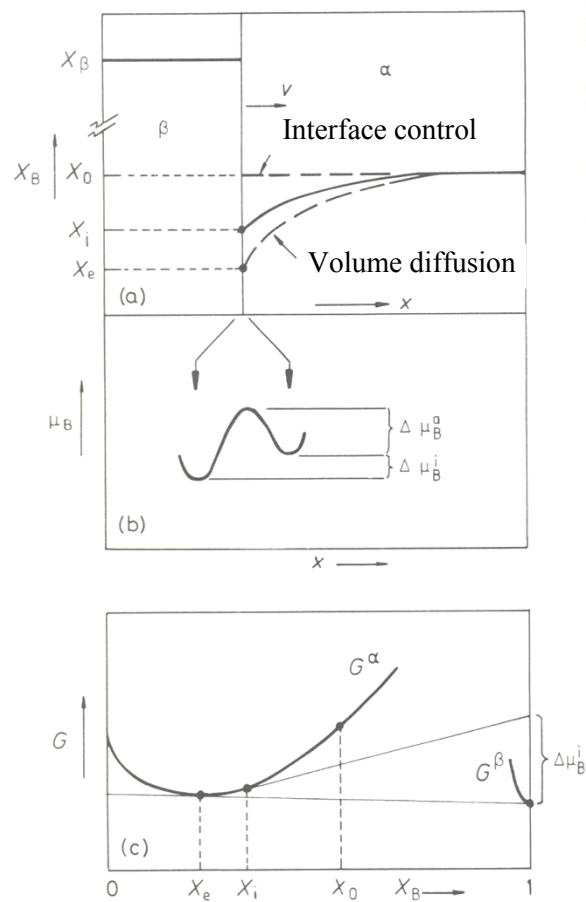


Fig. 4.5 Movement of interface with long-range diffusion, a) Composition profiles across the interface, b) Origin of driving force for migration of interface into phase  $\alpha$ , associated with differences in chemical potential ( $\mu$ ) of component B across the interface, c) schematic diagram of molar free energy showing relations among  $\Delta\mu_B^i$ ,  $X_i$  and  $X_e$ . Solubility of component A in phase  $\beta$  is so low that the full shape of curve showing the free energy of phase  $\beta$  could not be depicted.

#### 4.4.2 Migration of Glissile Interface

There are some circumstances, under which dislocations within a semi-coherent interface can be arranged in such manner that the interface may move by means of a coordinated glissile of dislocations present within the interface. That is possible in case, when dislocations have the Burgers vector enabling their glissile movement on the connecting atom planes in both adjacent crystals, Fig. 4.6. Glissile planes must pass across the interface smoothly but they do not have to be mutually parallel. Any moving dislocation would shift the lattice above glissile plane with respect to the plane below by the distance corresponding to the Burgers dislocation vector. The slip of dislocations within a glissile interface coordinated in the same manner causes a shear deformation of lattice, e.g. shear transforms the phase  $\alpha$  into the phase  $\beta$ .

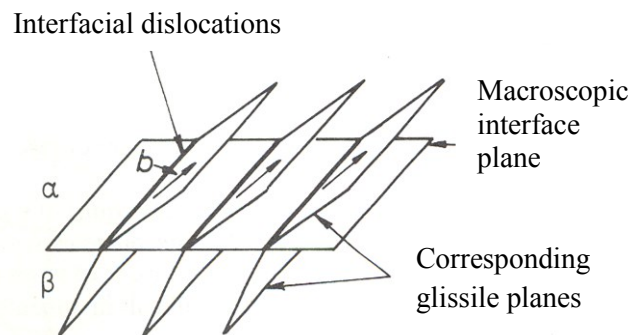
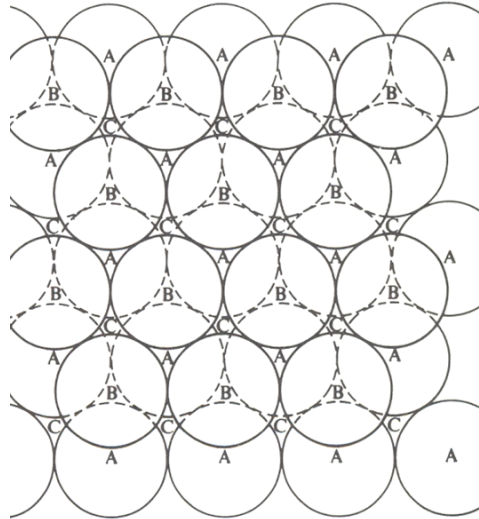


Fig. 4.6 Principle of glissile interface

The glissile interface can be illustrated by an example comprising the interface between FCC and HCP lattices. As you already know, both the FCC and HCP lattices can develop by stacking of atomic planes with the closest atomic configuration represented by solid spheres of identical size. With centres of atoms contained within the first layer marked with letter A, the second layer may occupy either positions B or C, Fig. 4.7. Assume that atoms in the second layer occupy B positions. This situation then shows two non-equivalent methods for creating the third layer.



*Fig. 4.7 Positions of atoms in close-packed layers represented by solid spheres of identical size*

In case the third layer is located right above the first layer, the stacking sequence is defined as ABA and repeating this sequence creates the ABABABAB..... configurations, which matches the HCP lattice. The basal plane features Miller - Bravais indices (0001) and the directions with the closest arrangement of atoms conform to the type  $\langle 11\bar{2}0 \rangle$ .

In case the atoms contained within the third layer occupy positions C, the resultant sequence will be ABC and it will form the ABCABCABC..... configuration when repeated, this is typical for a FCC lattice, Fig. 4.7. The plane with the closest atomic configuration exhibits Miller indices  $\{111\}$  and the close-packed directions conform to the type  $\langle 110 \rangle$ .

The spacing of B and C positions within the FCC lattice, measured along the plane parallel with the plane containing the closest atomic configuration, is equal to the vector type  $\frac{a}{6} \langle 11\bar{2} \rangle$ . This vector relates to the Shockley partial dislocation, which is shorter than the shortest vector linking two atoms within the FCC lattice. In case a dislocation with the vector  $\frac{a}{6} [11\bar{2}]$  slides between two planes (111) within the FCC lattice, e.g. between layers 4 and 5 in Fig. 4.8, all the planes above the slip plane (5, 6, 7...) will be shifted by vector  $\frac{a}{6} [11\bar{2}]$ . All the atoms at positions marked B are shifted to C positions above the slip plane, atoms from C positions are shifted to A positions and those from the A positions are shifted to B positions, Fig. 4.8.

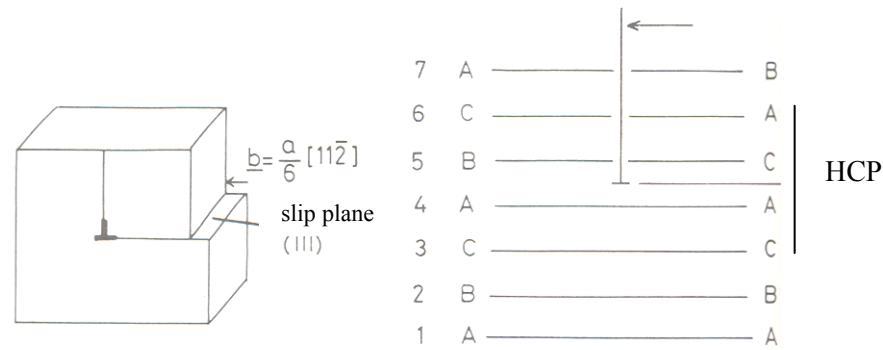


Fig. 4.8 Edge dislocation with Burgers vector  $\frac{a}{6} [11\bar{2}]$  on slip plane (111). The space behind a moving dislocation shows local changes in sequence of atomic planes (111)

The sliding movement of Shockley dislocation disrupts the crystal lattice and causes a stacking fault in the slip plane. Fig. 4.8 documents that such stacking fault includes four atomic planes with the CACA stacking sequence matching a HCP lattice. As far as thermodynamically stable FCC lattice is concerned, a stacking fault represents an area with high free energy. On the other hand, in case the FCC lattice is metastable with respect to the HCP lattice, the energy of stacking fault will be actually negative and the sliding of Shockley dislocations will reduce the system free energy.

Assume the impact of another moving dislocation with Burgers vector  $\frac{a}{6} [11\bar{2}]$  between layers 6 and 7 in Fig. 4.9. It is evident that the area with HCP structure has been extended by two more layers. That implies the configuration of Shockley dislocations at every second plane (111) within the FCC lattice may create a glissile interface separating the crystals of FCC and HCP, Fig. 4.10. Slip planes of interfacial dislocations run from the FCC into HCP lattice continuously and Burgers vectors lying within the sliding plane form an angle with the macroscopic plane of the interface. If such set of dislocations slides into a FCC crystal; it will result in transformation of FCC  $\rightarrow$  HCP, whereas the movement of the set of dislocations in the opposite direction would cause a reversed transformation of HCP  $\rightarrow$  FCC. From the macroscopic point of view, the interface plane makes an angle with the plane (111), or (0001) respectively; and this plane does not have to be parallel to any other plane with low indices, i.e. it may be irrational. However, the microscopic view shows interface comprising coherent facets parallel with the planes (111) FCC or (0001) HCP respectively, separated by cascades matching the thickness of two close – packed atomic layers.

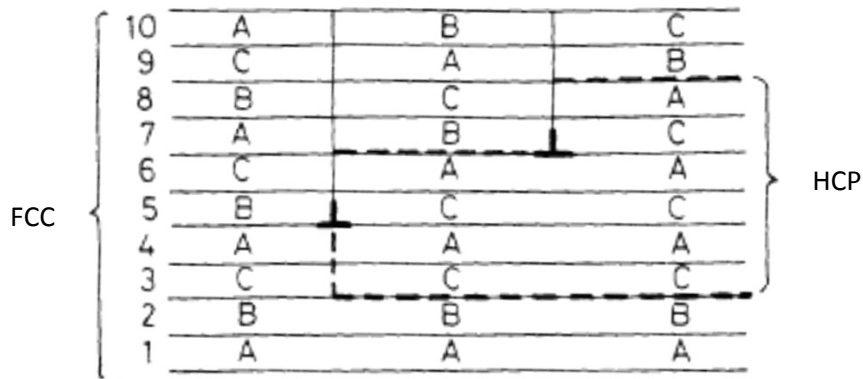


Fig. 4.9 Movement of two partial Shockley dislocations along two planes (111) FCC within the lattice separated by one layer (111) creates a HCP crystal with the thickness of 6 atomic layers

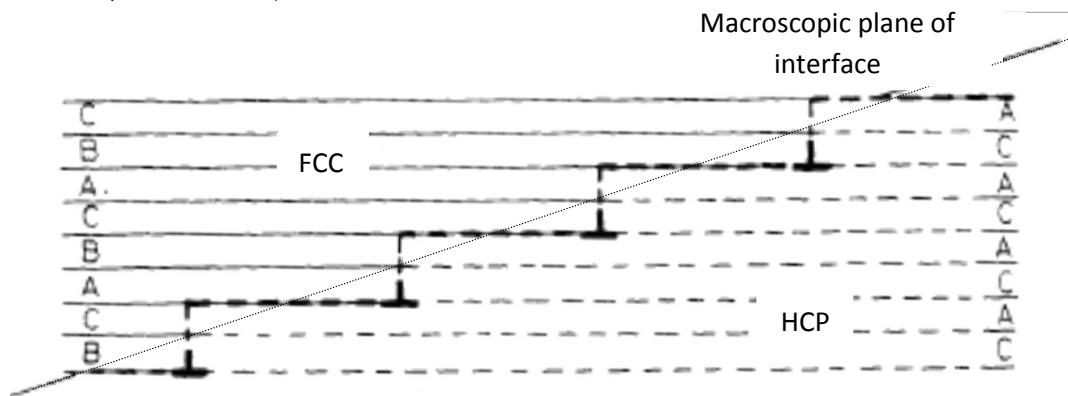


Fig. 4.10 Configuration of Shockley dislocations creating a glissile interface between FCC and HCP crystals, the macroscopic plane of interface is inclined to planes (111)

One of the important characteristics of the glissile interface is that its movement may induce a macroscopic change to the crystal shape. The transformation of FCC  $\rightarrow$  HCP is shown in the Fig. 4.11. Once a single FCC crystal is transformed into a HCP lattice by passing through the Shockley dislocation with identical Miller indices at every second plane (111), the macroscopic change of crystal shape occurs and it is similar to deformation by shear, Fig. 4.11a. Nevertheless, the plane (111) contains further two Shockley dislocations than can be used during transformation of FCC  $\rightarrow$  HCP. If the transformation of FCC  $\rightarrow$  HCP occurs with all three Shockley dislocations applied in equal numbers (Burgers vectors lie in the plane (111) and make angles of  $120^\circ$  each to other), no change in crystal shape will occur, Fig. 4.11b.

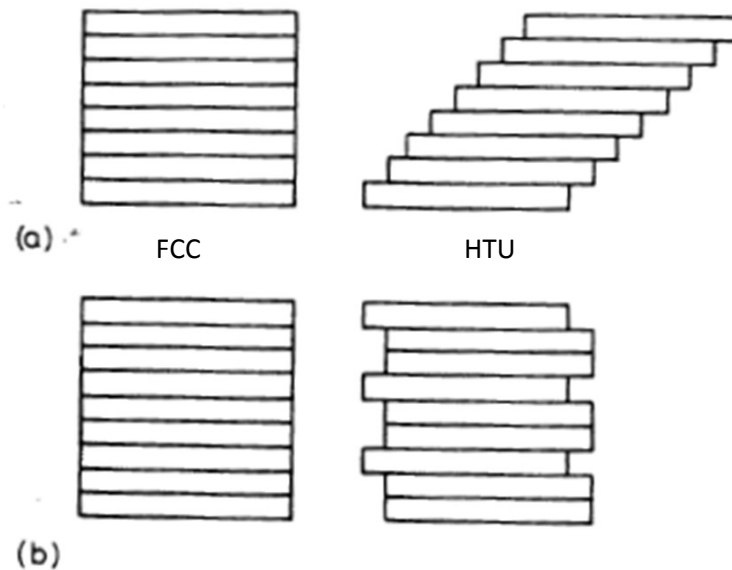


Fig. 4.11 Schematic depiction of various options for the transformation  $FCC \rightarrow HCP$ , a) using a Shockley dislocation of single type at every second plane (111) - shape change occurs, b) using the same number of all three types of Shockley dislocations possible at every second plane (111) – no macroscopic change of crystal shape

The glissile interface plays a vital role during martensitic transformations inducing macroscopic changes of crystal shape but the chemical composition of the parent phase and martensite remains the same.



### Summary of terms in this chapter

**Interphase interface:** an interface separating two phases.

**Coherent interface:** an interface with perfect atomic coherence within the interfacial plane. If there are two adjacent phases with identical crystal structure but their lattice parameters are slightly different, the misfit of lattice planes can be accommodated by coherent elastic deformations.

**Semicoherent interface:** misfit within the coherent interface reaches such an extent that it must be accommodated by the formation of dislocations.

**Incoherent interface:** the interfacial plane of adjacent crystals features very different atomic configurations; there is no possibility of good coherence within atomic configuration across the interface plane. An incoherent interface is characteristic for the high value of interfacial surface energy, whereas the contribution of coherent deformation energy is equal to zero.

**Glissile interface:** this interface contains dislocations with the Burgers vector which lies in

the slip planes of both old and new phases. Coordinated movement of these dislocations results in phase transformation, which may be accompanied by shape deformation.

**Non-glissile interface:** the movement of this interface is driven by random jumps of atoms across the interface. The movement of this interface can be controlled by volume diffusion or by the interface control.



### Questions addressing the content covered

1. What types of interface in solids do you know?
2. How do coherence strains develop?
3. What is the difference between interphase surface energy of coherent and semicoherent interfaces?
4. What is the definition of incoherence between crystal lattices and of the orientation relationship between phases?
5. Can elastic deformations play a role in incoherent interfaces? Where do they originate from?
6. What is the difference between a glissile and non-glissile interfaces?
7. Draw the layout of directions  $\langle 112 \rangle$  in the plane (111) of a FCC crystal lattice. Why the slip along all these vectors in equal numbers does not generate shape deformation during FCC transformation to HCP?
8. What is the difference between growth controlled by diffusion and growth controlled by the interface?

## 5. Solidification



**Study time:** 5 hours



**Objective:** Completion of this chapter will enable you:

- define difference between homogeneous and heterogeneous nucleation,
- define potential solidification mechanisms in single-phase alloys,
- explain the development of chemical heterogeneity during solidification of alloys,
- characterise dendritic growth in binary alloys,
- describe the rules of crystallisation of eutectic alloys.



### EXPLANATION

Solidification and melting represent transitions between the solid and liquid states. These phase transformations are essential for such technological applications as production of castings and ingots, continuous casting, growth of monocrystals for semiconductors, fusion welding and recently also metallic glasses. Understanding of the solidification mechanism and the impact of parameters such as the temperature gradient, rate of cooling and doping of alloys, is important for inspection of mechanical characteristics and structure of cast materials and welded joints.

#### 5.1 Nucleation in Pure Metals

##### 5.1.1 Homogeneous Nucleation

In this case, nucleation of the solid phase occurs right inside the melt overcooled to  $\Delta T$  below the melting point ( $T_m$ ). Assume the volume of melt depicted in Fig. 5.1a.

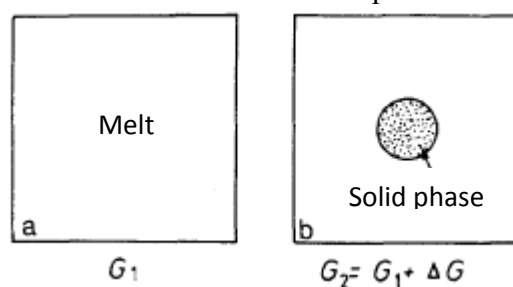


Fig. 5.1 Homogeneous Nucleation in Melt

The temperature  $T = T_m - \Delta T$  generates the Gibbs free energy in this system without any solid phase at the level of  $G_1$ . In case there are any atoms clustering inside the melt to form a small spherical solid nucleus (Fig. 5.1b), the Gibbs free energy of this system will change to  $G_2$  and it will be defined by the formula below:

$$G_2 = V_S G_V^S + V_L G_V^L + A_{SL} \gamma_{SL} \quad (5.1)$$

where:  $V_S, (V_L)$  is the volume of solid (liquid) phase,

$G_V^S (G_V^L)$  is the Gibbs free energy of solid (liquid) phase per unit of volume,

$A_{SL}$  is the surface area of solid/liquid phase interface,

$\gamma_{SL}$  is the surface energy of the solid/liquid phase interface.

The Gibbs free energy of the system without solid phase is defined as:

$$G_1 = (V_S + V_L) G_V^L \quad (5.2)$$

where  $V_S = 0$ .

Development of a solid phase therefore induces a change to the Gibbs free energy:

$$\Delta G = G_2 - G_1 = -V_S \Delta G_V + A_{SL} \gamma_{SL} \quad (5.3)$$

Where the Gibbs free energy (per unit of volume) is:

$$\Delta G_V = G_V^L - G_V^S$$

For undercooling  $\Delta T$ , the value of  $\Delta G_V$  is expressed by the following formula:

$$\Delta G_V = \frac{L_V \Delta T}{T_m} \quad (5.4)$$

where:  $L_V$  is the latent heat for solidification per unit of volume.

Wherever below the temperature  $T_m$ , the value of  $\Delta G_V$  remains positive, so the change of Gibbs free energy associated with development of a small quantity of the solid phase represents a negative contribution in the formula (5.3) but there is also a positive contribution associated with formation of the solid/liquid phase interface. Any redundant free energy relevant to solid particles in the melt can be minimised upon selection of the correct particle shape. Isotropy of surface energy  $\gamma_{SL}$  induces formation of a spherical particle with the radius  $r$

inside the melt and the formula (5.3) expressing the change of Gibbs free energy will be as below:

$$\Delta G_r = -\frac{4}{3}\pi r^3 \Delta G_V + 4\pi r^2 \gamma_{SL} \quad (5.5)$$

For graphic depiction of the formula (5.5) refer to Fig. 5.2. The resultant function is significant for the maximum point on curve showing Gibbs free energy matching the nucleus of critical size  $r^*$ . The growth of nuclei sized  $r < r^*$  would lead towards increase of the Gibbs free energy within the system, which is impossible and the nuclei below the critical size will be dissolved. That is followed by reduction of the Gibbs free energy of the system. Only a growth of nucleus with over-critical size ( $r > r^*$ ) causes reduction of the Gibbs free energy of the system, therefore the growth of these nuclei occurs automatically.

Critical radius of the nucleus  $r^*$  and the Gibbs free energy required for its formation  $\Delta G^*$  are vital parameters of nucleation. Relations enabling the determination of their sizes can be derived using a simple mathematical procedure of the formula (5.5) - searching for the extreme value of function ( $dG = 0$ , when  $r = r^*$ ):

$$r^* = \frac{2\gamma_{SL}}{\Delta G_V} \quad (5.6)$$

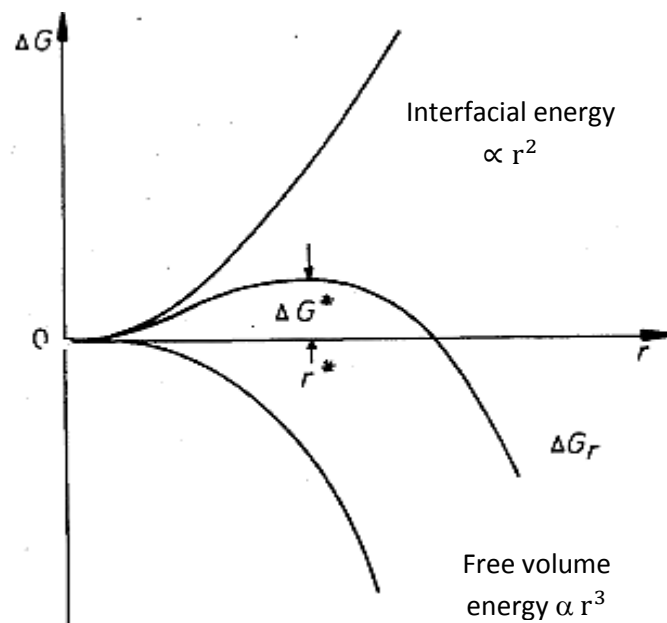


Fig. 5.2 Change of Gibbs free energy associated with homogeneous nucleation of sphere with radius  $r$

$$\Delta G^* = \frac{16\pi\gamma^3 SL}{3(\Delta G_V)^2} \quad (5.7)$$

Substitution of  $\Delta G_V$  in the equation (5.4) produces:

$$r^* = \left( \frac{2\gamma_{SL}T_M}{L_V} \right) \cdot \frac{1}{\Delta T} \quad (5.8)$$

$$\Delta G^* = \left( \frac{16\pi\gamma_{SL}^3 T_M^2}{3L_V^2} \right) \cdot \frac{1}{(\Delta T)^2} \quad (5.9)$$

Note how values of  $r^*$  and  $\Delta G^*$  decrease proportionally with undercooling  $\Delta T$ , Fig. 5.3.

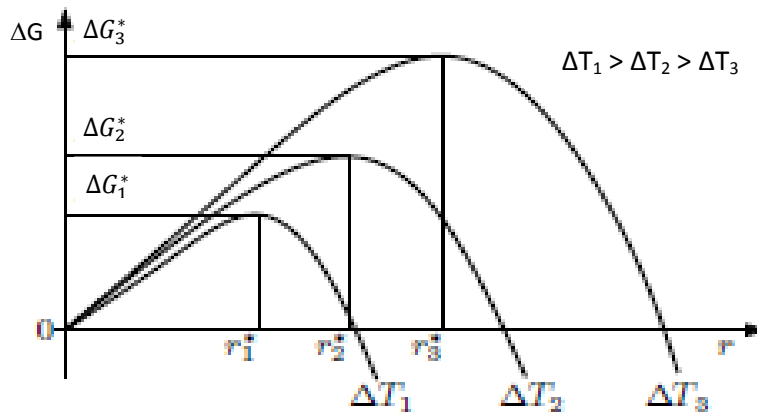


Fig. 5.3 Change of shape and position of the curve  $\Delta G$  depending on the magnitude of undercooling  $\Delta T$

The equation (5.6) could be also derived from the Gibbs-Thomson equation, see Chapter 2. As the value of  $r^*$  refers to a radius of a solid sphere, which is in equilibrium with the surrounding melt, the free energy of solidified sphere and melt must be the same. The equation (2.33) implies that the solid sphere of small radius  $r$  will contain the Gibbs free energy exceeding the large volume of solid phase by  $2\gamma V_m/r$  (per one mole) or  $2\gamma/r$  (per unit of volume). Fig. 5.4 shows that the equality of Gibbs free energy implies an expression identical with the equation (5.6):

$$\Delta G_V = \frac{2\gamma_{SL}}{r^*} \quad (5.10)$$

Proper understanding of possibilities for homogeneous development of stable solid nuclei in melts requires examination of atomic structure of the liquid phase first. Dilatometry

measurements have shown that the volume of a liquid phase will be 2-4 % higher compared to a solid phase at the melting point temperature. That is why atoms in melt can move more freely and take their positions at random. However, the melt can be inspected at any time to find numerous small clusters of atoms with their configuration temporarily identical to the one in solid phase (crystallisation centres).

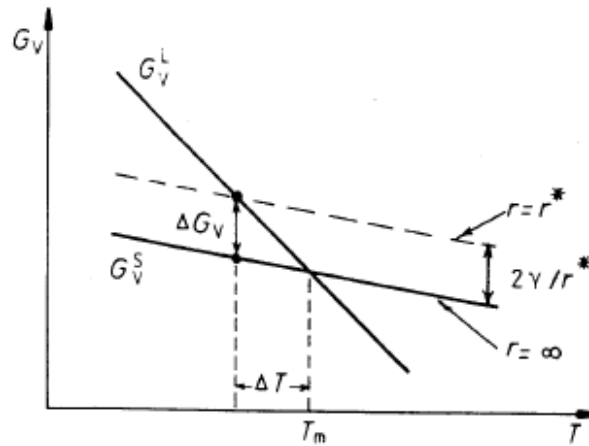


Fig. 5.4 Thermal dependency of the volume Gibbs free energy for liquid and solid phases

The average number of these spherical clusters with the radius of  $r$  is defined by the formula:

$$n_r = n_0 \exp\left(-\frac{\Delta G_r}{kT}\right) \quad (5.11)$$

where  $n_0$  is the total number of atoms in the system,  $\Delta G_r$  refers to the excess of Gibbs free energy associated with the cluster of atoms (equation 5.5) and  $k$  is the Boltzmann constant.

This relation shall apply for liquids exceeding the temperature  $T_m$  with any value of  $r$ . Its application below  $T_m$  shall be limited to  $r < r^*$ , as the clusters of over-critical size are formed by stable nuclei of solid phase and these are no longer parts of the melt. Owing to the fact, that  $n_r$  drops exponentially with respect to  $\Delta G_r$  (which actually rises fast by itself in proportion to  $r$ ), the probability of occurrence of the said cluster will drop very fast with the increase of cluster size. Fig. 5.5 represents a schematic depiction of the maximum size of cluster ( $r_{max}$ ) changing with  $\Delta T$ . Clusters larger than  $r_{max}$  can obviously form in systems of sufficient extent or in case there is enough time, yet the probability of finding clusters exceeding the size  $r_{max}$  by at least a slight extent is extremely low.

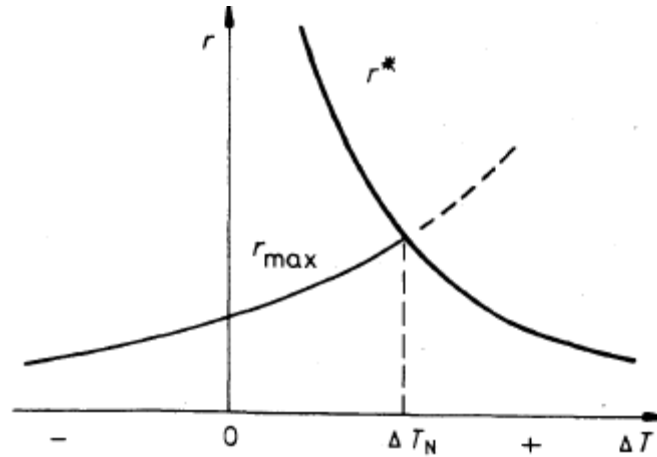


Fig. 5.5 Change of  $r_{max}$  and  $r^*$  with undercooling of  $\Delta T$  below the melting point

The Fig. 5.5 also shows the critical size of nucleus  $r^*$ . It is evident that low undercooling makes the critical radius  $r^*$  so big that the chance to create a stable nucleus will be basically eliminated. However, as  $\Delta T$  rises,  $r^*$  and  $\Delta G^*$  drop and the undercooling values equal or exceeding  $\Delta T_N$  mean fair chance that some clusters reach  $r^*$  and turn into stable solid particles. A small droplet of melt should therefore include a homogeneous nucleation upon its undercooling by  $\Delta T_N$ . Experiments have shown that most metals need to be overcooled by  $\Delta T_N \sim 0,2 T_m$  (i.e.  $\sim 200$  K).

### 5.1.2 Rate of Homogeneous Nucleation

Assume the rate, at which solid nuclei appear in a melt overcooled to the particular level. If the melt contains  $C_0$  of atoms per unit of volume, the number of clusters that have reached the critical size ( $C^*$ ) can be obtained from the equation (5.11) as:

$$C^* = C_0 \exp\left(-\frac{\Delta G_{\text{hom}}^*}{kT}\right) \quad (\text{number of clusters per m}^{-3}) \quad (5.12)$$

Adding one more atom to each cluster will produce stable nuclei and if that happens at the frequency  $f_0$ , the rate of homogeneous nucleation will be defined by the formula:

$$N_{\text{hom}} = f_0 c_0 \exp\left(-\frac{\Delta G_{\text{hom}}^*}{kT}\right) \quad (\text{number of nuclei per m}^{-3} \text{ s}^{-1}) \quad (5.13)$$

where  $f_0$  is the function of frequency of atomic vibrations, activation energy of diffusion in melt and the surface of critical nucleus.

The use of (5.9) and subsequent solving of (5.13) can also help to express the following:

$$N_{\text{hom}} = f_0 c_0 \exp\left(-\frac{A}{(\Delta T)^2}\right) \quad (5.14)$$

where the A parameter is defined by the formula:  $A = \frac{16\pi\gamma_{SL}^3 T_m^2}{3L_V^2 kT}$

The rate of homogeneous nucleation  $N_{\text{hom}}$  is expressed as a function of undercooling  $\Delta T$  in Fig. 5.6. Due to the expression  $(\Delta T)^2$  in the exponent of this equation  $N_{\text{hom}}$  will be changing basically from zero up to very high values within a very narrow temperature range, i.e. there is a truly critical undercooling for nucleation  $\Delta T_N$ . It is the same as  $\Delta T_N$  in Fig. 5.5 but the Fig. 5.6 is a more clear evidence of the fact that there are basically no clusters forming up to the critical undercooling point  $\Delta T_N$  followed by a very intense nucleation.

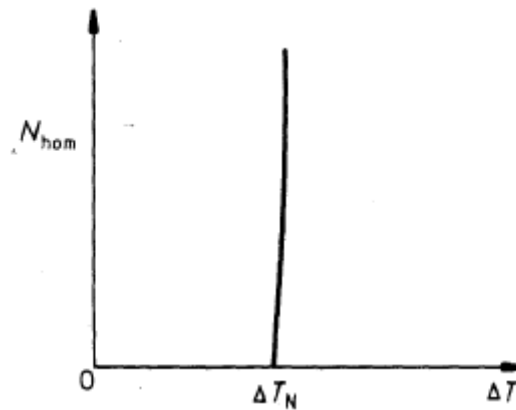


Fig. 5.6 The rate of homogeneous nucleation as a function of undercooling  $\Delta T$ .  $\Delta T_N$  represents the critical undercooling for homogeneous nucleation

The homogeneous nucleation during solidification is very scarce in practice, nucleation usually occurs on heterogeneous surfaces only. The points for heterogeneous nucleation are usually found on the walls of mould or impurity particles in the melt.

### 5.1.3 Heterogeneous Nucleation

The equation (5.9) implies that easier nucleation at low undercooling levels requires a reduction of surface energy in the interface between the solid phase and the melt. Formation of nucleus on the mould surface is an easy method to achieve that. Assume formation of a nucleus on the mould surface in accordance with Fig. 5.7. Assuming that  $\gamma_{SL}$  is isotropic, the shape of nucleus corresponding with the minimum total surface energy of the system consists of a spherical cap.

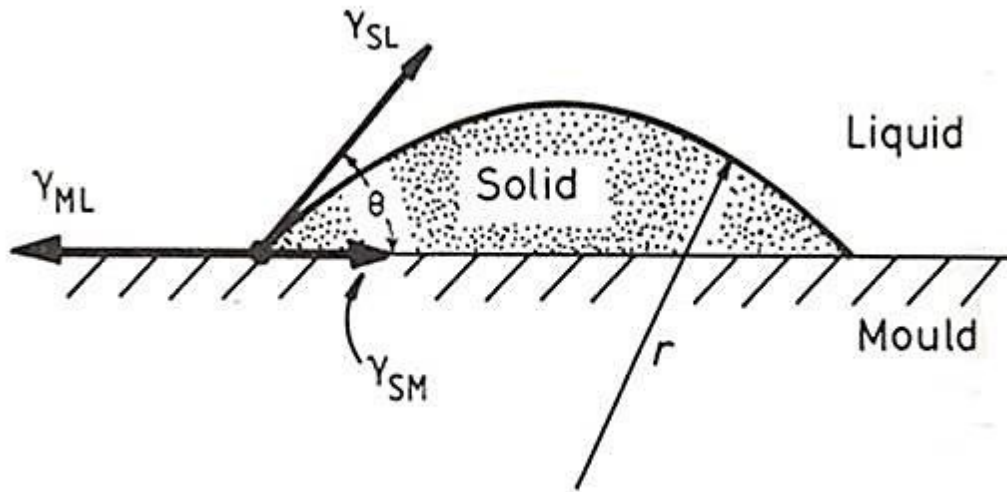


Fig. 5.7 Heterogeneous nucleation of solid phase on a planar wall of the mould

The prerequisite for equilibrium of surface tension at the mould wall plane can be expressed as:

$$\gamma_{ML} = \gamma_{SM} + \gamma_{SL} \cos\theta \quad (5.13)$$

where:  $\gamma_{ML}$  is the surface energy of interface between the mould (M) and the melt (L),  
 $\gamma_{SM}$  is the surface energy of interface between the solid phase (nucleus) and the mould,  
 $\gamma_{SL}$  is the surface energy of interface between the solid phase (nucleus) and the melt.

The contact angle is therefore  $\theta$  equal to:

$$\cos\theta = (\gamma_{ML} - \gamma_{SM}) / \gamma_{SL} \quad (5.14)$$

The total Gibbs free energy during a heterogeneous nucleation will be defined by the formula:

$$\Delta G_{\text{het}} = -V_S \Delta G_V + A_{SL} \gamma_{SL} + A_{SM} \gamma_{SM} - A_{SM} \gamma_{ML} \quad (5.15)$$

where:  $V_S$  is the volume of solid nucleus,

$A_{SM}$  is the area of interface between the nucleus and the mould,

$A_{SL}$  is the area of interface between the nucleus and the melt.

The equation (5.15) contains three terms relevant to the surface energy now. The first two terms are positive and they characterise the contribution of interfaces developed during nucleation. However, the third term corresponds with elimination of the interface between the

mould and the melt under the nucleus and that is why it is negative, i.e. reducing the total nucleation barrier.

Substitution of values for volume  $V_S$  and areas  $A$  helps altering the equation into the following form:

$$\Delta G_{het} = \left\{ -\frac{4}{3}\pi r^3 \Delta G_V + 4\pi r^2 \gamma_{SL} \right\} S(\theta) \quad (5.16)$$

where:

$$S(\theta) = (2 + \cos\theta)(1 - \cos\theta)^2 / 4 \quad (5.17)$$

The equation (5.16) is, except for the term  $S(\theta)$ , identical to the equation (5.5) describing the homogeneous nucleation in melt. The numerical value of expression (5.17) is always lower than or equal to 1 depending on the size of the wetting angle  $\theta$ . The expression  $S(\theta)$  is therefore marked as the *shape factor*.

The Fig. 5.8 shows the course  $\Delta G_{het}$  as well as  $\Delta G_{hom}$  for comparison purposes, depending on the radius of nucleus. Note that the actual critical radius of nucleus is independent of the nucleation type.

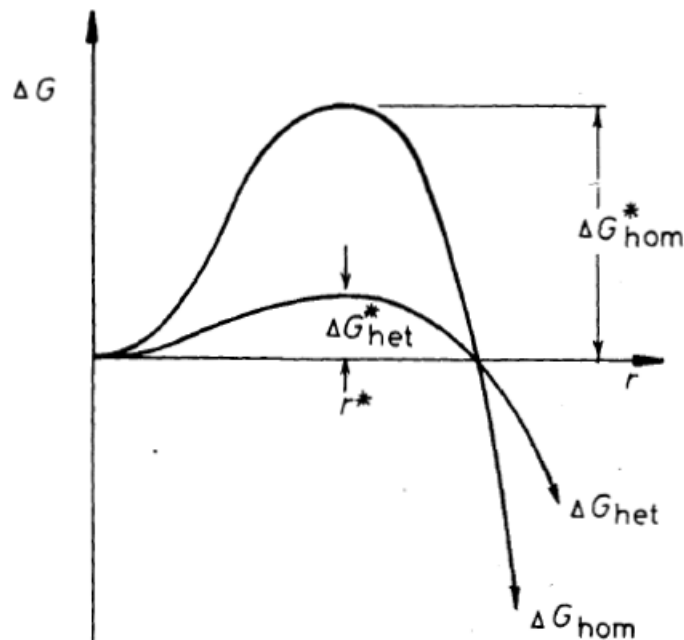


Fig. 5.8 Changes of the Gibbs free energy during homogeneous or heterogeneous nucleation

Formulas for calculation of critical values applicable to a heterogeneous nucleation can be obtained by derivation of the equation (5.16):

$$r^* = \frac{2\gamma SL}{\Delta G_V} \quad (5.18)$$

$$\Delta G^* = \frac{16\pi\gamma^3 SL}{3\Delta G_V^2} S(\theta) \quad (5.19)$$

The comparison of homogeneous and heterogeneous nucleation has produced the following conclusions:

$$r_{het}^* = r_{hom}^* \quad (5.20)$$

$$\Delta G_{het} = S(\theta)\Delta G_{hom}^* \quad (5.21)$$

The critical radius of nucleus  $r^*$  is not dependent on the nucleation type, Fig. 5.8. Small angles of contact are associated with a much lower energetic barrier to formation of heterogeneous nucleus compared to the homogeneous nucleation. Heterogeneous nucleation is feasible at lower undercooling temperature levels below the solidification point compared to the homogeneous nucleation.

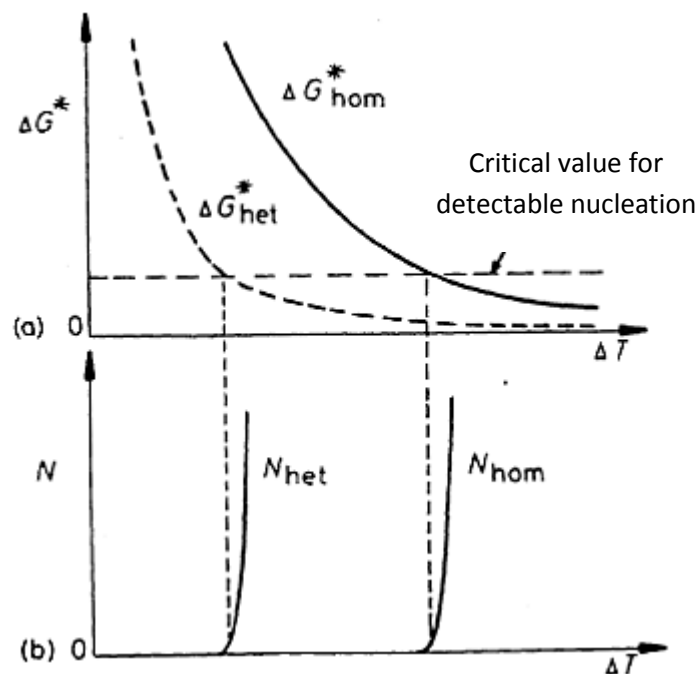


Fig. 5.9 a) The dependency of  $\Delta G^*$  on undercooling  $\Delta T$  for homogeneous and heterogeneous nucleation, b) corresponding rates of nucleation assuming the same critical value  $\Delta G^*$

The impact of undercooling to  $\Delta G_{het}^*$  and  $\Delta G_{hom}^*$  has been depicted in the Fig. 5.9. If there are  $n_1$  atoms in contact with mould walls, the number of nuclei is given by the formula:

$$n^* = n_1 \exp\left(-\frac{\Delta G_{het}^*}{kT}\right) \quad (5.22)$$

The heterogeneous nucleation should be possible, if the value  $\Delta G_{het}^*$  is low enough. That will depend mainly on the value of  $n_1$  in the above stated equation. The Fig. 5.9 shows that heterogeneous nucleation will be feasible at much lower undercooling levels than those required for the homogeneous nucleation. To be more precise, *the volume rate of heterogeneous nucleation* should be described by the following formula:

$$N_{het} = f_1 c_1 \exp\left(-\frac{\Delta G_{het}^*}{kT}\right) \quad (5.23)$$

where  $f_1$  is the frequency factor similar to  $f_0$  in the equation (5.13),  $c_1$  is the number of atoms touching the potential areas of heterogeneous nucleation per volume unit of melt.

### 5.2 Solid Phase Growth in Single-Component System

There are basically two types of the solid-phase - melt interface:

- a) *Uneven (diffusion interface)* - typical for metal systems, Fig. 5.10,
- b) *Smooth (planar) interface* - found mainly in non-metals.

The differences in atomic structure enable these two types of interface migrate by absolutely diverse ways. The diffusion interface migrates by means of continuous growth process, whereas the flat interface migrates by means of the lateral growth process using ledges.

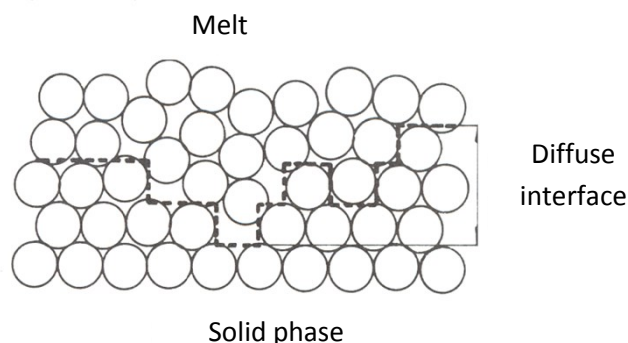


Fig. 5.10 Diffuse interface between a solid phase and melt

### 5.2.1 Continuous Growth

This is typical for metal systems with a diffusion (uneven) interface. The activation barrier  $\Delta G^a$  should be approximately similar as that for diffusion in liquid. The driving force for solidification  $\Delta G$  will be therefore defined by the equation:

$$\Delta G = \frac{L}{T_m} \Delta T_i \quad (5.24)$$

Where  $L$  is latent heat for solidification and  $\Delta T_i$  is undercooling of the interface below the equilibrium solidification point  $T_m$ . The rate of solidification should be expressed by the following formula:

$$v = k_i \Delta T_i \quad (5.25)$$

where parameter  $k_i$  characterizes the interface mobility.

The theoretical analysis shows the value of  $k_i$  is so high that normal rate of solidification can be achieved with undercooling  $\Delta T_i$  by a fraction of Kelvin only. The values of  $\Delta T_i$  can be therefore ignored in most cases and there is an assumption that the interface of solid/liquid (S/L) occurs at the equilibrium melting point. In other words, the process of metals solidification is usually controlled by diffusion. The process of growth of pure metals occurs by conducting of heat (diffusion), whereas solidification of alloys is controlled by diffusion of the dissolved components.

This mechanism can be applied to diffuse interfaces with the assumption that atoms may be captured at any point located on the solid surface. Such method is defined as the continuous growth. This method of growth is adequate, as the interface is disordered and atoms captured at random points will not cause any substantial interference with the equilibrium configuration of the interface.

### 5.2.2 Lateral Growth

It is worth reminding that materials with high melting entropy create primarily smooth atomic interfaces with close-packed configurations. As far as this type of interface is concerned, the Gibbs free energy also corresponds with the minimum intrinsic energy, i.e. the minimum number of disrupted "solid" bonds.

If there is any atom of liquid that joins the flat surface (Fig. 5.11a), it is evident that the number of disrupted bonds associated with the interface, i.e. the interfacial energy, will increase. Therefore, the probability of an atom bonding onto the solid phase is low and the

atom will likely jump back inside the melt. If the interface comprises atomic ledges, the atoms from melt will be allowed to settle at these ledges with much lower resultant increase of the interfacial energy, Fig. 5.11b.

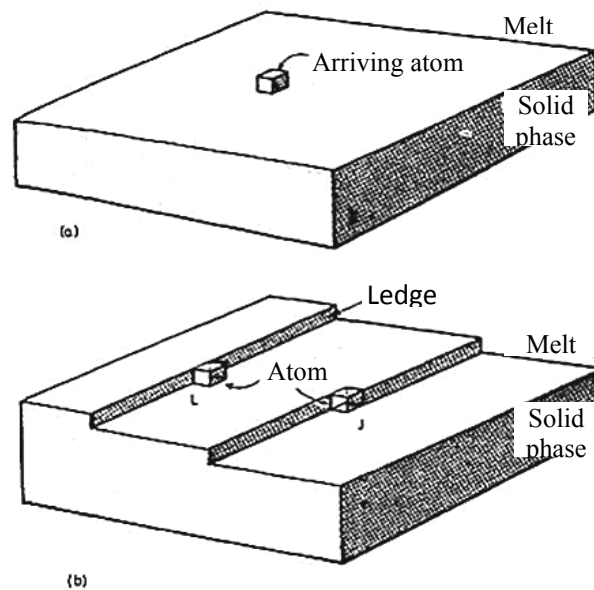


*Fig. 5.11 Smooth atomic interface of solid phase/liquid containing cube-shaped atoms, a) adding single atom to the interface surface will increase the number of "disrupted bonds" by four, (b) adding an atom to the ledge (L) will merely increase the number of disrupted bonds by two, whereas adding an atom to the jog (J) will not initiate any increase in the number of disrupted bonds at all.*

If the level contains a jog in a ledge (J), the atoms of liquid can bond onto the solid phase without any increase in number of the disrupted bonds and the inter-phase energy remains unchanged. That gives rise to the possibility that the remaining atoms join the solid phase at these points more likely than for an atom captured on a smooth surface. The smooth S/L interface can be expected to move by means of lateral growth of ledges. As the edges and jogs represent non-equilibrium states of the interface, their growth will depend on the potential methods of their development.

### **Surface Nucleation**

As stated above, lonely atoms "captured" on a flat surface will be unstable and they will tend to return back into the melt. However, if there is a sufficient quantity of atoms forming a disc-shaped layer, as shown in the Fig. 5.12, such body can be stabilised and grow further. The problem associated with the disc formation lies in two-dimensional analogy in development of atomic cluster by means of homogeneous nucleation. The disc edge contributes with

positive energy in this case; the energy must be counterbalanced by the volume free energy released during the process of disc development. The critical radius  $r^*$  associated with the two-dimensional nucleus will decrease with the increasing undercooling of the interface.

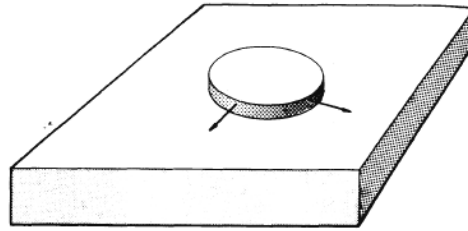


Fig. 5.12 Ledge by Surface Nucleation

### **Spiral Growth**

In case the solid phase contains dislocations intersecting the S/L interface, spiral growth of the solid phase may occur. Let us assume a simple screw dislocation protruding out of a perfect crystal. The resultant form will be a ledge on the crystal surface, as shown in the Fig. 5.13a. Anchoring of further atoms from the melt on this ledge will cause its rotation around the cross point between dislocation and the surface of solid, Fig. 5.13b.

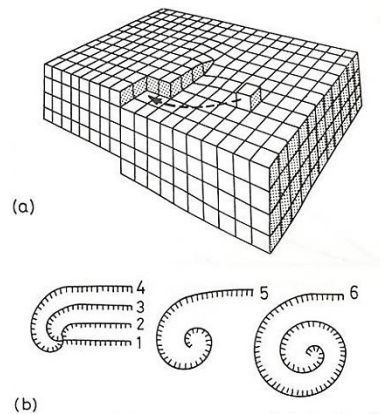


Fig. 5.13 Spiral growth, (a) ledge linked to the screw dislocation ending at the interface of solid/liquid phase. Settling of atoms on the ledge causes its rotation at angular velocity decreasing further from the dislocation core and the spiral growth occurs (b).

The Fig. 5.14 shows the impact of undercooling on the growth rate of various interface types.

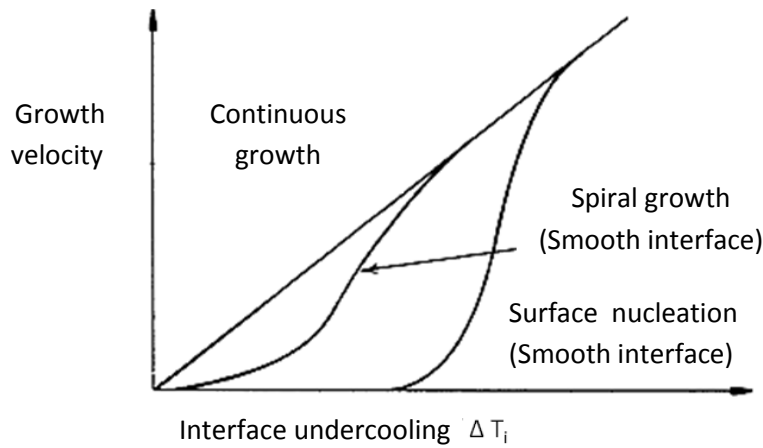


Fig. 5.14 Impact of the interface undercooling level ( $\Delta T_i$ ) on the growth rate of uneven and smooth interface on atomic scale

### 5.2.3 Heat Flow and Interface Stability

Solidification in pure metals is controlled by the rate at which the latent heat of solidification can be conducted away from the S/L interface. Heat can be conducted either via solid or liquid phase, depending on the temperature gradient within the interface area. Assume an example comprising a solid phase growing at the rate  $v$  with a planar interface into a melt (Fig. 5.15a). The heat flow via interface through the solid must be in equilibrium with the heat flow from melt increased by the latent heat of solidification developed in the S/L interface:

$$K_S T'_S = K_L T'_L + v L_V \quad (5.26)$$

where:  $K_{S,L}$  is the thermal conductivity of solid phase (S) and melt (L),

$T'_{S,L}$  is the temperature gradient ( $dT/dx$ ) in solid phase and melt,

$v$  is the growth rate of solid phase,

$L_V$  is the latent heat for solidification per unit of volume.

This equation applies generally to a planar interface, even holds in case when heat is conducted into liquid ( $T'_L < 0$ ) (Fig. 5.16a).

For two potential solidification methods refer to the Figs. 5.15 and 5.16. If the solid phase grows into an overheated liquid, the planar inter-phase interface is stable. Let us assume that the local increase of the rate of solidification creates a protrusion on the interface (Fig. 5.15c). If the projection curvature radius is so large that the Gibbs –Thomson effect can be ignored, then the S/L interface remains isothermal at the temperature of approx.  $T_m$ . That is why the temperature gradient in melt before the protrusion will be increased, while that in the solid will decrease. That will result in more heat conducted into the protrusion of the solid phase

and less away, so the rate of growth of protrusion will drop below the growth rate of planar areas and the protrusion will diminish progressively.

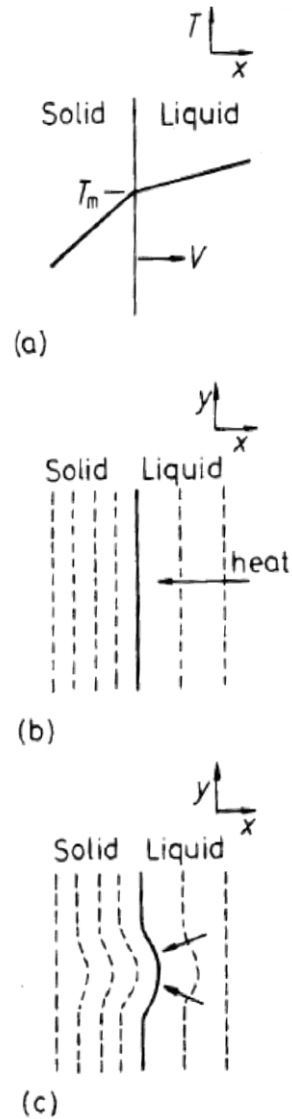


Fig. 5.15 Dissolution of Protrusion

a) Heat is extracted through solid;

b) Isotherms for planar S/L interface, c) Isotherms for a protrusion.

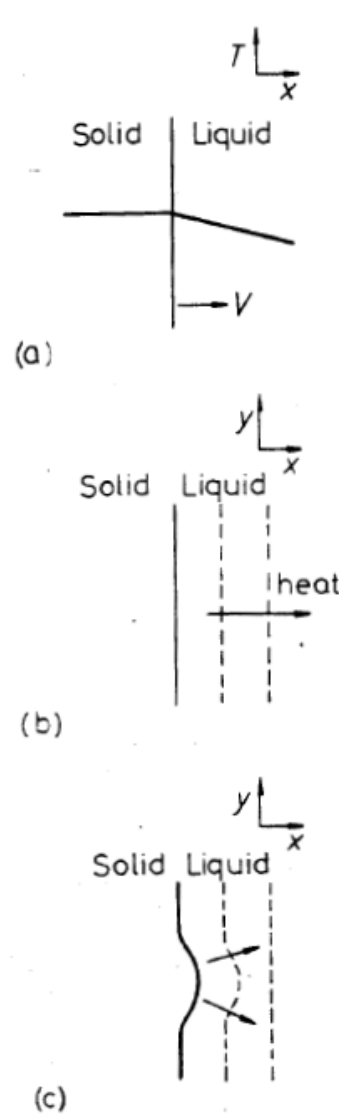


Fig. 5.16 Protrusion Growth

a) Heat is extracted through melt,

b) Isotherms for planar S/L interface, c) Isotherms for a protrusion.

However, the situation will be different in case of solid phase growth into an overcooled melt, Fig. 5.16. If the solidified interface forms a protrusion, it will result in even deeper temperature gradient inside melt in this case. That is why the heat is removed more efficiently from the protrusion tip rather than from surrounding regions, which promotes preferential growth of the protrusion. The S/L interface advancing into the overcooled melt is therefore unstable.

Conduction of heat through the solid phase (Fig. 5.15) occurs, when crystallisation occurs on walls of the mould that are colder than the melt. However, the heat flow into melt (Fig. 5.16) may occur only when the melt has been supercooled below  $T_m$ . Such a situation may take place at the beginning of solidification, if nucleation occurs on impurity particles within the melt. As there must be a certain undercooling before each nucleation, the first solid particles will grow into the overcooled melt and the latent heat of solidification will dissipate into the melt. That is why the originally spherical solid particles will develop branches in several directions, Fig. 5.17. As the primary branches elongate throughout the growth process, their surface becomes unstable and they split to form secondary or even tertiary branches. This solidified body is referred to as *dendrite* ("tree" in Greek language). Dendrites in pure metals are usually called *thermal dendrites* for better differentiation from dendrites in alloys. Experiments have proven that the growth of dendrite branches follows certain directions only, e.g. along  $\langle 100 \rangle$  directions in cubic metals.

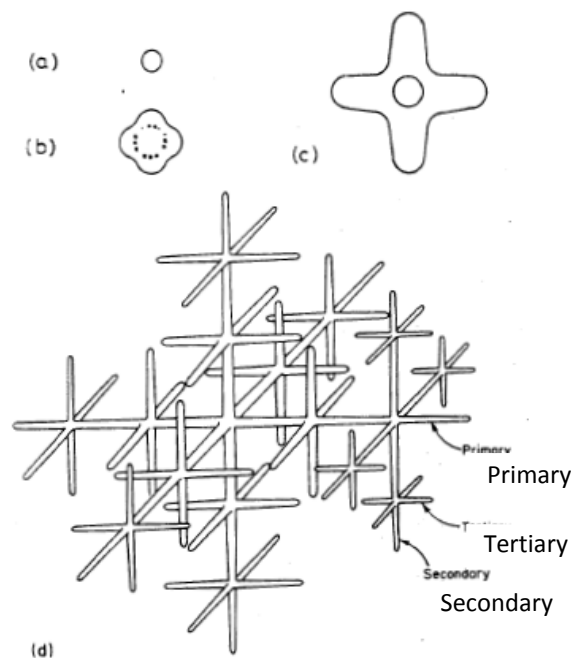


Fig. 5.17 Growth of thermal dendrites: a) Spherical nucleus, b) Unstable interface, c) Growth along primary dendrite axes, d) Development of secondary and tertiary axes (branches) of dendrites

### 5.3 Solidification of Binary Alloys

Solidification of pure metals occurs is a very rare event in practice. Even the commercially pure metals contain sufficient amount of impurities that turn the solidification characteristics

of pure metals into behaviour of alloys. The following chapters will deal with solidification of single-phase binary alloys.

### 5.3.1 Solidification of Single-Phase Alloys

The alloys concerned are of the same type as the one with composition  $X_0$  shown in the Fig. 5.18. This phase diagram has been somewhat simplified, as the *solidus* and *liquidus* curves are depicted as lines in this case. *The partition coefficient* is defined as follows:

$$k = \frac{X_S}{X_L} \quad (5.29)$$

with  $X_S$  and  $X_L$  representing the molar fractions of solute in solid or liquid in equilibrium at the given temperature. The partition coefficient in case shown in the Fig. 5.18 is independent on temperature.

Under practical circumstances, the mechanism of solidification of alloys shows complex dependency on the temperature gradient, the rate of cooling and the growth rate.

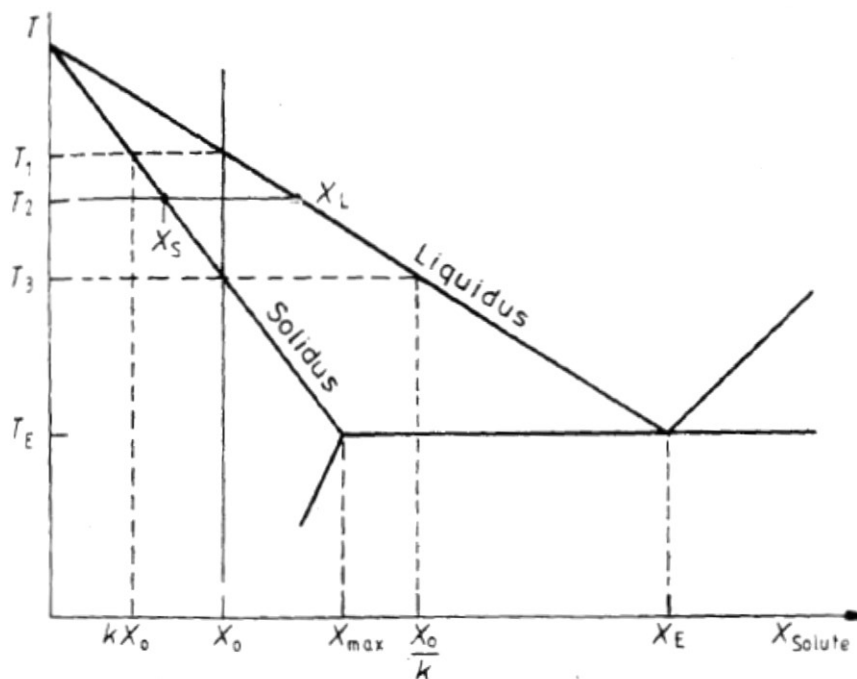


Fig. 5.18 Simplified binary phase diagram,  $k = X_S / X_L$  is constant

Assume a simple example with the movement of planar S/L interface along a cylindrical bar, as shown in the Fig. 5.19a. Such unidirectional solidification can be applied in practice on special equipment allowing a one-way heat flow only, along the longitudinal crystallizer axis.

This chapter will focus on three cases of solidification:

- a) Infinitely slow (equilibrium) solidification,
- b) Without diffusion in the solid phase with perfect mixing in melt,
- c) Without diffusion in the solid phase and only diffusional mixing in melt.

### 5.3.1.1 Equilibrium Solidification

An alloy with composition  $X_0$  shown in Fig. 5.18 starts solidifying at the temperature  $T_1$  by forming a small amount of solid phase with composition  $kX_0$ . Decrease in temperature will result in increasing quantity of solid phase and, provided the cooling is slow enough and there is intense diffusion in the solid phase, the solid and liquid phases will be always homogeneous with their composition compliant with curves of both solid and liquid (Fig. 5.19b). Relative amounts of solid and liquid phase at any temperature can be simply determined using the lever rule. Please note that when maintaining the one-dimensional solidification as assumed, preserving of the initial content of solute in the alloy requires that the two hatched areas in Fig. 5.19b are of the same size (differences in molar volumes between both phases will be ignored). Once the temperature  $T_3$  has been reached, the composition of last remainder of the alloy will be  $X_0/k$  and the composition of solidified bar will be  $X_0$  throughout its entire length.

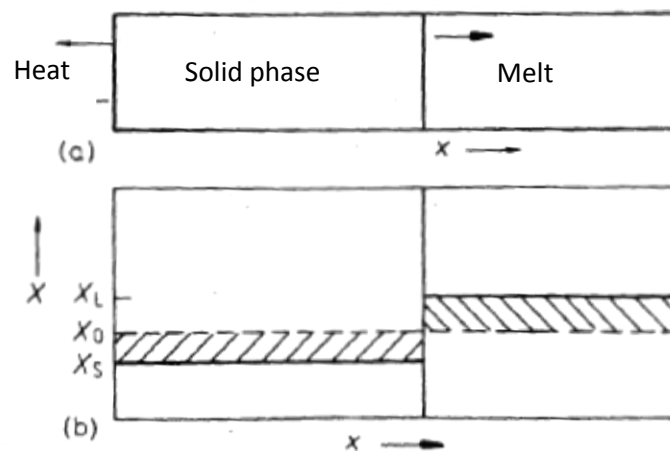


Fig. 5.19 Rectified solidification of an alloy with composition  $X_0$  in Fig. 5.18, a) planar interface of solid/liquid and one-way heat flow, b) corresponding profiles of composition at the temperature  $T_2$  in case of full equilibrium.

### 5.3.1.2 No Diffusion in Solid Phase, Perfect Mixing in Melt

Cooling will be often very fast under practical circumstances to allow diffusion in the solid phase. Assume that the solid phase will not allow any diffusion processes, yet the chemical homogeneity of melt will be maintained by efficient stirring during the solidification stage. There is also the rule that unidirectional solidification will develop the first solid, when the cooled end of bar reaches the temperature  $T_1$ , at which the composition of solid phase will be

equal to  $kX_0$ , Fig. 5.20a. As  $kX_0 < X_0$ , this first portion of solid will be purer than the melt from which it forms. Dissolved solute is forced into the melt, where its concentration rises above  $X_0$ , Fig. 5.20b. To resume the solidification process, the interface temperature must drop below  $T_1$ . Another layer of the solid phase will then contain slightly more of the dissolved component compared to the first layer. As the solidification process progresses, the melt will be successively enriched with the solute as the temperature of solidification is gradually decreasing, Fig. 5.20c.

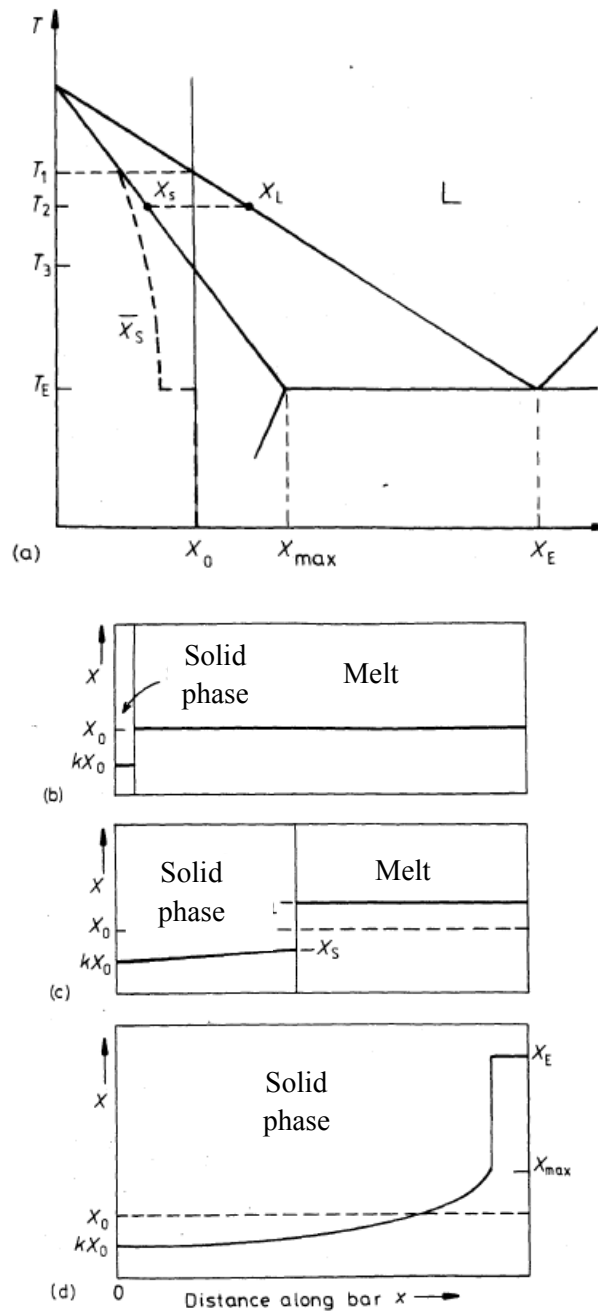


Fig. 5.20 The planar solidification front for alloy with composition  $X_0$  shown in Fig. 5.18 with no diffusion in solid phase and with perfect mixing in melt, a) as in Fig. 5.18 but including the

average composition (dashed line) of the solid phase, b) composition profile close to the temperature  $T_1$ , c) composition profile at temperature  $T_2$  (compare it with the profile and fraction solidified in Fig. 5.19b), d) composition profile at eutectic temperature.

At any moment the solidification process can be characterized by **local equilibrium** at the S/L interface, i.e. the composition of solid and liquid phase in mutual contact will correspond with the equilibrium phase diagram at the particular temperature. However, as there is no diffusion in solid phase, individual layers of the solid phase along the bar length keep their original compositions. The average chemical composition of solid phase ( $\bar{X}_S$ ) is always lower than the composition of S/L interface, as shown by the dashed line in Fig. 5.20a. The relative amount of solid and liquid phases for the particular temperature of interface is therefore determined by the lever rule using  $\bar{X}_S$  and  $X_L$ . That implies the melt may be much richer in dissolved component than the  $X_0/k$  and it may even achieve the eutectic composition  $X_E$ . The solidification process will therefore complete close to the temperature level  $T_E$  by forming the eutectic  $\alpha + \beta$ . To determine the ratio and composition of solid phase, this non-equilibrium model of solidification uses the *non-equilibrium lever rule*, the so called *Scheil equation*.

### 5.3.1.3 No Diffusion in Solid Phase, No Mixing in Melt

If the liquid phase does not involve any mixing or convection, the solute component rejected during the development of solid phase will be transported into the melt by diffusion only. This is the reason why there will be a prompt increase of solute ahead of the solid and the corresponding rapid enrichment of the solid formed, Fig. 5.21a. This stage of solidification is defined as the *initial transition*. In case the solidification process occurs at a constant rate  $v$ , it can be proven that once the interface temperature has reached the value  $T_3$  in Fig. 5.18, solidification will run in the *steady state*. The composition of melt adjacent to the solid phase at this stage will equal to  $X_0/k$  and the composition of solid phase will correspond with the average composition of alloy  $X_0$ .

The composition profile of melt in the steady state must be in such configuration that the rate of diffusion of dissolved component along the concentration gradient away from the interface is balanced by the rate of rejection of solute from the solidifying melt:

$$-DC'_L = v (C_L - C_S) \quad (5.31)$$

where:  $D$  is the coefficient of diffusion in melt,  $C'_L$  corresponds with the concentration gradient  $dC_L/dx$  at the interface,  $C_L$  and  $C_S$  refer to concentration of dissolved component in solid and liquid phases in case of equilibrium at the interface. The characteristic width of

concentration profile is  $D/v$ , Fig. 5.21b. When in the *final stage*, concentration of the dissolved component in melt grows rapidly and the solidification process ends by formation of a low fraction of eutectic.

Under practical circumstances, solidifying alloys will exhibit partial signs of all three models discussed above. There will be generally some mixing either due to turbulence in melt caused by casting, by the effect of convection currents or gravity. Concentration profiles established under practical circumstances may show characteristics shown between profiles in Fig. 5.20d and Fig. 5.21c. There are also numerous cases, where diffusion in the solid phase must be considered, e.g. interstitial atoms or BCC metals. In this case the solute may diffuse from the solidifying interface back into the solid as well as into the melt, which results in improved homogeneity after solidification.

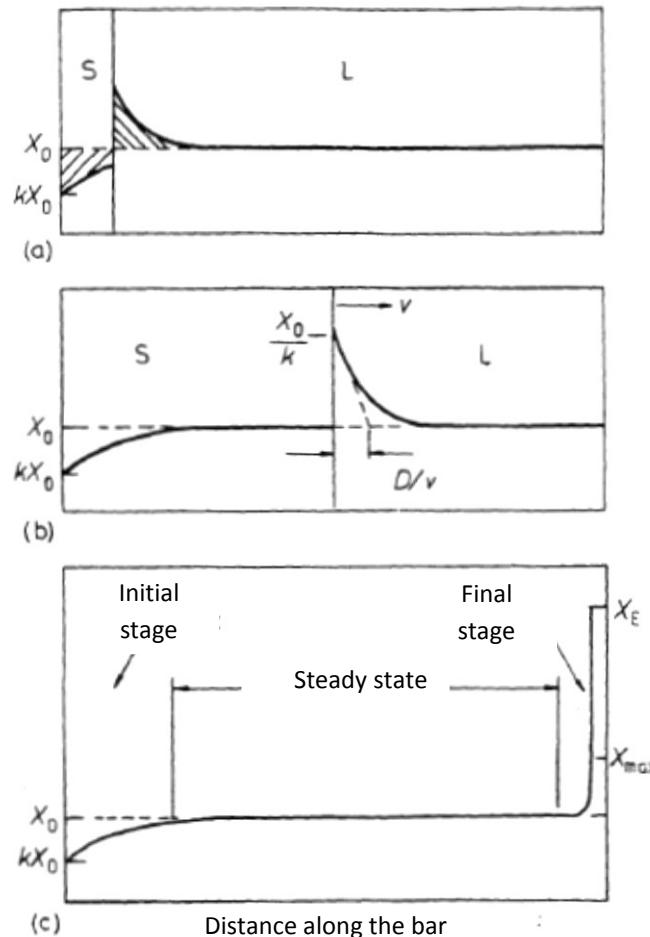


Fig. 5.21 Planar solidification front of alloy with composition  $X_0$  in Fig. 5.18 considering no diffusion in solid phase and no mixing in melt, a) composition profile in case the temperature of S/L interface lies between  $T_2$  and  $T_3$  in Fig. 5.18, b) steady solidification at the temperature

$T_3$ , the solid phase composition is equal to the composition of melt away from the S/L interface ( $X_0$ ),  $c$ ) the composition profile at the temperature  $T_E$  (final transition).

Unidirectional solidification finds its commercial use in production of heat resistant alloys, for example, those are utilised in manufacturing of blades for gas turbines. It is also used in manufacturing of very pure metals (zone refining).

### 5.3.2 Cellular and Dendritic Solidification

The examples examined so far have dealt with solidification processes, when the growth front is planar. Nevertheless, the diffusion of solutes into the melt during alloy solidification is analogical to convection of latent heat into the melt during solidification of pure metal. The first impression then is that the planar front should break up to form dendrites. This problem is complicated further by potential occurrence of gradients in the melt.

Assume a steady-state solidification with planar interface, as shown in the Fig. 5.22a. The consequences of changing concentration of solute in melt ahead the solidification front are represented by corresponding changes to the equilibrium solidification temperature, i.e. the temperature of liquid shown in the Fig. 5.22b as the line  $T_e$ . Besides the interface temperature determined by the local equilibrium, the actual melt temperature may correspond to any line, e.g. the line  $T_L$ . The values applicable to the interface are  $T_L = T_e = T_3$ , Fig. 5.18. In case the temperature gradient is lower than the critical value shown in Fig. 5.22b, the melt before the solidification front will exist even below its equilibrium solidification temperature, i.e. it is supercooled. As undercooling develops due to composition (constitution), it is defined as the **constitutional undercooling**.

The precondition necessary for development of stable protrusions on the planar interface is their existence in the area of constitutional undercooling in melt. Provided the value of  $T_L$  in Fig. 5.22b changes, the temperature on tip of each protrusion will exceed that of the surrounding interface. However, if any protrusion tip remains below the local liquid temperature ( $T_e$ ) of concentrated melt, there is still a chance for further solidification and the protrusion can grow. On the other hand, if the temperature gradient before interface is steeper than the critical gradient shown in Fig. 5.22b, the protrusion will be exceeding the local liquid temperature and it will therefore melt back.

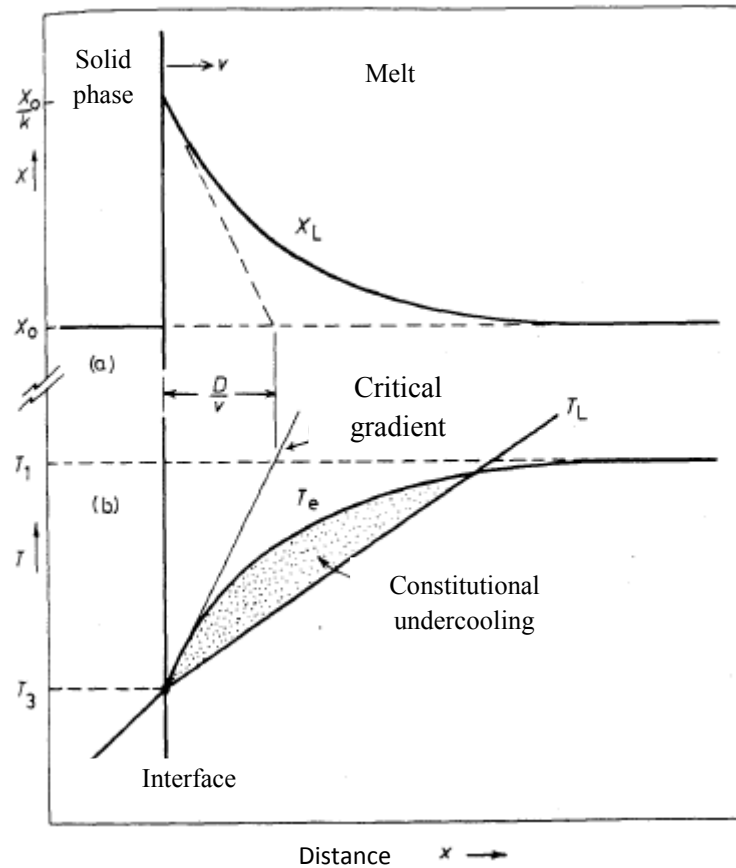


Fig. 5.22 Constitutional supercooling ahead the planar solidification front, a) The composition profile before the S/L interface in steady state of solidification. The dashed line shows  $dX_1/dx$  in the S/L interface, b) The temperature of melt ahead the solidification front corresponds with the line  $T_L$ . The equilibrium temperature of liquid for the melt near the S/L interface is characterized by the curve  $T_e$ . The constitutional undercooling develops, when the line  $T_L$  lies below the critical gradient.

Provided the growth state is steady, the critical gradient shown in Fig. 5.22b will be determined by the formula  $(T_1 - T_3)/(D/v)$ , where  $T_1$  and  $T_3$  refer to the temperature of liquid and solid for alloy with composition  $X_0$  (Fig. 5.18). The precondition for stable planar interface is defined as:

$$T_L' > \frac{(T_1 - T_3)}{(D/v)} \quad (5.32)$$

where  $T_L'$  refers to the temperature gradient ( $dT_L/dx$ ) at the S/L interface and  $D/v$  is the characteristic width of concentration profile. Rearrangement of the experimentally adjustable parameters  $T_L'$  and  $v$  determines the precondition for absence of constitutional undercooling as follows:

$$T_L'/v > (T_1 - T_3)/D \quad (5.33)$$

where  $(T_1 - T_3)$  characterises the *solidification equilibrium interval* of the alloy.

It is evident that the planar solidification front is very hard to reach in alloys with great solidification interval and at high solidification rates. Except for well controllable experimental conditions, alloys would seldom solidify with the planar S/L interface. Temperature gradients and growth rates cannot be controlled independently under normal conditions; those are determined by the rate of heat conduction out of the solidifying alloy.

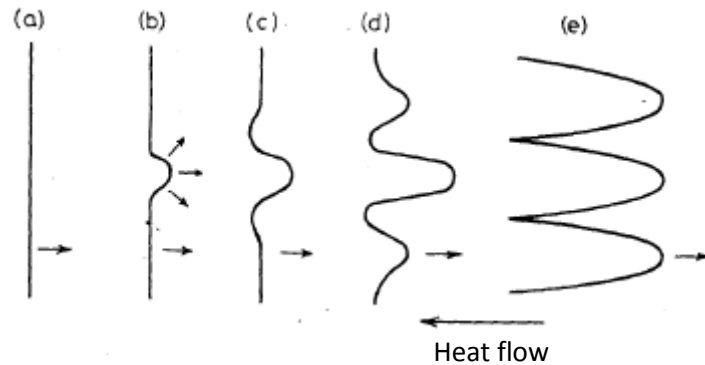


Fig. 5.23 Breakdown of initially planar solidification front to cells

In case the temperature gradient before an initially planar interface passes through a gradual decrease below the critical value, the first stage of breakdown of such interface is the development of cellular structure, Fig. 5.23. The development of the first protrusion forces the solute in the transverse direction to accumulate at the root of protrusion, Fig. 5.23b. That reduces the equilibrium solidification temperature and causes occurrence of recesses at the interface (Fig. 5.23c) that induce development of further protrusions (Fig. 5.23d). Protrusions finally develop into long branches or cells that grow in parallel with the heat flow direction, Fig. 5.23e. The dissolved component forced out of the solidifying melt concentrates between walls of cells forming eutectic at the lowest temperature. However, tips of those cells grow into the hottest melt and that is why these contain the least solute. Actually, when  $X_0 \ll X_{\max}$  (see Fig. 5.18) the melt between cells may achieve the eutectic composition and therefore the intercellular spaces will contain eutectic. Mutual relations between the temperature gradient, the shape of cell and segregation of the dissolved component are shown in Fig. 5.24.

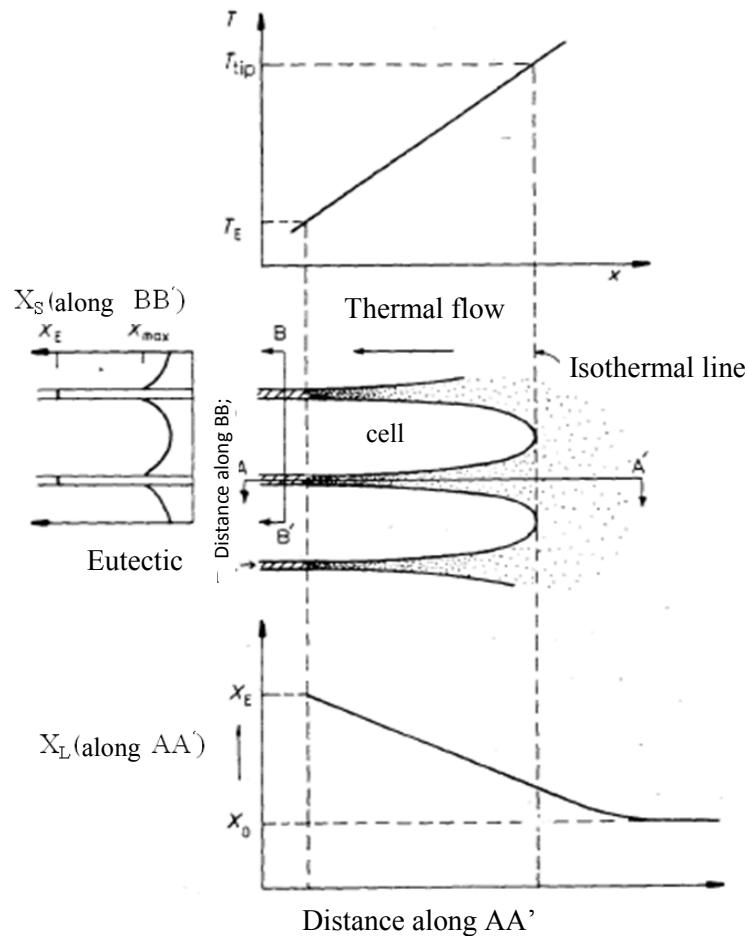


Fig. 5.24 Distribution of temperature and solute during cellular solidification. Please note that the dissolved component concentrates in the melt between cells, the composition across cells shows the concentration profile ("coring"), eutectic forms in between cells.

As far as the cellular structure is concerned, individual cells are oriented in the same direction and they all form a single as-cast grain. Cellular microstructures are stable within a particular interval of the temperature gradient only. When the temperature gradient is low enough, walls of cells or primary branches of the solid phase show a development of secondary branches and even lower temperature gradient will induce creation of the tertiary branches, i.e. formation of dendrites. The morphological change will be also followed by a change in direction of the main branches out of the heat flow direction to the preferential crystallographic orientation, e.g.  $\langle 100 \rangle$  in cubic metals. The reasons for conversion of cells into dendrites are still not very clear. This is probably relevant to occurrence of constitutional undercooling in the melt between cells, which causes transverse instability of the interface. For morphology of dendrites created during solidification of a transparent organic compound refer to the Fig. 5.25.

The general rule implies that the tendency towards development of dendrites rises with the increase of equilibrium solidification interval. That is the reason why effectiveness of different solutes can vary widely. As far as systems with a very low partition coefficient ( $k$ ) are concerned, the cellular or dendritic growth may be associated with a very little additive of a solute.

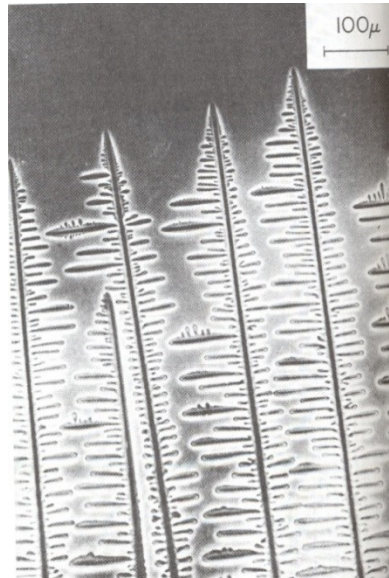


Fig. 5.25 Columnar dendrites in a transparent organic compound. Please note the low thickness of secondary branches at the point of contact with primary dendritic branches.

Finally, it is worth mentioning that even though the discussion on solidification of alloys is focused on systems, where  $k < 1$ , similar arguments can be exercised also in those cases, when  $k > 1$ .

### 5.3.3 Eutectic Solidification

Solidification of a binary eutectic alloy produces two cooperative solid phases, i.e.  $L \rightarrow \alpha + \beta$ . Different alloys exhibit different types of eutectic solidification, those are usually defined as *normal* or *anomalous*. Normal structures will feature both phases either as alternating lamellae or as small bars of minor phase embedded in the other phase. The growth of both phases during solidification is simultaneous, while the S/L interface is basically planar. Normal structures develop, when both phases have low entropy of formation. On the other hand, anomalous structures occur in systems, where one of the solid phases possesses the high entropy of melting. There are many versions of such degenerated structures, where the most commercially important ones can be found in Al - Si alloys. This didactic text will deal with normal structures featuring lamellar morphology only.

Figure 5.26 shows how two phases can grow in cooperative manner at a basically planar solidification front. Development of phase  $\alpha$  rich in component A is followed by diffusion of excessive atoms of component B along the S/L interface over a short distance, where they will be integrated into phase  $\beta$  (rich in component B).

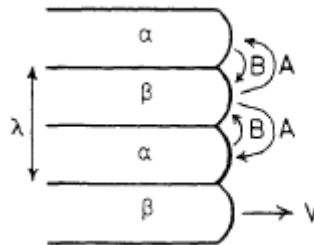


Fig. 5.26 Interdiffusion in melt ahead of eutectic front

Similarly, atoms of the component A forced out of the phase  $\beta$  diffuse towards the ends of adjacent  $\alpha$  lamellae. The rate of eutectic growth will depend on the rate of diffusion processes, which will depend on the interlamellar spacing  $\lambda$ . Short interlamellar spacing should result in faster growth.

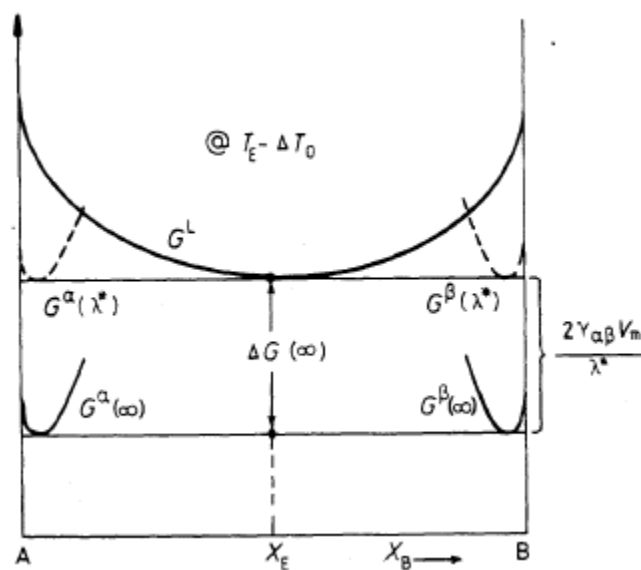


Fig. 5.27 Illustration of the Gibbs free energy at the undercooling  $\Delta T_0$  below the eutectic temperature for two limit cases of interlamellar spacing:  $\lambda = \lambda^*$  and  $\lambda = \infty$

Nevertheless, there is also the bottom threshold for interlamellar spacing  $\lambda$ , which is determined by the total interfacial energy required to form the  $\alpha/\beta$  interface. The interlamellar spacing  $\lambda$  determines the total area of  $\alpha/\beta$  interface: in the unit volume of eutectic it is equal to  $2/\lambda$  ( $\text{m}^{-2}$ ). The change of Gibbs free energy relevant to solidification of 1 mole of the melt is expressed by the formula:

$$\Delta G(\lambda) = -\Delta G(\infty) + \frac{2\gamma_{\alpha\beta}V_m}{\lambda} \quad (5.34)$$

where  $V_m$  is the molar volume of the eutectic and  $\Delta G(\infty)$  is the drop of free energy for very large values  $\lambda$ . Solidification will not take place, if  $\Delta G(\lambda)$  is positive and therefore  $\Delta G(\infty)$  must ensure full compensation of the interfacial energy, i.e. the eutectic/melt interface must be undercooled below the equilibrium eutectic temperature  $T_E$ , Fig. 5.27. If the total undercooling is  $\Delta T_o$ , then  $\Delta G(\infty)$  is approximated by the formula:

$$\Delta G(\infty) = \frac{\Delta H \Delta T_o}{T_E} \quad (5.35)$$

where  $\Delta H$  is the enthalpy. The minimum possible interlamellar spacing  $\lambda^*$  corresponds with the condition  $\Delta G(\lambda^*) = 0$ , Fig. 5.27:

$$\lambda^* = \frac{2\gamma_{\alpha\beta}V_m T_E}{\Delta H \Delta T_o} \quad (5.36)$$

Presence of such interlamellar spacing in eutectic will result in situation, where the Gibbs free energy liquid and eutectic are the same, i.e. all three phases are in equilibrium. That is due to the fact that the  $\alpha/\beta$  interface raises the levels of Gibbs free energy  $\alpha$  and  $\beta$  phases from values  $G^\alpha(\infty)$  and  $G^\beta(\infty)$  to the values of  $G^\alpha(\lambda^*)$  and  $G^\beta(\lambda^*)$ , see Fig. 5.27. The cause of this increase lies in curvature of the interfaces  $\alpha/L$  and  $\beta/L$  arising from the need for balancing of the interfacial tensions at the triple point  $\alpha/\beta/L$ , Fig. 5.26. The increase will be generally different for either phase but for simple cases it can be shown that  $\frac{2\gamma_{\alpha\beta}V_m}{\lambda^*}$  applies for both phases, Fig. 5.27.

#### 5.4 Crystallisation Example - Ingot

Production of heavy forgings makes use of cast semi-products called ingots. Those are products created by solidification of liquid metal in metal moulds. -Heavy forgings are made of ingots at the weight of several hundreds of tonnes. Ingots solidify very slowly and they can obviously develop various defects to impair their further processing ability. This chapter focuses on evolution of structure during solidification of ingots only.

Solidified ingots involve three basic zones, Fig. 5.28:

- External, fine-grained, undercooled layers of equiaxed crystals,
- Columnar crystal bands,
- Centre zone of equiaxed crystals.

Once the liquid metal comes into contact with walls of the mould, the melt will cool down below the temperature of liquid rapidly. The mechanism of heterogeneous nucleation will form a large number of fast growing nuclei. Different orientations of individual crystals cause their mutual crashing and the growth will stop fast, which results in formation of a fine-grained external zone of ingot, Fig. 5.29.

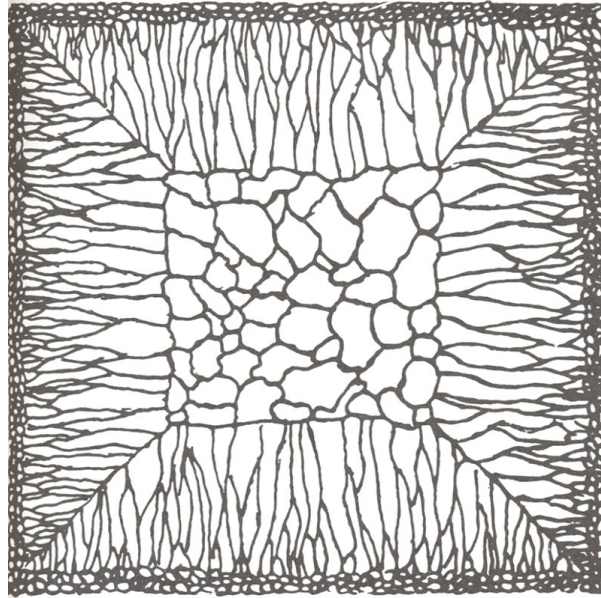


Fig. 5.28 Cross section of an ingot

Crystals with their primary axes approximately parallel with the direction of heat flow will be the fastest-growing ones and they will form columnar crystals, i.e. dendrites. Preferred growth of crystals along the crystallographic directions of type  $\langle 100 \rangle$  occurs in cubic metals. A large number of dendrites forms with parallel primary axes. Fig. 5.30 illustrates an optional multiplication mechanism for primary branches of dendrites during the solidification process.

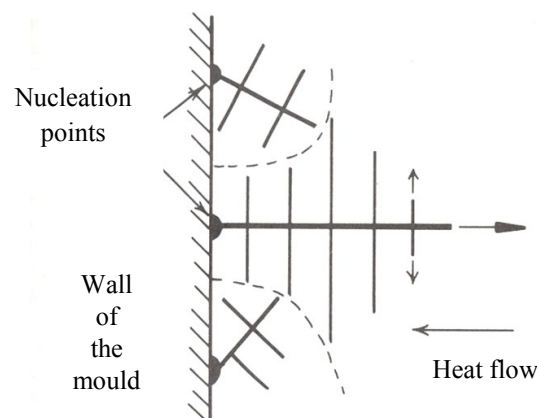
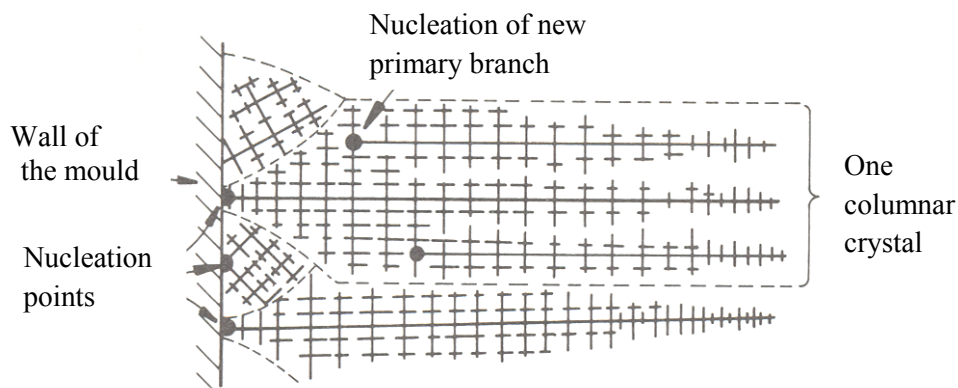


Fig. 5.29 Competitive growth of crystals right after pouring, dendrites with primary branches perpendicular to the mould walls grow faster than less conveniently oriented crystals the growth of which ceases rapidly.

The volume fraction of solidified melt increases with the rise of spacing behind dendrite tips. The area between dendrite tips and the last portions of the melt is called the "mushy" zone. The length of this zone depends on the temperature gradient and the equilibrium solidification interval of alloy. The spacing of primary and secondary dendrites often increases with the rise of distance from the mould wall. That relates to the drop in cooling rate during solidification of ingots.

The equiaxed zone at the central section of ingots comprises equiaxed grains with random orientation. Remelted ends of dendrite branches are considered an important source of these crystals. The temperature around the newly developed dendrites will increase, which may result in melting of certain portions of the dendrites, especially at contact points between the primary and secondary branches, see Fig. 5.25. Such released parts of dendrites may serve as nuclei of new crystals. Turbulent flows caused due to differences in temperature or concentration in the remaining melt volume represent an effective source of temperature differences within a solidifying ingot. Convection flows can transport dendrite fragments into the liquid area, where they can grow into equiaxed crystals.



*Fig. 5.30 Columnar crystals are formed by conveniently oriented dendrites. Each columnar crystal starts from separate points of heterogeneous nucleation but it may contain a range of primary dendrite branches.*

Most metals shrink during the solidification process. Alloys with narrow solidification intervals have narrow mushy zones and as the zone of solidified metal grows in thickness, the quantity of liquid metal decreases continuously with a deep shrinkage cavity at the centre of cross section of the solidified ingot. In alloys with wider solidification intervals, shrinkage cavity close to the ingot top is created.

The occurrence of chemical heterogeneity is a very important consequence of segregation processes during solidification of steel ingots; it is expressed by formation of macro-segregation bands as well as micro-segregation areas. Further details of these issues can be also found in [1].



### Summary of terms in this chapter

**Homogeneous nucleation:** nucleation of a solid phase occurs within a homogeneous melt. It is very rare under practical circumstances.

**Heterogeneous nucleation:** nucleation of a solid phase occurs on foreign surfaces, e.g. the mould walls. Heterogeneous nucleation may occur after a very slight undercooling only.

**Rate of nucleation:** the number of stable nuclei formed within a unit of volume over a unit of time.

**Dendrite:** preferential growth of crystals during crystallisation results in formation of columnar crystals. These may form in pure metals as well as in alloys.

**Constitutional undercooling:** the dendritic growth in binary alloys is subject to the condition, when the temperature gradient in melt lies below the equilibrium liquid temperature of the solute enriched melt ahead the liquid/solid interface.

**Critical nucleus:** the drop of free chemical energy relevant to the formation of critical nucleus is equal to the interfacial energy necessary for the development of nucleus/matrix interface. A jump of an atom from the melt to the surface of critical nucleus is associated with the drop of its total Gibbs free energy enabling its further growth.

**Local equilibrium:** chemical composition of solid phase and melt at an interface moving in the course of crystallisation process at a particular temperature corresponds with values of the solid and liquid in the equilibrium phase diagram.



### Questions addressing the content covered

1. What is the latent heat of solidification?
2. What is the difference between homogeneous and heterogeneous nucleation?
3. What is a thermal dendrite?
4. What is the constitutional undercooling?
5. What mechanisms of binary alloy solidification do you know?
6. What is the definition of the partition coefficient?

7. What limits the minimum interlamellar spacing in eutectic?
8. How does the chemical heterogeneity develop during solidification of alloys?
9. Explain the helical growth of crystals.
10. What is an ingot mould?



## Exercises

### Exercise 1

Use the formulas below to estimate the number of clusters of atoms within 1 mm<sup>3</sup> of copper at its melting point for spherical clusters contains: a) 10 atoms, b) 60 atoms. What amount of liquid copper is probably contained in a single cluster formed by 100 atoms? The atomic volume of copper is  $\Omega = 1.6 \times 10^{-29} \text{ m}^3$ ,  $\gamma_{SL} = 0.177 \text{ Jm}^{-2}$ ,  $k = 1.38 \times 10^{-23} \text{ JK}^{-1}$ ,  $T_m = 1,356 \text{ K}$ .

$$\Delta G_r = -\frac{4}{3}\pi r^3 \Delta G_V + 4\pi r^2 \gamma_{SL} \quad (\text{A})$$

$$n_r = n_o \exp\left(-\frac{\Delta G_r}{kT}\right)$$

*Solution:*

At the equilibrium melting point  $\Delta G_V = 0$ , the equation (A) is:

$$\Delta G_r(T = T_m) = 4\pi r^2 \gamma_{SL}$$

The cluster comprising  $n_c$  atoms with the atomic volume  $\Omega$  is defined by:

$$\frac{4\pi r^3}{3} = n_c \Omega$$

Alteration of term for  $\Delta G_r$ :

$$\Delta G_r = 4\pi \left(\frac{3n_c \Omega}{4\pi}\right)^{2/3} \gamma_{SL}$$

Substitution of values  $\Omega$  a  $\gamma_{SL}$ :

$$\Delta G_r = (5,435 \times 10^{-20}) n_c^{2/3}$$

$$\text{For } 1 \text{ mm}^3, n_o = 6.25 \times 10^{19} \text{ atoms}$$

for  $n_c = 10$  atoms,  $n_r = 9 \times 10^{13}$  of clusters per 1 mm<sup>3</sup>

for  $n_c = 60$  atoms,  $n_r = 3$  clusters per 1 mm<sup>3</sup>

for  $n_c = 100$  atoms,  $n_r = 4 \times 10^{-8}$  clusters per 1 mm<sup>3</sup> and this can be used to calculate the following:

1 cluster is in the volume of  $2.5 \times 10^7 \text{ mm}^3$ .

**Exercise 2**

Calculate the rate of homogeneous nucleation in liquid copper for undercooling levels of 180, 200 and 220 K.

$$N_{\text{hom}} = f_0 c_0 \exp\left(-\frac{A}{(\Delta T)^2}\right); \quad A = \frac{16\pi\gamma_{\text{SL}}^3 T_m^2}{3L_V^2 kT}$$

Data:

$$L = 1.88 \times 10^9 \text{ Jm}^{-3}, \quad T_m = 1,356 \text{ K}, \quad \gamma_{\text{SL}} = 0.177 \text{ Jm}^{-2}, \quad f_0 = 10^{11} \text{ s}^{-1}, \quad c_0 = 6 \times 10^{28} \text{ atoms m}^{-3},$$

$$k = 1.38 \times 10^{-23} \text{ JK}^{-1}$$

*Solution:*

The values given imply:

$\Delta T$ (K)	$N_{\text{hom}}$ ( $\text{m}^{-3}\text{s}^{-1}$ )	$N_{\text{hom}}$ ( $\text{cm}^{-3}\text{s}^{-1}$ )
180	0.7	$7 \times 10^{-7}$
200	$8 \times 10^6$	8
220	$1 \times 10^{12}$	$1 \times 10^6$

The results show the scope of changes to rate of homogeneous nucleation occurring within a relatively narrow range of temperature.

## 6. Diffusional Transformations



**Study time:** 6 hours



**Objective:** Completion of this chapter will enable you:

- define basic types of diffusional transformations,
- describe the precipitation from an oversaturated solid solution,
- characterise the individual stages of precipitation,
- explain the term "precipitation sequence",
- describe the kinetics of diffusional transformations,
- identify products of massive transformation and discontinuous precipitation.

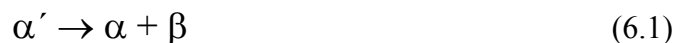


### EXPLANATION

Most phase transformations in solid state occur pursuant to thermally activated movement of atoms, i.e. the diffusion mechanisms. The basic types of diffusional phase transformations can be classified as follows:

- Precipitation reactions,
- Eutectoid transformations,
- Reactions of atom ordering,
- Massive transformations,
- Allotropic transformations.

Precipitation reactions may be characterised by the following formula:



where  $\alpha'$  is a metastable oversaturated solid solution,  $\beta$  is a stable or metastable precipitate and  $\alpha$  is a solid compound with its crystal structure identical to the  $\alpha'$  phase, but its chemical composition is closer to the equilibrium state. The precipitation process can be divided into three stages: *nucleation, growth and coarsening of precipitate*.

Eutectoid transformations represent a replacement of metastable phases ( $\gamma$ ) with a more stable mixture of two other phases ( $\alpha+\beta$ ):



Precipitation and eutectoid transformations include the formation of phases with different compositions and that is why these must involve long-range diffusion. The remaining reactions may run without any composition changes or long-distance diffusions. Ordering reactions may be expressed as follows:



Massive transformation deals with breakdown of the original phase to form one or more phases with the chemical constitution matching the master phase, yet these phases differ in terms of crystal structures:



Allotropic transformations occur in single-component systems with various crystal structures within certain temperature ranges.

## 6.1 Precipitation

### 6.1.1 Homogeneous Nucleation

In the course of precipitation from an  $\alpha$  oversaturated solid solution, atoms of the component B must diffuse and form small quantities matching the composition of phase  $\beta$ ; and if needed, these atoms must be re-arranged into a crystal structure of  $\beta$  phase. This process must result in the formation of the  $\alpha/\beta$  interface and this leads to the **activation energy barrier**.

The change of Gibbs free energy associated with this process involves three contributions:

1. At the temperature where the  $\beta$  phase is stable, formation of the  $\beta$  phase in volume  $V$  causes a drop of the volume free energy by  $V\Delta G_V$ .
2. Assuming the  $\alpha/\beta$  inter-phase energy  $\gamma$  is isotropic, formation of the interface with the area  $A$  will result in an increase of the free energy by  $A\gamma$ .
3. Generally, the transformed volume will differ from the initial volume occupied by the matrix and that situation will result in development of deformation energy of misfit  $\Delta G_S$  per unit volume of  $\beta$  phase.

The total change of free energy during homogeneous nucleation in solid solution is:

$$\Delta G = -V\Delta G_V + A\gamma + V\Delta G_S \quad (6.5)$$

As for nucleation in solids, the value of surface energy may undergo significant modifications from very low values, for coherent interfaces up to very high values for incoherent interfaces. That is why the term  $A\gamma$  should be replaced with summation over individual surfaces of the nucleus  $\sum\gamma_i A_i$ .

If the changes to surface energy associated with interface characteristics are ignored and assuming the development of a spherical nucleus with the radius  $r$ , the equation (6.5) will be in form of:

$$\Delta G = -\frac{4}{3}\pi r^3(\Delta G_V - \Delta G_S) + 4\pi r^2\gamma \quad (6.6)$$

Graphic dependence  $\Delta G$  versus  $r$  is illustrated in the Fig. 6.1. The first derivation of equation (6.6) can be used to obtain terms for critical radius of the nucleus and the critical nucleation barrier:

$$r^* = \frac{2\gamma}{(\Delta G_V - \Delta G_S)} \quad (6.7)$$

$$\Delta G^* = \frac{16\pi\gamma^3}{3(\Delta G_V - \Delta G_S)^2} \quad (6.8)$$

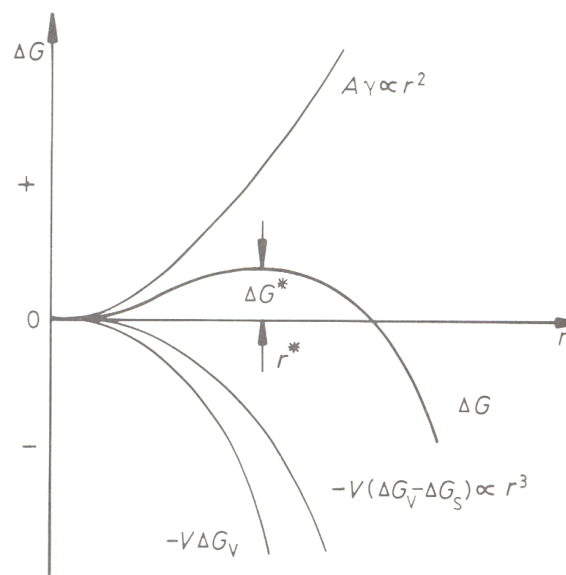


Fig. 6.1 Change of  $\Delta G$  with the radius  $r$  for a homogeneous nucleus,  $\Delta G^*$  - activation barrier of nucleation

If an alloy with constitution  $X_0$  is subject to solution annealing at the temperature  $T_1$  and subsequently cooled down to the temperature  $T_2$ , the  $\alpha$  solid solution will be oversaturated with the component B, Fig. 6.2. The oversaturation may be gradually eliminated by means of

precipitation of particles of the  $\beta$  phase. Once the transformation has been completed, the Gibbs free energy of alloy will drop by  $\Delta G_0$  per 1 mole.  $\Delta G_0$  is therefore the total driving force of transformation, i.e. decomposition of the oversaturated solid solution. Nevertheless, this is not a driving force of nucleation. The first nuclei that appear will have no significant impact towards changes of the constitution of solid compound  $\alpha$  from its value  $X_0$ . The Gibbs free energy released upon formation of 1 mole of nuclei may be determined as follows: if the phase  $\alpha$  is deprived of a small amount of material comprising the composition of nucleus of  $\beta$  phase ( $X_B^\beta$ ), the total Gibbs free energy of the system will be reduced by  $\Delta G_1$ :

$$\Delta G_1 = \mu_A^\alpha X_A^\beta + \mu_B^\alpha X_B^\beta \quad (\text{per 1 mole of } \beta \text{ phase removed}) \quad (6.9)$$

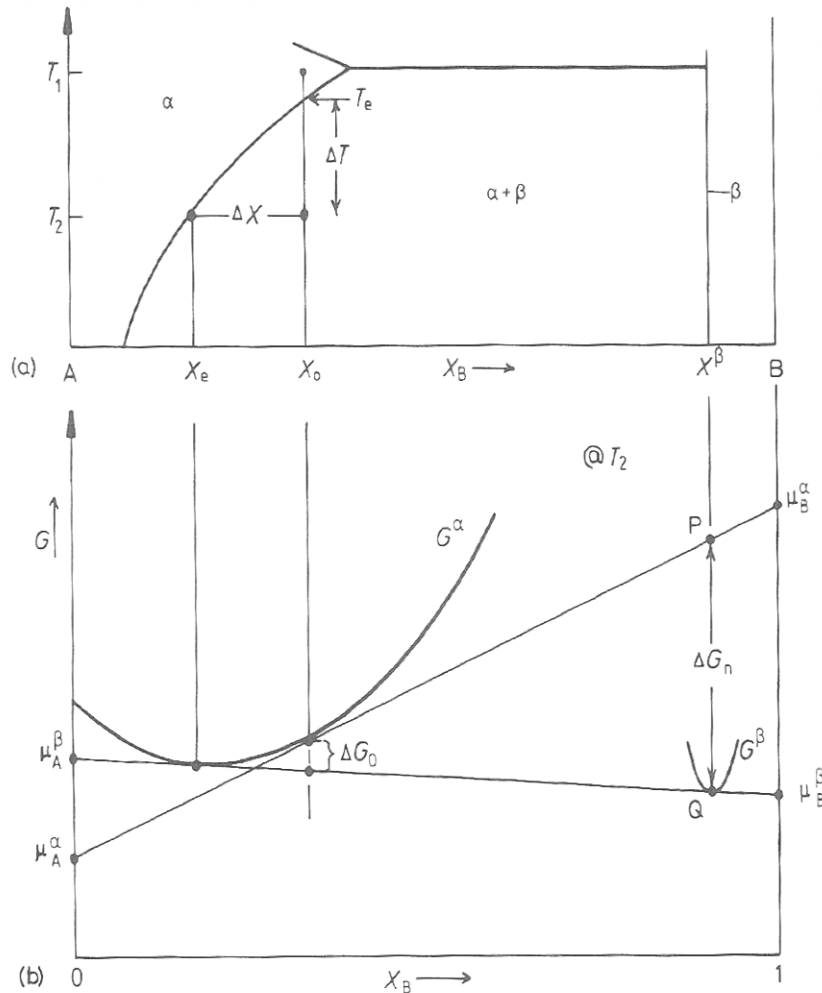


Fig. 6.2 Changes of the free energy during precipitation, a) development of an oversaturated solid solution in the alloy with constitution  $X_0$ , b) driving force for nucleation of the first precipitate is  $\Delta G_n = \Delta G_V V_m$ . The total decrease of free energy at the end of precipitation and achievement of equilibrium is  $\Delta G_0$ .

That is implied by the definition of chemical potential. The value  $\Delta G_1$  is shown in Fig. 6.2 as the point P. If the atoms inside nucleus are further re-arranged into the crystal structure of  $\beta$  phase, the total free energy of the system will increase by the value of  $\Delta G_2$ :

$$\Delta G_2 = \mu_A^\beta X_A^\beta + \mu_B^\beta X_B^\beta \quad (\text{per 1 mole of } \beta \text{ phase developed}) \quad (6.10)$$

The value of  $\Delta G_2$  is shown in the Fig. 6.2 as the point Q. Therefore, the **driving force for nucleation** is defined as follows:

$$\Delta G_n = \Delta G_2 - \Delta G_1 \quad (\text{per 1 mole of } \beta \text{ phase}) \quad (6.11)$$

That matches the vector PQ. The drop of Gibbs free volume energy associated with nucleation of the  $\beta$  phase can be expressed as follows:

$$\Delta G_V = \frac{\Delta G_n}{V_m} \quad (\text{per unit of volume of the } \beta \text{ phase}) \quad (6.12)$$

where  $V_m$  is the molar volume of the  $\beta$  phase. The approximate rule for diluted solutions is:

$$\Delta G_V \propto \Delta X \quad \text{where } \Delta X = X_o - X_e \quad (6.13)$$

It is evident that the driving force for precipitation increases with the increasing of undercooling  $\Delta T$  below the temperature of equilibrium solubility.

Concentration of nuclei of critical size  $C^*$  is determined by the formula:

$$C^* = C_o \exp(-\Delta G^* / kT) \quad (6.14)$$

where  $C_o$  is the number of atoms per unit of volume of the phase. If each nucleus can become supercritical with frequency  $f$ , the rate of homogeneous nucleation will then be given as:

$$N_{hom} = f \cdot C^* \quad (6.15)$$

where the frequency factor  $f$  depends on the frequency shown by critical nucleus in obtaining an atom from the surrounding  $\alpha$  matrix. That will depend on surface area of the nucleus and the rate of diffusion. If the energy for activation of atomic migration is given by  $\Delta G_m$  per atom, the factor  $f$  can then be expressed using the formula  $\omega \cdot \exp(-\Delta G_m / kT)$ , where  $\omega$  is the factor including the vibration frequency of atoms as well as the surface area of the critical nucleus. The formula to determine the rate of homogeneous nucleation is then:

$$N_{hom} = \omega C_o \exp\left(-\frac{\Delta G_m}{kT}\right) \exp\left(-\frac{\Delta G^*}{kT}\right) \quad (6.16)$$

To express this equation as a function of temperature, one shall assume that  $\omega$  and  $\Delta G_m$  are constant but  $\Delta G^*$  is strongly dependent on temperature. The main factor controlling the  $\Delta G^*$  is the driving force for precipitation  $\Delta G_V$ . As the composition varies, the value  $\Delta G_V$  must be obtained from the diagram showing dependency between the Gibbs free energy and the composition.

The change of  $\Delta G_V$  depending on temperature applicable to an alloy with composition  $X_0$  has been illustrated by the diagram in Fig. 6.3b. Bearing in mind the element of misfit strain energy  $\Delta G_S$ , the effective driving force will be determined by the difference  $(\Delta G_V - \Delta G_S)$  and the effective equilibrium temperature is reduced to the value of  $T'_e$ , Fig. 6.3a. If the value of  $(\Delta G_V - \Delta G_S)$  is known, the activation energy  $\Delta G^*$  can be calculated. The Fig. 6.3c shows two exponential terms for rate of homogeneous nucleation. The second term  $(\exp(-\frac{\Delta G^*}{kT}))$  is basically an expression of potential concentration of nuclei of critical size, it is virtually zero until reaching the critical undercooling value of  $\Delta T_C$  and then it grows rapidly. The first exponential term  $(\exp(-\frac{\Delta G_m}{kT}))$  characterises the mobility of atoms. As the value of  $\Delta G_m$  is constant, this term experiences a rapid drop with decrease of temperature.

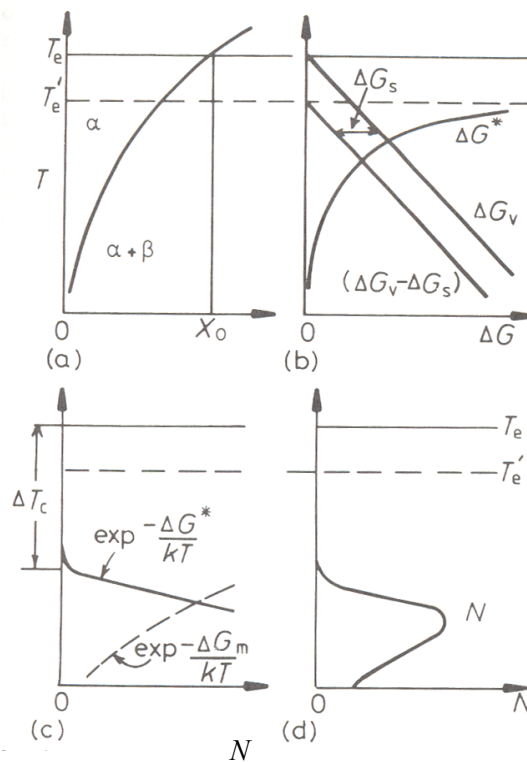


Fig. 6.3 Changes to the rate of homogeneous nucleation in an alloy with constitution  $X_0$ , a) phase diagram, b) effective driving power  $(\Delta G_V - \Delta G_S)$  and the resultant energetic barrier

$\Delta G^*$ , c) two exponential terms to determine the resultant rate of nucleation illustrated in the Fig. 6.3d.

These two exponential terms determine the rate of homogeneous nucleation, Fig. 6.3d. The rate of nucleation will be negligible for undercooling below  $\Delta T_C$ , as the driving power  $\Delta G_V$  is too low, whereas large undercooling is matched by low rate of nucleation owing to the too slow diffusion. The maximum rate of nucleation is achieved at medium levels of undercooling. Systems with a lower concentration of solute reach the undercooling level at lower temperature with slower diffusion. The rate of nucleation in such alloy will be always lower than in an alloy with higher concentration of the solute, Fig. 6.4. This issue of nucleation was handled with assumption that the rate of nucleation is constant. However, in practice the rate of nucleation at the beginning of transformation is rising gradually and later it drops, as the growth of nuclei developed at the initial stage of nucleation works towards progressive reduction of the supersaturation of  $\alpha$  solid solution. The equation for  $\Delta G^*$  implies the most effective method for minimising the energetic barrier is to form nuclei within the minimum total interfacial energy. Incoherent interfaces reach the  $\gamma$  value so high that it makes any homogeneous nucleation basically impossible. If there is an orientation relationship between the nucleus and matrix and if the interphase interface is incoherent, then the value of  $\Delta G^*$  will be reduced significantly and homogeneous nucleation will be enabled. An example of homogeneous nucleation may include precipitation of particles of  $\text{Ni}_3\text{Al}$  (phase  $\gamma'$ ) in nickel superalloys.

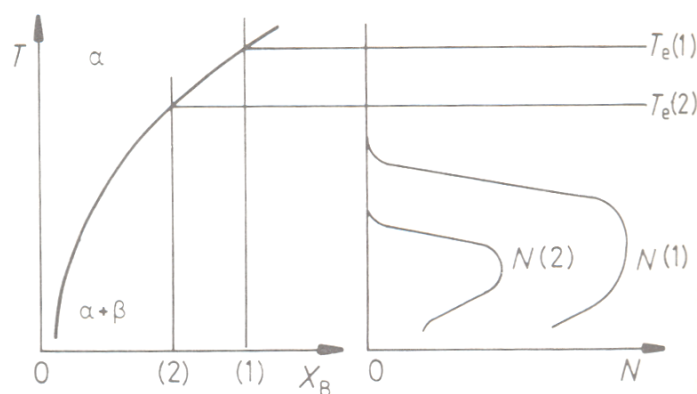


Fig. 6.4 Impact of alloy composition on the rate of nucleation. The rate of nucleation in alloy No. 2 will be always lower than in the alloy No. 1 - read the text for explanation.

### 6.1.2 Heterogeneous Nucleation

Nucleation in solids mostly takes place by means of a heterogeneous mechanism. Suitable nucleation points may be identified as non-equilibrium defects, e.g. dislocations, grain interfaces, stacking faults, inclusion particles, free surfaces etc. All these defects increase the free energy of material. In case the development of nucleus induces destruction of the defect; there will be a certain amount of energy released ( $\Delta G_d$ ) which causes a drop of the energy nucleation barrier:

$$\Delta G_{het} = -V(\Delta G_V - \Delta G_S) + A\gamma - \Delta G_d \quad (6.17)$$

One of the most common cases of nucleation is the development of nuclei at grain boundaries. If the missfit strain energy is neglected, the optimal shape of nucleus will be the one minimising the total interfacial free energy. In case of incoherent grain boundary the optimal shape of nucleus will be in form of a lens, see Fig. 6.5. The value of the contact angle  $\theta$  may be expressed as follows, assuming that the value  $\gamma_{\alpha\beta}$  is isotropic and the same for both grains:

$$\cos \theta = \gamma_{\alpha\alpha} / 2\gamma_{\alpha\beta} \quad (6.18)$$

The free energy of nucleus can be expressed as follows:

$$\Delta G = -V\Delta G_V + A_{\alpha\beta}\gamma_{\alpha\beta} - A_{\alpha\alpha}\gamma_{\alpha\alpha} \quad (6.19)$$

where  $V$  is the volume of nucleus,  $A_{\alpha\beta}$  is the area of  $\alpha/\beta$  interface with the surface energy  $\gamma_{\alpha\beta}$ , and  $A_{\alpha\alpha}$  is the initial surface area of the grain boundary with the energy of  $\gamma_{\alpha\alpha}$  eliminated during the nucleation process. The last term in this equation is identical for the term  $\Delta G_d$  in the formula (6.17).

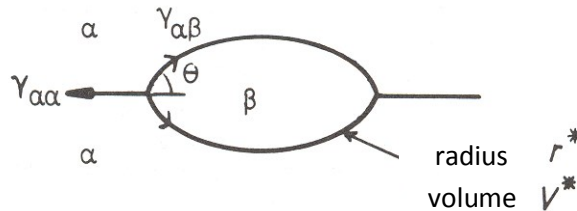


Fig. 6.5 Critical size and shape of nucleus at the grain interface

Critical radius of lenticular nucleus at the grain boundary can be expressed by the formula:

$$r^* = \frac{2\gamma_{\alpha\beta}}{\Delta G_V} \quad (6.20)$$

and the ratio of activation energy barriers for heterogeneous and homogeneous nucleation will be equal to the shape factor:

$$\frac{\Delta G_{het}^*}{\Delta G_{hom}^*} = \frac{V_{het}^*}{V_{hom}^*} = S(\theta) \quad (6.21)$$

where  $S(\theta) = \frac{1}{2}(2 + \cos \theta)(1 - \cos \theta)^2$

The potential of interface as the point of heterogeneous nucleation depends on  $\cos \theta$ , i.e. on the ratio  $\gamma_{\alpha\alpha}/2\gamma_{\alpha\beta}$ . The activation barrier of heterogeneous nucleation at grain boundaries can be reduced further at the point of contact of three or four grains, Fig. 6.6.

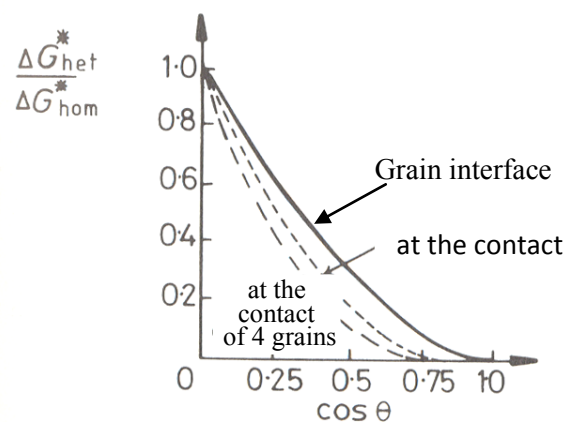


Fig. 6.6 Impact of angle  $\theta$  on the activation nucleation barrier at grain boundaries

Exceptionally effective nucleation points for incoherent precipitates are on the high-angle grain boundaries. Further reduction of the activation energy may occur in case one of the interfaces contains a single grain and it is planar, while the other one is curved, Fig. 6.7. The nucleus will have an orientation relationship to the grain on the side of planar interface and it will grow into the grain adjacent by means of the curved incoherent interface. The nuclei with the lowest nucleation barrier will develop at the fastest rate.

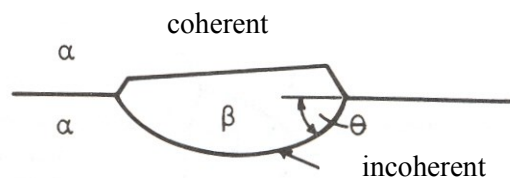


Fig. 6.7 The critical size of nucleus may be reduced, if the energy of interface with one grain is low (coherent - planar interface)

The effectiveness of various defects with respect to heterogeneous nucleation will increase in this order:

- Vacancies,
- Dislocations,
- Stacking faults,
- Grain boundaries or interphase interfaces,
- Free surfaces.

The easiest and the most rapid nucleation should therefore occur on defects stated in the bottom of the list. Nevertheless, the importance of these defects with respect to the overall rate of transformation also depends on their relative frequency.

If the concentration of heterogeneous nucleation points per unit of volume is marked  $C_1$ , the rate of heterogeneous nucleation will be expressed as:

$$N_{hom} = \omega C_1 \exp\left(-\frac{\Delta G_m}{kT}\right) \exp\left(-\frac{\Delta G^*}{kT}\right) \quad (\text{nuclei m}^{-3} \text{ s}^{-1}) \quad (6.22)$$

For the rate of nucleation as a function of temperature refer to the Fig. 6.8. Measurable rate of nucleation apparently occurs at very low undercooling levels below  $T_e$ .

Relative differences in the heterogeneous and homogeneous rates of nucleation are defined by the formula:

$$\frac{N_{het}}{N_{hom}} = \frac{C_1}{C_0} \exp\left(\frac{\Delta G_{hom}^* - \Delta G_{het}^*}{kT}\right) \quad (6.23)$$

Remark: small differences in values of parameters  $\omega$  and  $\Delta G_m$  have been ignored in the formula above.

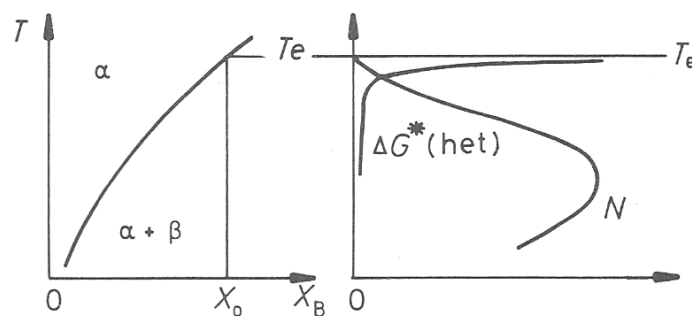


Fig. 6.8 Rate of heterogeneous nucleation during precipitation of the phase  $\beta$  in alloy with composition  $X_0$  as a function of undercooling

The factor  $\frac{c_1}{c_0}$  makes provision for the number of atoms at the point of heterogeneous nucleation with respect to the quantity of atoms in matrix. The following formula applies to nucleation at the grain boundary:

$$\frac{c_1}{c_0} = \frac{\delta}{D} \quad (6.24)$$

where  $\delta$  is the thickness of grain boundary and  $D$  refers to grain diameter.

For very low driving force of transformation, when the activation energy for nucleation is very high, the greatest rates of nucleation will be experienced by points of the contact of three or four grains respectively. Increase of the driving force will establish grain boundaries as dominant defects for heterogeneous nucleation. Very high driving forces of transformation may result in the situation, when the greatest rate of nucleation corresponds with the homogeneous nucleation.

The remarks mentioned above were relevant to nucleation during the isothermal nucleation process only. If the nucleation process runs under continuous cooling conditions, the driving force for nucleation will be increasing progressively in time. Under such circumstances, the initial stages of transformation will be associated with those points of nucleation, which may generate measurable rate of nucleation as fast as possible.

### 6.1.3 Growth of Precipitates

Successful critical nuclei are those with the lowest nucleation barrier, i.e. **the lowest critical volume**. When strain energy is absent, the shape of precipitate compliant with this rule will be convenient for minimising the total interface energy. Nuclei are usually bounded by a combination of coherent and semicoherent facets and smoothly curved incoherent interfaces. While the precipitate grows, these interfaces must be in motion and the shape of precipitate will be determined by relative rates of migration of particular interfaces. The mobility of incoherent interfaces is usually higher than in case of (semi)coherent interfaces.

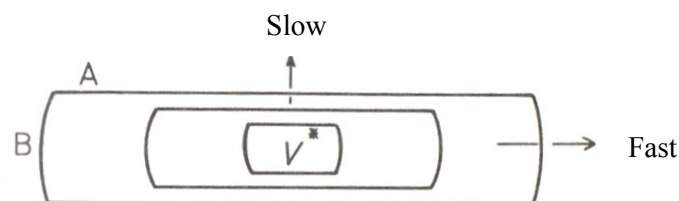


Fig. 6.9 The effect of interface type on morphology of a growing precipitate, A - semicoherent interface with low mobility, B – incoherent interface with high mobility

The Fig. 6.9 shows growth of the nucleus bounded with the curved incoherent interface and low-energy planar interface (the plane of good crystallographic matching with the matrix) into a disc or thin plate shape.

Concentration profiles of the solute around particles of the  $\beta$  phase precipitating from the oversaturated matrix  $\alpha$  have been illustrated in the Fig. 6.10. The initial concentration of component B in the oversaturated matrix is  $c_0$ . The process of precipitate growth is accompanied by a gradual decrease in concentration of the solutes in matrix; the time  $t$  refers to the concentration of atoms of the solutes at great distance from particles equal to  $c^\alpha(t)$ . The value  $c_e^\beta$  refers to equilibrium concentration inside particles of the phase  $\beta$  and the value  $c_e^\alpha$  characterises the equilibrium concentration within the matrix. The concentration  $c^{\alpha\beta}$  in matrix in the close vicinity to the interface  $\alpha/\beta$  is determined by the local equilibrium between the  $\alpha$  matrix and  $\beta$  particle - this equilibrium concentration is defined as the **solubility of particles**.

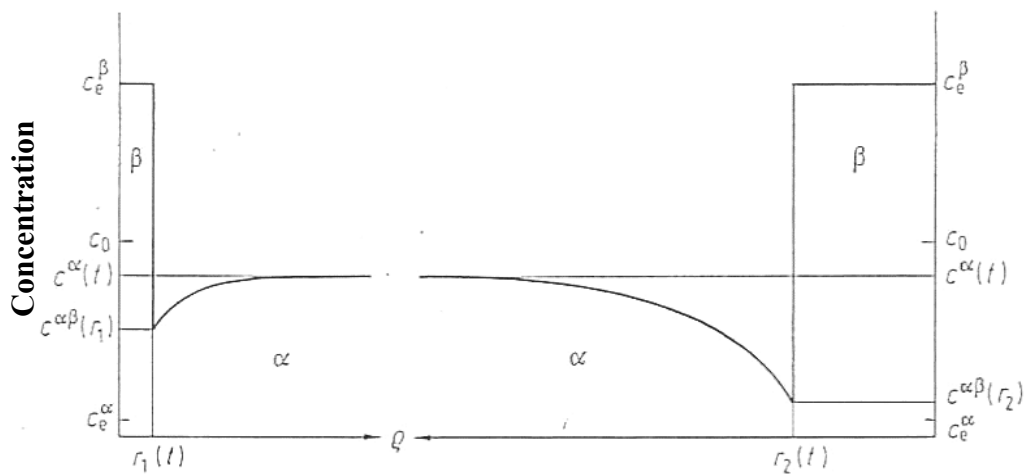
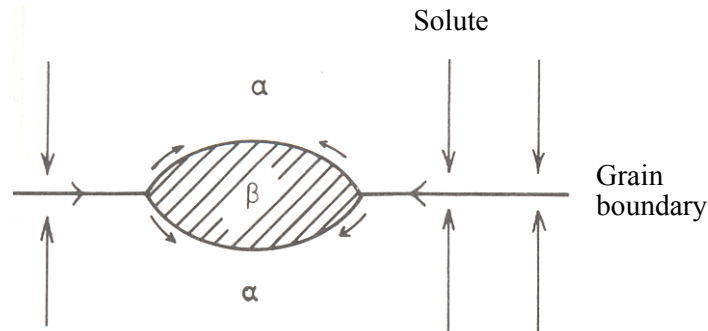


Fig. 6.10 Diagram showing the changes of concentration of dissolved component depending on the distance from the centre of two growing particles of the  $\beta$  phase with radii  $r_1(t)$  and  $r_2(t)$ ,  $r_2(t) > r_1(t)$

The concentration  $c^\alpha(t)$  of an oversaturated matrix at the initial stage of precipitate growth is much greater than the solubility value  $c^{\alpha\beta}(r)$ . The difference  $(c^\alpha(t) - c^{\alpha\beta}(r))$  controlling the growth of particles is greater for larger particles. The concentration  $c^\alpha(t)$  in matrix goes through a gradual decrease during the precipitate growth and that is why concentration  $c^\alpha(t)$

reaches the value  $c^{\alpha\beta}$  for the smallest particles after a certain time, so this particle reaches the critical size and its growth stops. Extension of the growth time will result in further decrease of  $c^{\alpha}(t)$  and the critical size will be achieved gradually by particles of larger dimensions. The solubility of small particles  $c^{\alpha\beta}(r)$  (concentration of dissolved component in the vicinity to the interface) exceeds the concentration of solutes in solution now and that is why these particles dissolve.



*Fig. 6.11 Diffusion along the grain boundaries may result in fast growth of precipitates on the grain boundaries*

Precipitates along the grain boundaries usually do not create a continuous layer and they are rather isolated particles. The growth of these particles can run at a much faster rate than allowed by the volume diffusion, Fig. 6.11. The growth of particles at grain boundaries comprises three steps:

- Volume diffusion of the solute to the grain boundary,
- Diffusion of solute along the grain boundary towards the edge of precipitate,
- Diffusion along the  $\alpha/\beta$  interface enabling accelerated precipitate growth.

This mechanism plays a very important role in diffusion of substitution elements, e.g. precipitation of  $\text{Cr}_{23}\text{C}_6$  carbides in Cr - Ni austenitic steels.

#### **6.1.4 Coarsening of Precipitates**

The final stage of precipitate growth is terminated with absolute removal of atoms of component B from oversaturated solution  $\alpha$  ( $\Delta G_v = 0$ ). However, the microstructure of a two-phase alloy will remain in a non-equilibrium state until it reaches the lowest value of the total interfacial energy possible ( $A\gamma$ ). That is the reason for progressive replacement of a high number density of fine particles of the precipitate with a smaller number of coarser precipitates with the generally smaller interfacial area. The rate of precipitate coarsening is

increased with temperature. Coarsening of precipitates is usually followed by degradation of mechanical properties of materials.

As far as alloys hardened through precipitation are concerned, the particle dimensions will always lie within a certain size interval due to difference in nucleation time and the growth rate of particles. The Fig. 6.12 shows two precipitates with different radii. Capillary effect causes the increase of concentration of the solute in the matrix in the vicinity of particles, as a function of the decreasing curvature of the particle, Fig. 6.13. That is the reason for occurrence of concentration gradients in the matrix; those will cause diffusion of the dissolved component from the smallest particles towards the largest ones. Small particles will be dissolving and the large ones will continue growing. The outcome of these processes will comprise gradual reduction of the particle number and enlargement of the mean particle radius. The first particles to dissolve will be the ones that formed nuclei with a great delay, Fig. 6.14. Particles that formed nuclei with time delay will also dissolve during the stage of precipitate growth, Fig. 6.14. Long annealing will leave the matrix with coarse particles of the  $\beta$  phase, which developed in the initial stage of precipitation, only.

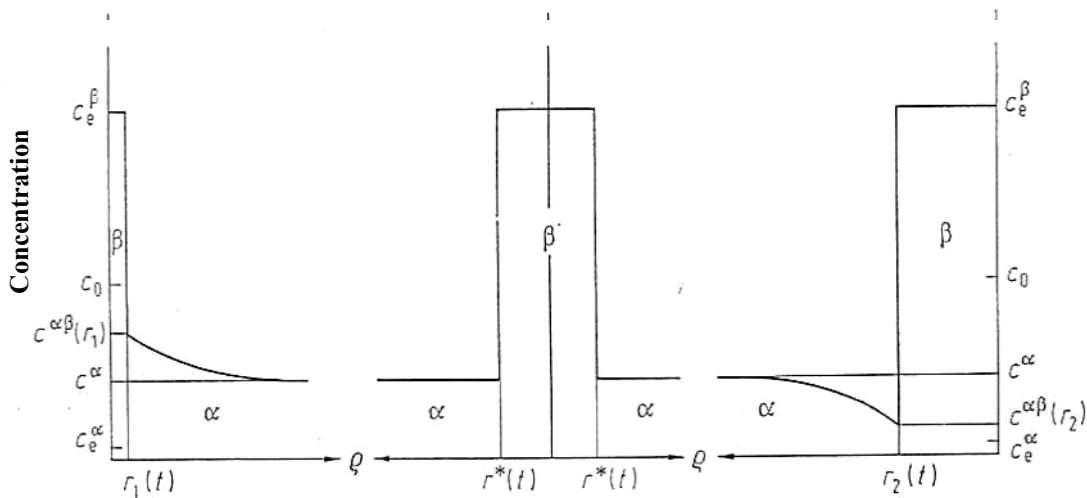


Fig. 6.12 Diagram showing the changes of concentration of the dissolved component during the particle coarsening process: dissolution of particles with radius  $r_1(t)$ , particles with the critical radius  $r^*(t)$  and the growing particles  $r_2(t)$ ,  $r_2(t) > r_1(t)$

Assuming that volume diffusion will be the mechanism controlling growth, the following relation, the so called *Wagner equation*, will apply:

$$\bar{r}^3 - r_0^3 = kt \quad (6.25)$$

where  $k \propto D\gamma X_e$ ,  $r_0$  is the mean radius of particles in time  $t = 0$ ,  $\bar{r}$  is the mean radius of particles in time  $t$ ,  $D$  is the diffusion coefficient,  $\gamma$  is the interfacial energy and  $X_e$  is the equilibrium solubility of very large particles. As the values of  $D$  and  $X_e$  grow exponentially with respect to temperature, the rate of coarsening will grow with the temperature rapidly.

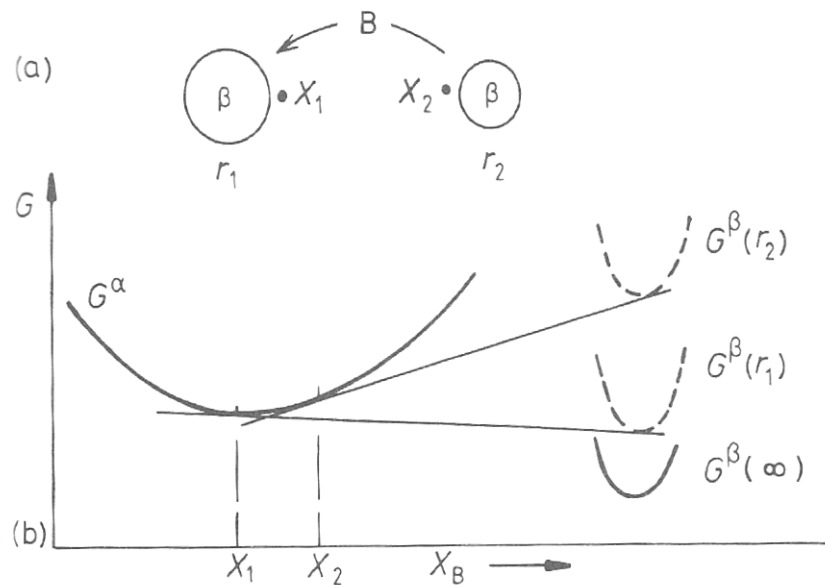


Fig. 6.13 Precipitate particles  $\beta$  with small radius ( $r_2$ ) have a higher molar Gibbs free energy than the particles with greater curvature radius ( $r_1$ ). The concentration of dissolved component  $B$  within the matrix  $\alpha$  in the vicinity of the  $\alpha/\beta$  interface will be the greatest close to the smallest particles  $\beta$ .

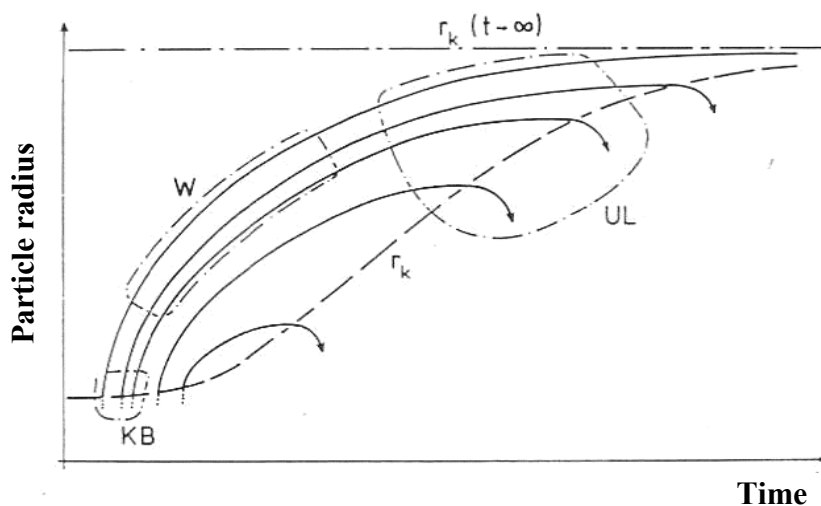


Fig. 6.14 Growth trajectory of precipitate radius as a function of time and changes of the critical particle radius  $r_k$  – dashed line, KB – nucleation stage, W – growth stage, UL – ultimate limit.

*UL – coarsening stage*

The rate of particle coarsening in certain systems is not proportional to the cube of particle radius. Deviations from this relation may be caused by other diffusion mechanisms, e.g. along dislocations or grain boundaries or the rate of coarsening may be controlled by the interface. Nevertheless, except for situation with the rate controlled by interface, the rate of coarsening should depend on the product of  $D\gamma X_e$ . High-temperature alloys, the strength of which depends on the precipitation hardening, must show low value of one of these parameters at least.

**6.1.5 Precipitation Sequence**

In a number of systems, the metastable phases having the lowest activation energy barrier nucleate first. While the duration of exposure to higher temperature extends, these phases will dissolve gradually to be replaced with thermodynamically more stable phases. The driving force of these **transcrystalline processes** lies in difference between the mean concentration of solute in matrix  $c_w$  and solubility of particles.

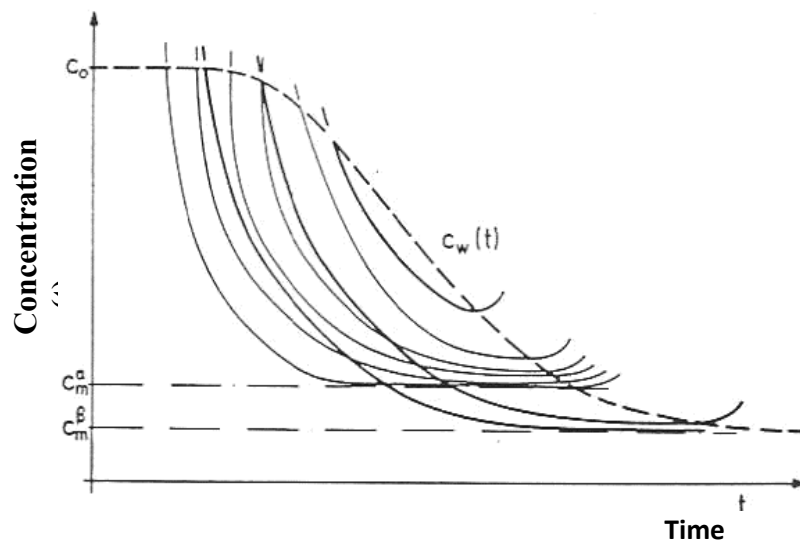


Fig. 6.15 Diagram showing dependency of particle solubility for phases  $\alpha$  and  $\beta$  on the time of exposure

The Fig. 6.15 shows trajectories of growth for individual particles and the dashed line identifies the curve  $c_w(t)$  defining gradual depletion of the matrix. If the particles of phase  $\alpha$  are small enough, they may be less soluble than particles of the  $\beta$  phase. The particles of phase  $\alpha$  will grow faster in this case, i.e. the gradient of their growth will be greater than on the curve of already existing  $\beta$  particles. The bottom limit for concentration  $c_a^\alpha$  is defined

by equilibrium concentration  $c_m^\alpha$ , therefore the growth trajectory of particles  $\alpha$  show asymptotic approach to the limit value  $c_m^\alpha$ . The growth trajectory of particles  $\beta$  approach the equilibrium concentration  $c_m^\beta$  by asymptotic means. The concentration of dissolved component  $c_w(t)$  in matrix drops continuously together with the exposure time and once it drops below the value  $c_m^\alpha$ , particles of the  $\alpha$  phase have to dissolve. The lower the difference between solubility of  $c_m^\alpha$  and  $c_m^\beta$ , the more similar the behaviour of  $\alpha$  and  $\beta$  phases, the longer the potential coexistence of both phases in the matrix.

### 6.2 Kinetics of Diffusional Transformations

The course of diffusional phase transformation  $\alpha \rightarrow \beta$  conducted by means of a diffusion mechanism can be presented clearly by illustration of the transformation fraction ( $f$ ) as a function of time and temperature, Fig. 6.16.

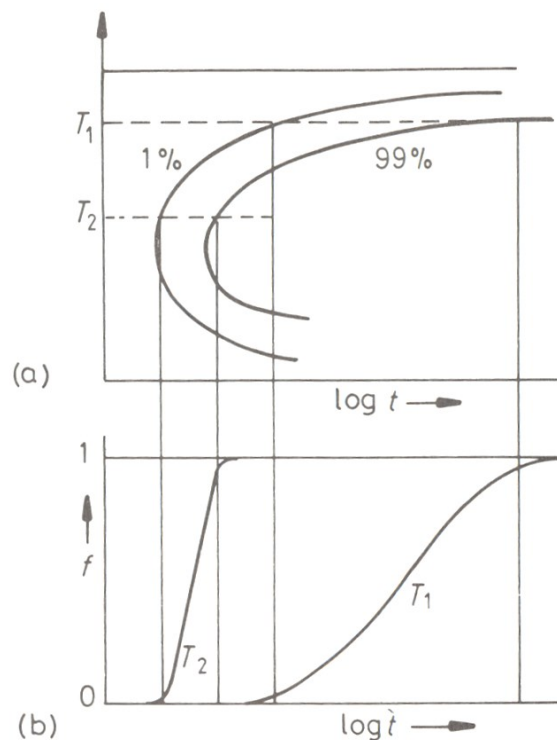


Fig. 6.16 a) Kinetic diagram of diffusional decomposition, b) kinetic curves for  $T_1$  and  $T_2$ , the growth of volume fraction of the new phase ( $f$ ) occurs after a certain **incubation period**, which is a function of  $T$

The parameter  $f$  refers to volume fraction of the  $\beta$  phase at particular moment; it changes from 0 to 1 at the end of the transformation process. The C-curve marked 1 % represents a link of

points representing 1 % of phase  $\beta$  in the matrix of phase  $\alpha$  and the curve 99 % identifies the end of decomposition of the  $\alpha$  phase (microstructure contains 99 % of the phase  $\beta$ ). The factors that determine dependency among  $f$ ,  $t$  and  $T$  include the rate of nucleation, the rate of growth, density and distribution of nucleation sites, overlapping of diffusion fields of adjacent transformed volumes and the mutual influence of adjacent transformed volumes. Some of the problems are illustrated in the Fig. 6.17. After a rapid cooling to the transformation temperature, the metastable phase  $\alpha$  can form at many nucleation sites, usually of heterogeneous type. One of the possibilities deals with a constant nucleation rate during the transformation, so there will be a broad range of particle sizes at any moment, Fig. 6.17a. Another option may be that all the nuclei develop at the beginning of transformation already, Fig. 6.17b. This is defined as saturation of nucleation sites. In the first case, the volume fraction of new phase will depend on the rate of nucleation as well as on the growth rate. In the second case, the volume fraction of new phase depends on the number of nucleation sites and the growth rate only.

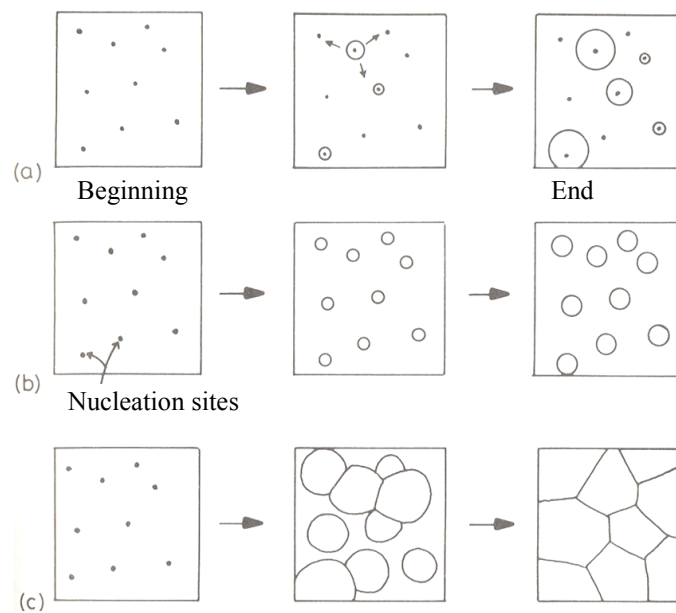


Fig. 6.17 a) Nucleation at a constant rate throughout the entire transformation, b) saturation of nucleation points – all the nuclei develop at the beginning of transformation, c) cellular transformation

Transformations of type  $\alpha \rightarrow \beta$  involve gradual replacement of the whole master phase with the transformation product, Fig. 6.17c. Transformation will not complete with gradual reduction of the growth rate in these cases, it will end with mutual contact between adjacent

cells growing at a constant rate. This category includes the ferrite transformation in steel, for example.

Assume a simple example for determination of the dependency between the volume fraction of a new phase (f) and the time and temperature during cellular transformation  $\alpha \rightarrow \beta$ , when cells  $\beta$  go through gradual nucleation at a constant rate N during the transformation process. If the cells grow as spheres at a constant rate  $v$ , the volume of cell that forms nucleus at the beginning of transformation will be defined by the formula:

$$V = \frac{4}{3}\pi r^3 = \frac{4}{3}\pi(vt)^3 \quad (6.26)$$

where t is the time of transformation.

The volume of cell to form nucleus with a delay  $\tau$  will be defined as follows:

$$V' = \frac{4}{3}\pi v^3(t - \tau)^3 \quad (6.27)$$

The number of nuclei developed within the time increment  $d\tau$  will be defined by the term  $Nd\tau$  per unit of volume of the non-transformed  $\alpha$  phase. If cells do not impinge each other, the total unit volume will be expressed as:

$$f = \sum V' = \frac{4}{3}\pi N v^3 \int_0^t (t - \tau)^3 d\tau \quad (6.28)$$

The equation for volume fraction of the new phase after integration will be:

$$f = \frac{\pi}{3} N v^3 t^4 \quad (6.29)$$

The equation will apply in case  $f \ll 1$  only. Cells of the  $\beta$  phase will start impinge each other as the time progresses and the rate of transformation will be reduced. The equation applicable to randomly distributed nuclei for short or long transformation times will be:

$$f = 1 - \exp\left(-\frac{\pi}{3} N v^3 t^4\right) \quad (6.30)$$

Note that the equation is the same as for short intervals, as  $1 - \exp(-z) \cong z$ , if  $z \ll 1$ . This equation is also applicable to long intervals, as both  $t \rightarrow \infty$ , as well as  $f \rightarrow 1$ .

This equation is defined as the **Johnson-Mehl-Avrami model**. Expected mechanisms of nucleation and growth can be used to several equations in the form:

$$f = 1 - \exp(kt^n) \quad (6.31)$$

where  $n = (1 - 4)$ . Unless the mechanism of nucleation is changed, the coefficient  $n$  is independent on temperature. The coefficient  $k$  depends on rates of nucleation and growth and it is therefore very sensitive to the transformation temperature. Rapid transformations will be associated with high values of  $k$ .

Diffusional transformations are in the TTT (or CCT) diagrams characterized by typical C-shaped curves. That can be explained pursuant to changes in the rate of nucleation together with increase of undercooling. When the temperature approaches  $T_e$ , the driving force of transformation will be very low, so both the rate of nucleation as well as the rate of growth are very low and the rate of transformation will be very slow. If  $\Delta T$  is very high, the rate of transformation is limited by slow rates of diffusion. The maximum rate of transformation is then obtained at medium transformation temperatures.

### 6.3 Spinodal Decomposition

The spinodal decomposition, which falls within the category of homogeneous transformations, does not involve any nucleation barrier. Assume a binary diagram with the miscibility gap in solid state, Fig. 6.18a. When heating an alloy with composition  $X_0$  to a high temperature  $T_1$  followed by cooling to the temperature  $T_2$ , the initial composition of the alloy will be the same and its free energy will be illustrated by the point  $G_0$  on the curve of Gibbs free energy shown in the Fig. 6.18b. However, the alloy is in unstable condition, as low fluctuations of its composition will produce adjacent A-rich and B-rich areas which will induce a drop of the Gibbs free energy in the system. That is why diffusion up the concentration gradient will be in progress until achievement of the equilibrium composition of  $X_1$  and  $X_2$ , Fig. 6.19a. This process may occur only in alloys with such composition, where the curve of Gibbs free energy shows a negative curvature ( $\frac{d^2G}{dX^2} < 0$ ). That means constitution of such alloy must be located between inflection points on the curve of Gibbs free energy. The dashed curve in Fig. 6.18a represents a link of inflection points for various temperatures and it is defined as a *chemical spinodal*.

If the chemical composition of alloy lies outside the chemical spinodal, small changes in chemical composition of the solid solution  $\alpha$  will result in an increase of free energy in the system. The free energy may be reduced only in case the chemical composition of nuclei is very different from the matrix composition. That is the reason why decomposition of an oversaturated solid solution takes place in areas outside the chemical spinodal by means of

nucleation and growth processes. Such case deals with diffusion occurring down the concentration gradient, Fig. 6.19b.

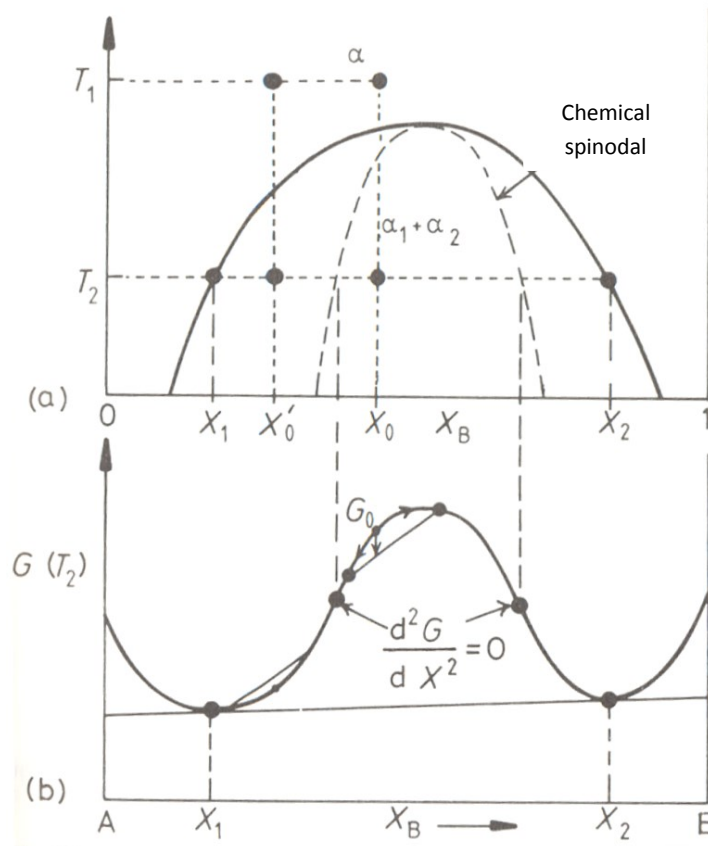


Fig. 6.18 Alloys between spinodal points are unstable and they may decompose to form two coherent phases  $\alpha_1$  and  $\alpha_2$  without overcoming the activation energy barrier. Alloys between the curves of limited solubility and chemical spinodals are metastable and they may decompose only in case after nucleation of another phase.

The rate of spinodal decomposition is controlled by the interdiffusion coefficient  $D$ . The value inside the chemical spinodal is  $D < 0$  and fluctuations of the composition will increase exponentially with time. The rate of transformation will rise with the decrease of wavelength  $\lambda$ , to a certain critical value only. When calculating the value  $\lambda$ , the following two vital factors need to be considered: the interfacial energy and the coherent strain energy.

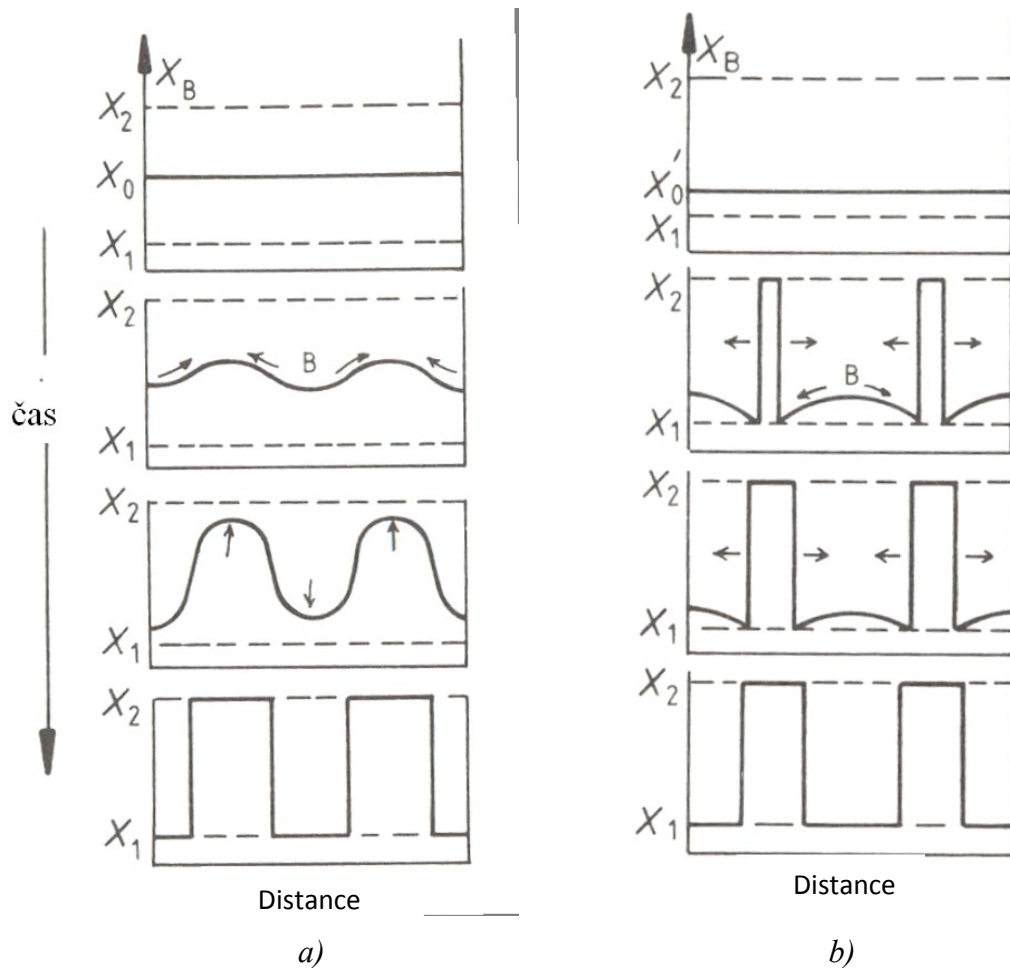


Fig. 6.19 Schematic profiles of composition for decomposition of an oversaturated solid solution, a) composition  $X_0$  between curves of the chemical spinodal, b) composition  $X'_0$  outside the curves of chemical spinodal, Fig. 6.18

#### 6.4 Discontinuous Transformation

In some cases, precipitation on grain boundaries does not result in formation of allotriomorphic particles or Widmanstätten patterns. The so called discontinuous or cellular precipitation is characteristic for movement of grain boundaries with the growing particles of precipitate, as shown in the Fig. 6.20. Morphology of transformation products is reminiscent of an eutectoid reaction. The general schema of a discontinuous reaction will be as follows:



where  $\alpha'$  is the over-saturated matrix,  $\alpha$  is the same phase with a lower level of over-saturation by solute and  $\beta$  is the equilibrium precipitate. Mechanisms leading towards development of cellular precipitates nucleated at grain boundaries may be different for different alloys.

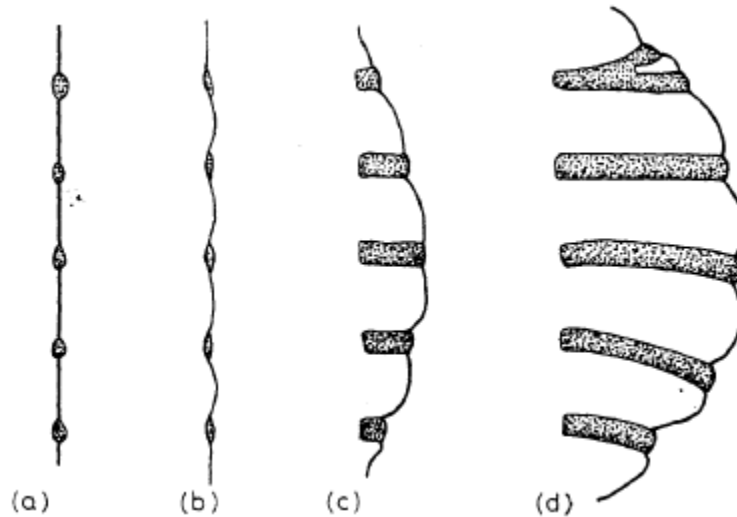


Fig. 6.20 Diagram showing individual stages of discontinuous precipitation

The "discontinuous precipitation" reflects the fact that contents of solute undergo a discontinuous change when passing through the front of cellular precipitation. As far as mechanical characteristics are concerned, this type of precipitation is undesired, as the interior of cells often involves development of coarse precipitates. The Fig. 6.21 documents cells of discontinuous precipitation of  $M_{23}C_6$  in an austenitic weld overlay of 19Cr – 12Ni type. The mechanism for development of these cells is shown in the Fig. 6.22a – c.

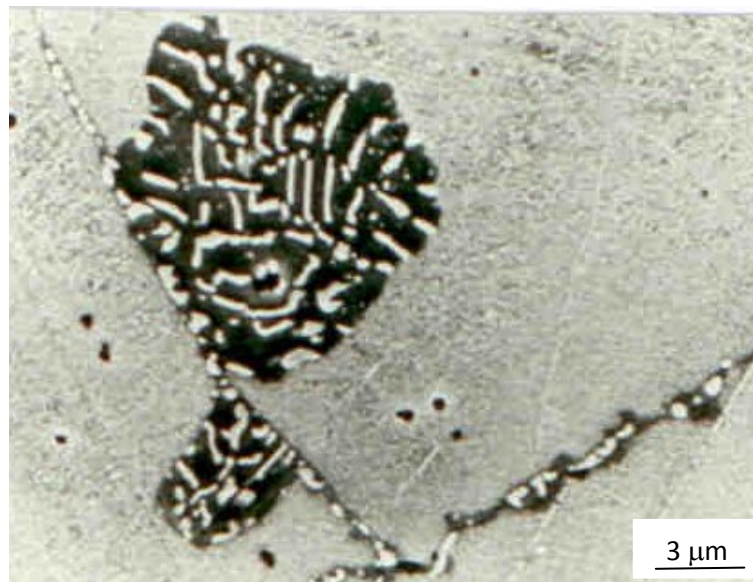


Fig. 6.21 Discontinuous precipitation of  $M_{23}C_6$  in an austenitic weld overlay of 19Cr – 12Ni type

The Fig. 6.22a documents the condition, when the interior of austenitic grains includes numerous fine particles of  $M_{23}C_6$  which is rich in chromium, whereas the particles of identical phase found on grain boundaries are significantly coarser. That relates to easier diffusion of

chromium along the grain boundaries compared to the volume of grains. This precipitation mechanism is defined as continuous, as the precipitation of precipitate particles is followed by a continuous change to the matrix composition during the precipitation process. A coarse precipitate found at grain boundary comprises a semi-coherent planar interface with grain  $\gamma_1$ . There is an orientation relationship between this particle K and the grain  $\gamma_1$ , it is the "cube-to-cube" ( $(001)_K // (001)_{\gamma_1}$ ,  $[100]_K // [100]_{\gamma_1}$ ). The growth of this particle occurs by movement of the curved incoherent interface into the grain  $\gamma_2$  and it is accompanied with migration of the grain boundary, Fig. 6.22b. Easy growth of particles at grain boundaries is enabled by diffusion of chromium along the grain boundaries, fine intragranular particles of  $M_{23}C_6$  dissolve upon contact with the moving interface to form a surrounding zone depleted in precipitates ("denuded zone"). The area behind such moving interface will show formation of lamellae of  $M_{23}C_6$  particles with the orientation relationship of "cube-to-cube" type with grain  $\gamma_1$ . Spherical particles inside cells of discontinuous decomposition represent "inherited" particles of  $M_{23}C_6$ , which initially precipitated in the grain  $\gamma_2$  and were not dissolved during movement of the grain boundary. That is proven by the orientation relationship of these particles with the grain  $\gamma_2$ . The orientation of austenite inside the cell of discontinuous precipitation corresponds with the grain  $\gamma_1$ . In this case the discontinuous decomposition can be described using the following equation:



The discontinuous precipitation was followed by a drop in oversaturation of austenite, the type of precipitating phase in the continuous precipitation area was the same as in cells of discontinuous decomposition. As the fine particles in the initial microstructure were replaced with coarse lamellae, one could expect the discontinuous decomposition was followed by a drop of interfacial energy.

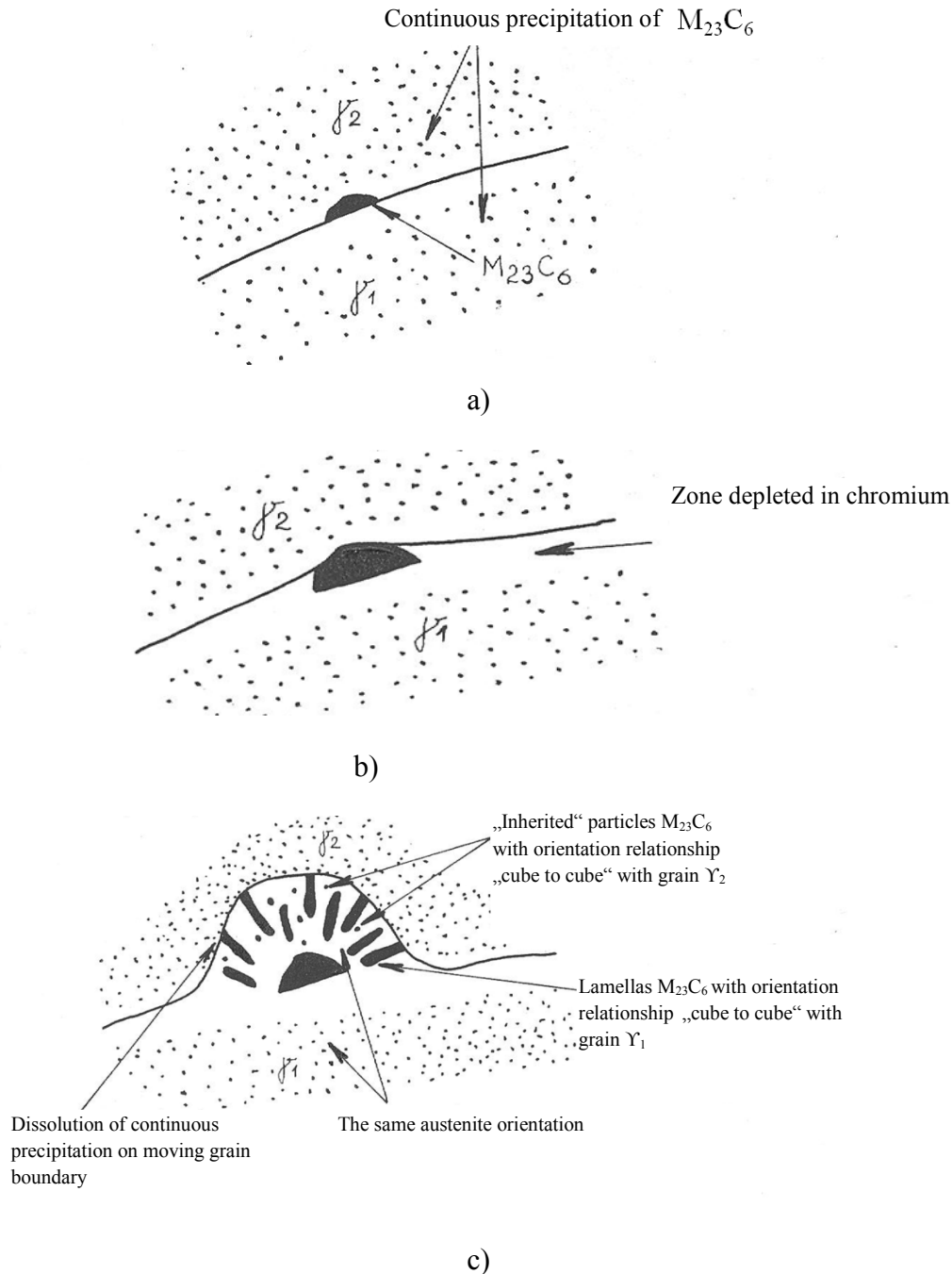


Fig. 6.22a-c Mechanism of discontinuous precipitation of  $M_{23}C_6$  in a carburized austenitic weld overlay of 19Cr – 12Ni type

### 6.5 Massive Transformation

The Fig. 6.23 shows the binary diagram of Cu – Zn emphasizing the alloy with approx. 38 at. % Zn. For temperature levels exceeding approx. 800°C, the most stable condition of this alloy is represented by the phase  $\beta$ , whereas below approx. 500°C the most stable phase will be  $\alpha$  phase and the area between these temperatures show the stable mixture of phases  $\alpha + \beta$ . The type of transformation during decomposition of the phase  $\beta$  depends on the rate of cooling.

Slow and medium rates of cooling result in precipitation of particles of  $\alpha$  phase from the oversaturated  $\beta$  phase. Slow cooling prefers transformation at low undercooling levels with development of equiaxed grains of  $\alpha$  phase. Higher rates of cooling lead to transformation at lower temperature forming the Widmanstätten needle like morphology. As shown by the phase diagram of Cu – Zn, precipitating  $\alpha$  particles will contain more copper than the initial  $\beta$  phase, therefore the growth of  $\alpha$  phase will be subject to diffusion of zinc over a long distance, away from the moving  $\alpha/\beta$  interface. As copper and zinc occupy substitution positions, the diffusion process is relatively slow and that is why the curves showing formation of the  $\alpha$  phase in a CCT diagram are present at relatively long time intervals, Fig. 6.24.

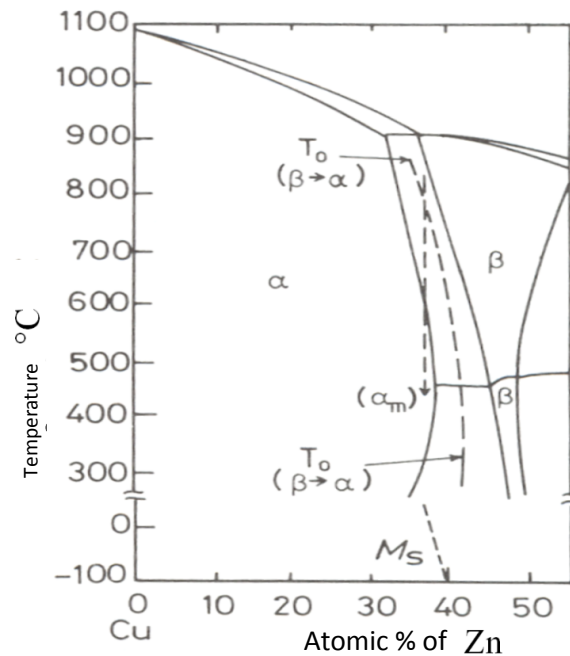


Fig. 6.23 Part of the Cu – Zn binary diagram showing equilibrium between phases  $\alpha$  and  $\beta$ . The values of Gibbs free energy will be the same in both phases at temperature  $T_0$  ( $G^\alpha = G^\beta$ ).

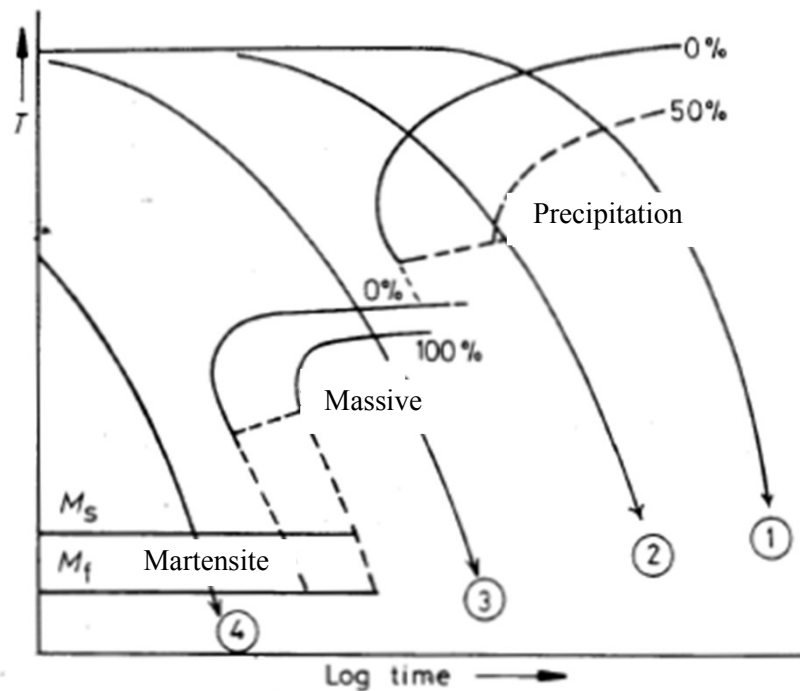


Fig. 6.24 Schematic CCT diagram for a system with massive transformation. Slow cooling (1) leads to precipitation of equiaxed grain of the  $\alpha$  phase, whereas faster cooling (2) creates the Widmanstätten morphology. Medium-rate cooling (3) results in development of a massive transformation, fast cooling (4) creates martensite.

In case the alloy is cooled fast enough, there is insufficient time for precipitation of the  $\alpha$  phase and the  $\beta$  phase can be preserved up to temperature levels below  $500^{\circ}\text{C}$ , where  $\beta \rightarrow \alpha$  transformation can occur without any change of the chemical composition. This is defined as the massive transformation. The Fig. 6.25 illustrates grains of the  $\alpha$  phase, which developed through the mechanism of massive transformation on interfaces of the master  $\beta$  phase; the starting temperature during hardening process is  $850^{\circ}\text{C}$ . A fast movement of the interface  $\alpha/\beta$  causes uneven appearance of grain boundaries. As the composition of phases  $\alpha$  and  $\beta$  is the same during massive transformation, massive particles  $\alpha$  ( $\alpha_m$ ) may grow as fast the atoms of Cu and Zn are able to cross the  $\alpha/\beta$  interface without the need to diffuse over a long distance. CCT diagrams show the massive transformation in the form of a separate C-curve. Migration of the  $\alpha/\beta$  interface is very similar to migration of grain boundaries during recrystallisation of a single-phase material. However, the driving force of massive transformation is several levels higher, which explains the high rate of massive transformation.



*Fig. 6.25 Massive  $\alpha$  phase grains at grain boundaries of  $\beta$  in the alloy Cu – 38 at. % Zn hardened at the temperature of 850°C using ice brine at 0°C. Dark particles along the grain interfaces represent precipitates that developed by means of the nucleation and growth mechanism (precipitation) at a high temperature.*

The  $\beta$  phase may transform into the  $\alpha$  phase via the massive mechanism, if the phase is cooled fast into the phase field of stable  $\alpha$  phase to prevent precipitation of the  $\alpha$  phase along the grain boundaries of  $\beta$  phase. As far as the thermodynamics is concerned, there is a theoretical possibility that massive transformation occurs at a higher temperature. One of the necessary prerequisites for massive transformation is that the free energy of the new phase is lower than the free energy of master phase of the same composition. Looking at an alloy comprising Cu – 38 at. % Zn, the value of  $G^\alpha$  is lower than  $G^\beta$  at temperatures below approx. 700°C. The temperature levels, at which  $G^\alpha = G^\beta$ , are linked with a dashed line in the Fig. 6.23. The massive transformation may theoretically occur within the two-phase field of the phase diagram anywhere below  $T_0$ . However, practical experience has proven that the massive transformation occurs within the single-phase area of the phase diagram only.

Massive transformations occur in a number of alloys. Iron and its alloys require that the rate of cooling within the austenite field is high enough to prevent development of equilibrium decomposition products and insufficient for progress of martensitic transformation too. Microstructure of massive ferrite in iron with uneven grain boundaries is shown in the Fig. 6.26.

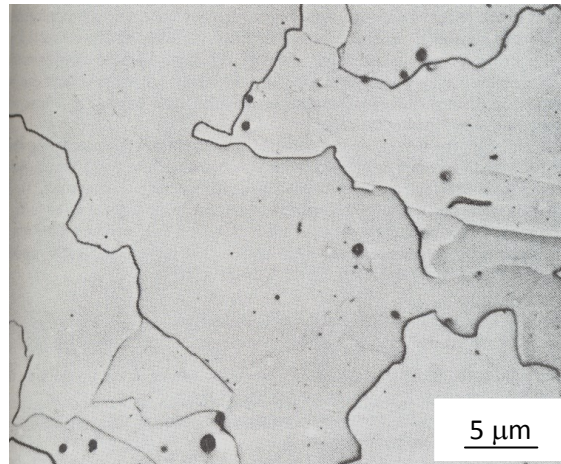


Fig. 6.26 Massive  $\alpha$  phase in Fe – 0,002%C alloy hardened from the temperature of 1000 °C into icy bath



### Summary of terms in this chapter

**Diffusional transformations:** caused by thermally activated movements of atoms across the interface. However, these phase transformations do not have to be accompanied by a change of chemical composition of phases. These transformations usually involve nucleation and the subsequent growth of nuclei.

**Precipitation:** a phase transformation associated with gradual removal of oversaturation from a solid solution due to formation of particles of the new phase. It is formally divided into three stages: nucleation, growth and coarsening.

**Coarsening of precipitates:** the final stage of precipitation, when the Gibbs free energy of the system drops due to a reduction of the total interfacial area. Small particles dissolve, large particles grow further but the volume fraction of precipitates remains constant.

**Precipitation sequence:** the initial stage of precipitation may produce metastable phases with a low nucleation barrier, these are gradually replaced with thermodynamically more stable phases.

**Kinetics of diffuse transformations:** the change of volume fraction of the new phase with time at a particular temperature can be described using the Johnson – Mehl - Avrami model. Knowledge of the progress of transformations in time at various temperatures enables processing of kinetic diagrams, e.g. TTT or CCT diagrams.

**Incubation period:** the period until the start of diffusion transformation, it corresponds to a detection time of stable particles of the new phase in the matrix. This parameter is strongly temperature dependent.



## Questions addressing the content covered

1. Write the general scheme of eutectoid transformation.
2. What are the characteristics of massive transformation?
3. Derive the equation 6.6 and conclude the relations applicable to the critical radius of nucleus and the critical nucleation barrier.
4. What makes the heterogeneous nucleation more efficient as compared to the homogeneous nucleation?
5. What are the stages of precipitation process?
6. What is the difference between the stages of growth and coarsening of precipitates?
7. Write and explain the Wagner equation.
8. What is the incubation period of diffusion transformations?
9. Write and explain the Johnson-Mehl-Avrami model.
10. What are the precipitation sequences?
11. Describe the mechanism of spinodal decomposition.
12. What are the basic characteristics of massive transformations?



## Exercises

### Exercise 1

The approximate formula for the total driving force for precipitation in a regular solution is:

$$\Delta G_o = RT \left[ X_o \ln \frac{X_o}{X_e} + (1 - X_o) \ln \frac{(1 - X_o)}{(1 - X_e)} \right] - \Omega (X_o - X_e)^2 \quad (6.34)$$

- a) Use this equation to evaluate the total driving force released during transformation of  $\alpha' \rightarrow \alpha + \beta$  at 600K, if  $X_o=0,1$ ,  $X_e = 0,02$  and  $\Omega = 0$  (ideal solution),
- b) Estimate the volume fraction of precipitate in the equilibrium state, if  $\beta$  is the pure component B ( $X_B^\beta = 1$ ). Assume the molar volume is constant.
- c) If there is an alloy thermally processed to create a dispersion of precipitate with the pattern of 50 nm, determine the total of the  $\alpha/\beta$  interface in  $1\text{m}^3$  of alloy. Assume the precipitate distribution in corners of cubes with the edge length of 50 nm.
- d) If the interfacial energy is  $\gamma_{\alpha\beta} = 200 \text{ mJm}^{-2}$ , what is the total interfacial energy per  $1\text{m}^3$  and per 1 mole of alloy? ( $V_m = 10^{-5} \text{ m}^3$ ).
- e) What amount of the driving force will remain as the interfacial energy in the above mentioned case?
- f) Repeat steps c – e for precipitation of particles with the distance of  $1 \mu\text{m}$ .

*Solution:*

a) Substitution into the equation (5.32) above produces the following result:  $\Delta G_o = 420,3 \text{ J mol}^{-1}$

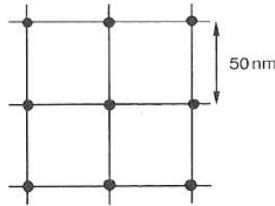
b) Using the lever rule, calculate the following:

$$\text{molar fraction of precipitate} = \frac{(X_o - X_e)}{(X_\beta - X_e)} = 0.08$$

Provided the molar volume is independent of composition, this will be the volume fraction of precipitate too.

c) Assuming the particles precipitate in corners of a cube with edge length of 50 nm, the number of particles per

$1 \text{ m}^3$  will be calculated as follows:  $\frac{1}{(50 \times 10^{-9})^3} = 8 \times 10^{21} \text{ particles per m}^{-3}$



Assume the volume of each particle is the same, the particles are spherical with the radius  $r$ . The total volume of particles per  $1 \text{ m}^3$  can be calculated as follows:

$$8 \times 10^{21} \times \frac{4}{3} \pi r^3 = 0,08 \text{ m}^3, \text{ particle radius } r = 13.4 \text{ nm}.$$

The total surface area of the interphase interface per  $1 \text{ m}^3$ :  $8 \times 10^{21} \times 4\pi r^2 = 1.8 \times 10^7 \text{ m}^2$

d) If  $\gamma_{\alpha\beta} = 200 \text{ mJm}^{-2}$

The total interfacial energy =  $200 \times 1.8 \times 10^7 = 3,6 \times 10^6 \text{ Jm}^{-3}$  of the alloy =  $36 \text{ Jmol}^{-1}$

e) Ratio remaining as the interfacial energy =  $\frac{36}{420,3} = 9\%$

f) with the particle spacing of  $1 \mu\text{m}$ :

$$\text{the number of particles per } 1 \text{ m}^3 = \frac{1}{(1 \times 10^{-6})^3} = 1 \times 10^{18} \text{ m}^{-3}$$

Using the same method as for item c) the particle radius is 267 nm.

The total interfacial surface area of particles per  $1 \text{ m}^3 = 1 \times 10^{18} \times 4\pi \times (2.67 \times 10^{-7})^2 = 8.96 \times 10^5 \text{ m}^2$

Total interfacial energy =  $1.8 \times 10^5 \text{ Jm}^{-3}$  of alloy =  $1.8 \text{ Jmol}^{-1}$

Ratio remaining as the interfacial energy = 0.4 %.

## 7. Diffusionless Transformations



**Study time:** 5 hours



**Objective:** Completion of this chapter will enable you:

- define the basic characteristics of diffusionless transformations,
- define the characteristic temperatures of martensitic transformation,
- explain the shape deformation and surface relief during martensitic transformation,
- describe the crystallography of martensitic transformation in steels,
- characterize terms as "thermoelastic martensitic transformation" and "self-accommodation martensite",
- explain the models of pseudoelastic behaviour and shape memory effect.



### EXPLANATION

Transformations defined as *diffusionless transformations* are associated with individual atomic movements shorter than one interatomic spacing. This product develops in steels during cooling from the austenitizing temperature at the rate exceeding the critical rate – the cooling curve may not intersect the C curves defining diffusional decomposition of austenite in the CCT diagram. The product of diffusionless transformation in iron-based alloys is called *martensite*. However, this term is also used in other metal and non-metal materials. Because of the technological importance of hardened steel, significant part of this chapter will be dedicated to characteristics of martensite in iron-based alloys.

#### 7.1 Martensite in Iron Alloys

Martensite in steels represents oversaturated solid solution of carbon in ferrite. As you already learnt in the course called *Materials Science*, cavities present between the basic atoms in elementary cells are defined as tetrahedral or octahedral. The size of these cavities can be calculated provided atoms are seen as solid spheres of the same size. For a FCC lattice, the size (diameter) of these cavities will be:  $d_{\text{tet.}} = 0.225D$  and  $d_{\text{oct.}} = 0.414D$ , where  $D$  is the diameter of basic atom in the elementary cell. As for  $\gamma$  iron ( $D = 0.252 \text{ nm}$ ), the size of

interstitial cavities reaches the following values:  $d_{\text{tetr.}} = 0.0568 \text{ nm}$  and  $d_{\text{oct.}} = 0.104 \text{ nm}$ . The diameter of one atom of carbon is approx.  $0.154 \text{ nm}$ . This means that the presence of interstitial atom of carbon in the FCC elementary cell of iron induces a significant distortion of the lattice. Octahedral positions are occupied with preference.

The size (diameter) of interstitial cavities in the BCC lattice is:  $d_{\text{tetr.}} = 0.291D$  and  $d_{\text{oct.}} = 0.155D$ . Although the octahedral position is smaller than the tetrahedral one, interstitial atoms occupy it with preference. This is related to the magnitude of shift of basic atoms surrounding the octahedron cavity: shift of two atoms is larger than that of the rest four atoms. The BCC lattice contains more "free" space than lattices with close-packed configurations of atoms (FCC, HCP). However, the greater number of interstitial positions in the BCC elementary cell causes the situation, when the "free" space pertaining to each interstitial position within the BCC lattice is smaller. Occupying of octahedral positions by carbon atoms can cause a significant distortion of the BCC lattice, Fig. 7.1.

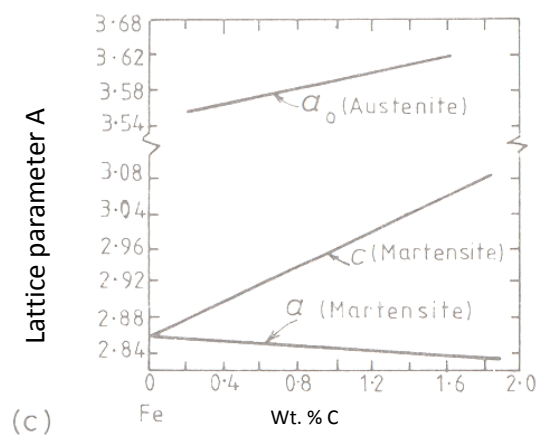
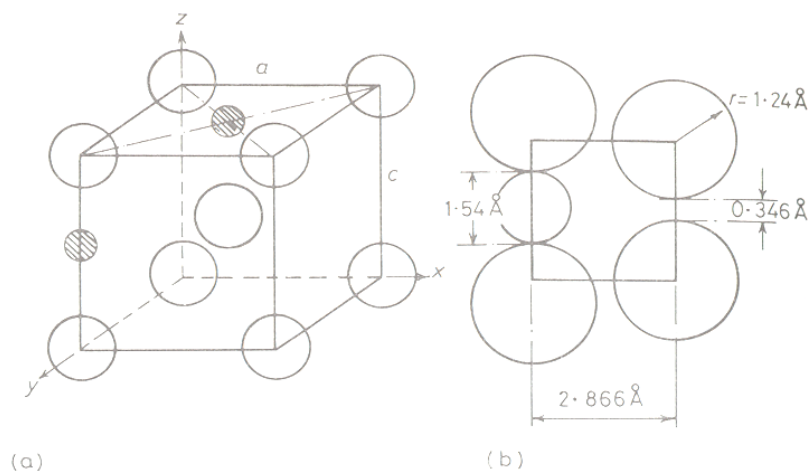


Fig. 7.1 Martensite in Fe – C alloys, a) octahedral positions (dashed) for interstitial atoms in the BCC lattice, b) large lattice distortion caused by the atom of carbon in octahedral

position, *c*) changes of lattice parameters *a* and *c* as a function of carbon content in Fe – C alloys

Preferential occupation of octahedral positions  $00\frac{1}{2}$  with carbon atoms results in distortion of the BCC elementary cell to form a tetragonal body centred cell. Distortion of the elementary cell of martensite by carbon atoms causes high hardness of martensite in Fe – C alloys. X-ray diffraction analysis at the temperature of  $-100^{\circ}\text{C}$  (to prevent diffusion of carbon) has found out that the ratio of axes *c/a* in the tetragonal unit cell is a linear function of carbon content in Fe – C alloys:

$$c/a = 1.005 + 0.045 (\text{hm.\%C}) \quad (7.1)$$

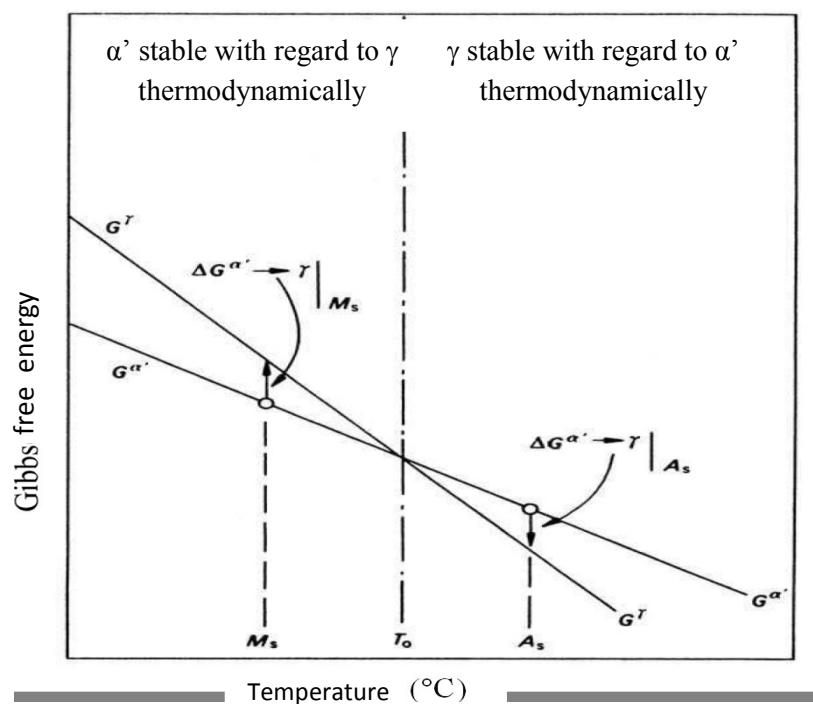


Fig. 7.2 Thermodynamic driving force during martensitic transformation ( $M_s$ ) and reverse transformation ( $A_s$ )

Martensite starts to develop during undercooling below the temperature  $M_s$ , which is called "martensite start". This temperature is associated with a certain driving force for diffusionless transformation of austenite into martensite, Fig. 7.2. The temperature  $M_s$  in low-carbon steels is approx.  $550^{\circ}\text{C}$ , it will drop rapidly with the rising content of carbon in the system of Fe – C, Fig. 7.3. The temperature  $M_f$ , which is called "martensite finish", represents the temperature, under which the fraction of martensite will stop rising.  $M_f$  does not have to correspond with 100 % of martensite, microstructure may retain some retained austenite. Maintenance of a certain fraction of austenite in the resultant microstructure can be supported by high value of elastic tensile stress between plates developing in the final stage of

transformation. This limits further growth and thickness increase of martensitic plates. The fraction of austenite remaining in Fe – C alloy generally increases with the rising carbon content.

Deformation of austenite leads to the rise of temperature of martensite transformation start. The temperature  $M_d$  is defined by the maximum rise in temperature  $M_s$  due to plastic deformation of austenite. Nevertheless, it is very likely that deformation of austenite below the temperature  $M_d$  will change the temperature  $M_s$  during the subsequent undercooling of alloys into the range of martensite formation. These circumstances will usually lead to a reduction in temperature  $M_s$  – the improved stability of austenite is defined as mechanical stabilisation.

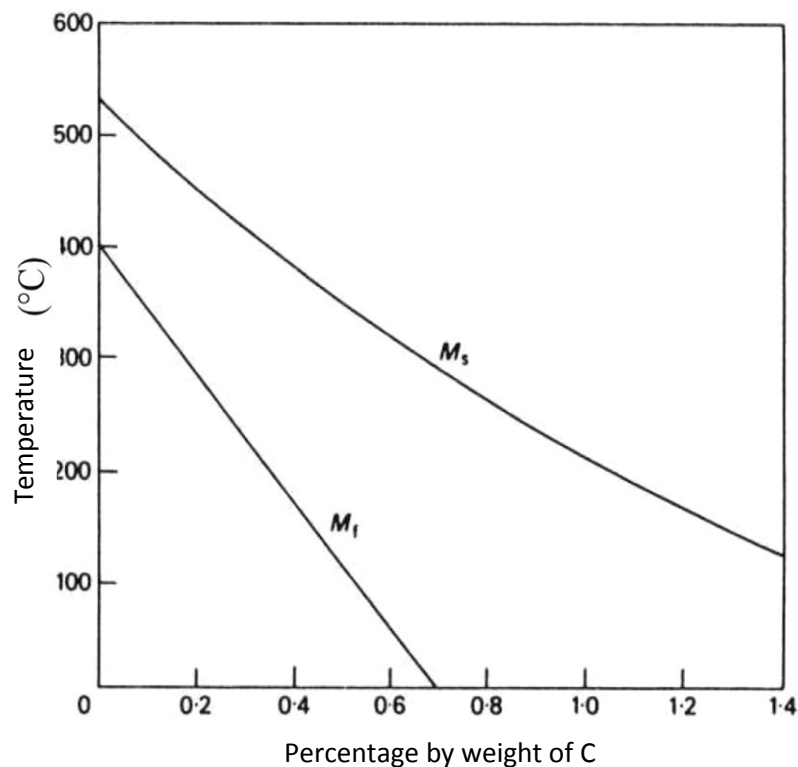


Fig. 7.3 Dependency of temperatures  $M_s$  and  $M_f$  on carbon content in Fe – C alloys

Similar deformations of martensite will be accompanied by shift of temperatures  $A_s$  (austenite start) towards lower values. The minimum temperature of the deformed martensite transformation to austenite is defined as temperature  $A_d$ . The temperature  $T_0$  in Figs 7.2 and 7.4 represents the temperature, at which the values of Gibbs free energy of austenite and martensite are the same.

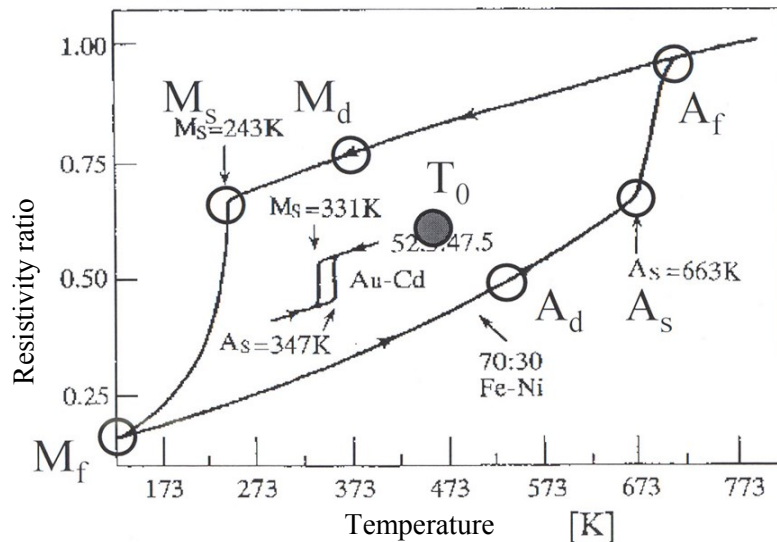


Fig. 7.4 Effect of deformation on the shift of transformation temperatures

### 7.1.1 Shape Deformation during Martensitic Transformation

Profile distortion is a characteristic feature of martensitic transformation. The glissile movement of dislocations creates a level step at the point, where the glissile plane cuts the crystal, Fig. 7.5. Movement of many dislocations at parallel glissile planes causes a macroscopic shear. Glissile movement of dislocations includes a change to the crystal shape but it does not alter the crystal structure. Martensitic transformation brings a change to the atomic configuration by means of process, which reminds of shear deformation, into new positions corresponding with martensite. That is why the crystal undergoing transformation must be subject to the corresponding macroscopic change of shape. Dislocations responsible for deformation are located within the interface  $\alpha'/\gamma$ , these induce deformation when moving, together with a change of crystal structure to martensite. This is the so called *glissile interface*.

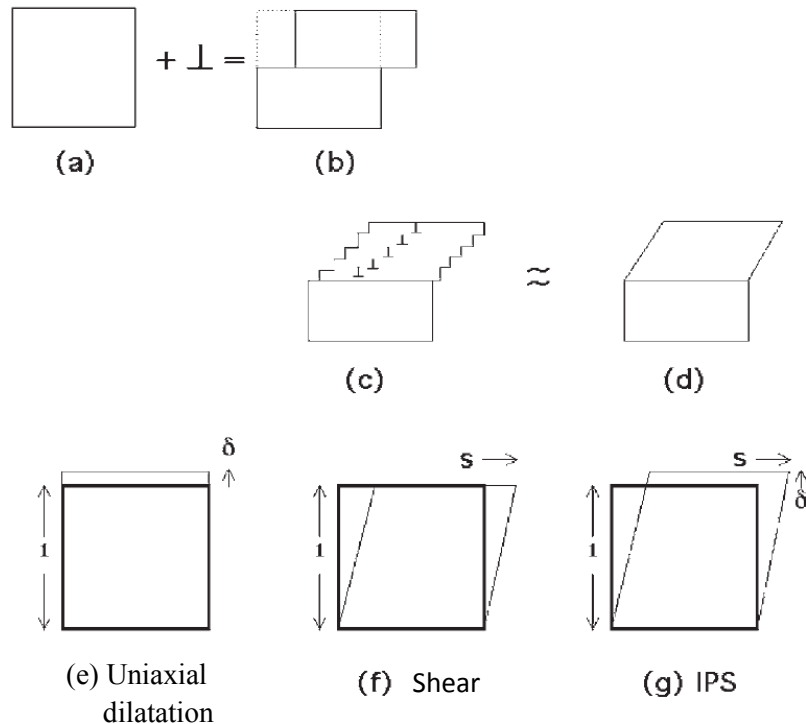


Fig. 7.5a) and b) level caused by glissile movement of dislocations, c) and d) a big number of glissile dislocations causes a macroscopic shear, e) deformation with an invariant plane associated with a uniaxial dilatation, f) deformation with an invariant plane associated with shear, g) IPS - deformation with an invariant plane, which represents a combined effect of dilatation and shear

Due to the elastic deformation during martensitic transformation, the initial straight surface of the sample is inclined around the line that represents intersection of the interface plane and the free surface, it gives rise to so called **surface relief**. The metallographic examination shown in the Fig. 7.6a carried out on a polished sample which was scratched with a series of parallel lines before undercooling to the temperature  $M_s$ . Creation of a martensitic crystal caused a change to inclination of lines but the continuity of lines in the vicinity of the  $\alpha'/\gamma$  interface remained intact. Intact coherence of lines shows that the shape deformation does not cause any rotation of the interface plane – otherwise keeping of coherence between austenite and martensite would require plastic deformation to cause additional shift of lines within the interface. In order to keep the interface plane  $\alpha'/\gamma$ , the so called **habit plane** (Fig. 7.6b), undistorted during transformation, martensitic transformation can be imagined as a homogeneous shear deformation at the direction parallel to the interface - see the arrows in Fig. 7.6a. The transformation  $\gamma \rightarrow \alpha'$  is also associated with approx. 3 – 4% dilatation, which takes place perpendicularly to the habit plane, see Fig. 7.5.

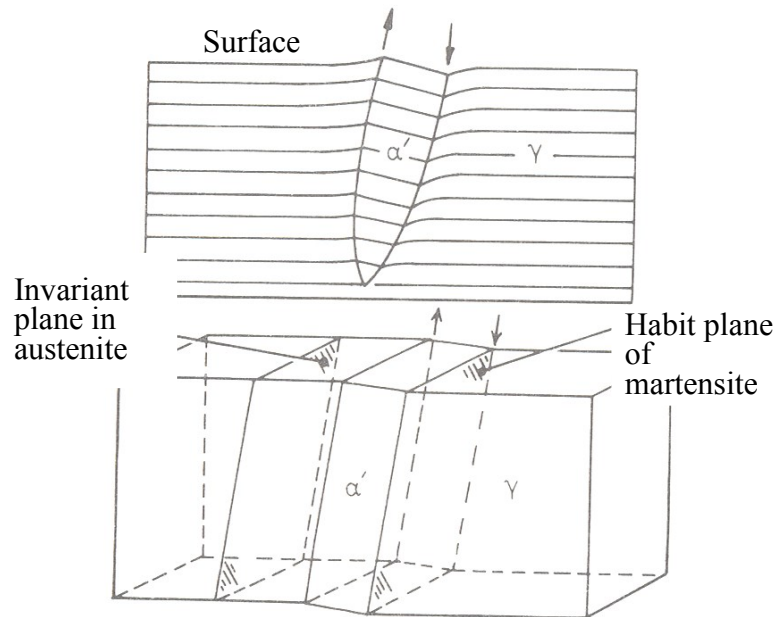


Fig. 7.6 a) Development of surface relief during martensitic transformation, b) unrotated and undistorted interface plane  $\gamma/\alpha'$  is called "the habit plane"

Creation of martensite is associated with coordinated movement of atoms. That results in a close relationship between the lattices of austenite and martensite. Every martensitic transformation has a reproducible **orientation relationship** between lattices of the master phase and martensite. This relationship is usually expressed by parallelism of close - packed planes and close - packed directions lying in these planes.

X-ray diffraction was used to define the following two orientation relationships in various iron-based alloys:

$$\text{Kurdjumov – Sachs relation: } \{1\ 1\ 1\}_{\gamma} // \{0\ 1\ 1\}_{\alpha}, \langle 1\ 0\ \bar{1} \rangle_{\gamma} // \langle 1\ \bar{1}\ 1 \rangle_{\alpha}, \quad (7.2)$$

$$\text{Nishiyama – Wasserman relation: } \{1\ 1\ 1\}_{\gamma} // \{0\ 1\ 1\}_{\alpha}, \langle 1\ 0\ \bar{1} \rangle_{\gamma} // \langle 1\ 00 \rangle_{\alpha} \quad (7.3)$$

These orientation relationships differ in terms of rotation around  $\langle 1\ 1\ 1 \rangle_{\alpha}$  by the angle of  $5.3^{\circ}$ . Progressive development in experimental methods led to conclusion that the definition of above mentioned orientation relationships is approximate only. The actual orientation relationships are irrational, i.e. these cannot be exactly expressed by parallelism of planes with low Miller indices.

### 7.1.2 Crystallography of Martensitic Transformation in Steels

Martensitic transformation is diffusionless, so the change of crystalline structure occurs in terms of homogeneous deformation of the initial austenite. The deformation required for transformation of FCC lattice of austenite into BCC lattice of martensite was firstly designed

by Bain, Fig. 7.7. The FCC lattice shows a tetragonal body - centred elementary cell (parameters  $a_\gamma/\sqrt{2}$ ,  $a_\gamma$ ). Its transformation into a BCC unit cell with lattice parameter  $\alpha'$  of martensite requires an even expansion in the plane  $(001)_\gamma$  by approx. 12 % and compression along the axis  $[001]_\gamma$  by approx. 17 %. The **Bain model** implies the following orientation relationship between the initial lattice of austenite and martensite:

$$[001]_\gamma // [001]_\alpha \quad [1\bar{1}0]_\gamma // [100]_\alpha \quad [110]_\gamma // [010]_\alpha \quad (7.4)$$

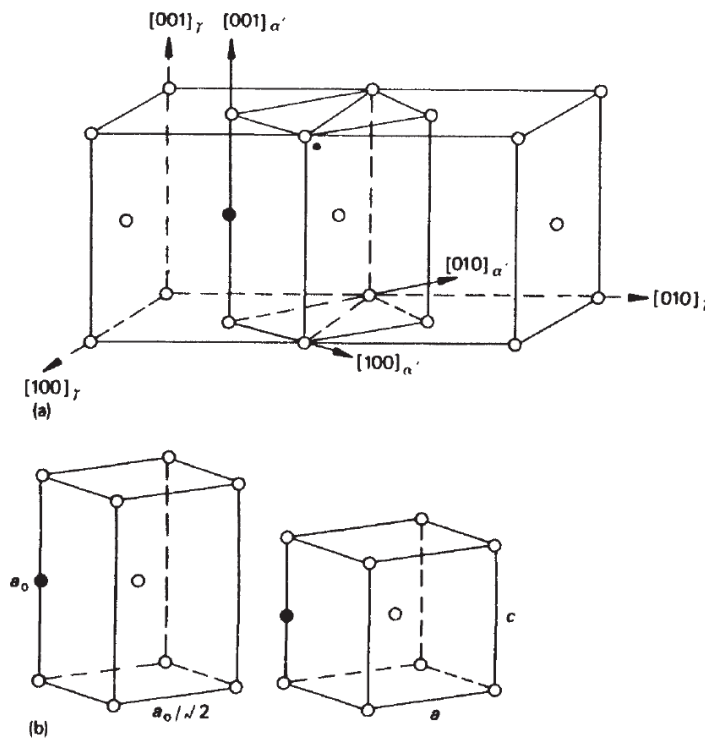


Fig. 7.7 Model of lattice correspondence for development of martensite out of austenite, a) tetragonal elementary cell in austenite, b) distortion of a tetragonal cell of austenite with development of a tetragonal or BCC unit cell of martensite

However, this orientation relationship has not been confirmed by experiments. The main cause is that the Bain deformation does not represent a full deformation, as it requires a high level of interface coherence. Any deformation transformation of austenite into martensite must keep one line invariant, i.e. undeformed and undistorted. Such deformation is called **deformation with invariant line**. The Fig. 7.8 shows austenite as a sphere deformed into a rotation ellipsoid due to Bain deformation (**B**). Deformation **B** does not leave any line that is undeformed and undistorted. Lines  $wx$  and  $yz$  are undistorted but they are rotated into new positions  $w'x'$  and  $y'z'$ . Such rotated lines are not invariant. Nevertheless, a combination of **Bain deformation (B)** and **rotation of a solid body (R)** results in overlapping of lines  $yz$  and

$y'z'$ , it is therefore a deformation with invariant line. That is the reason, why the orientation relationship derived from the Bain correspondence has not been proven by experiments.

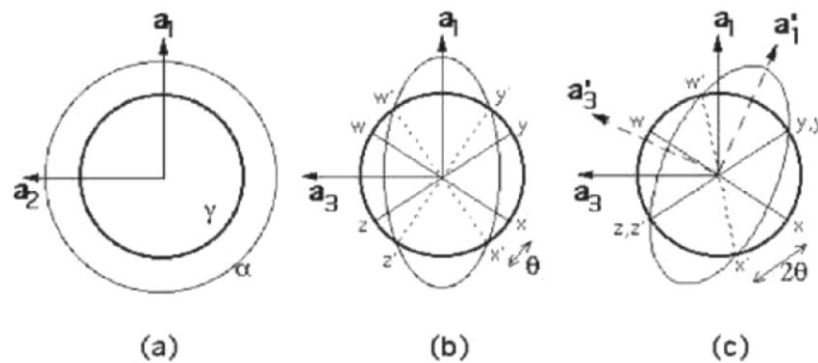


Fig. 7.8 a) and b) show the impact of Bain deformation on austenite, which is represented by a sphere in its initial state. Pure deformation transforms the sphere into a rotation ellipsoid. c) deformation with invariant line is obtained by combination of Bain deformation and rotation of the solid body by the angle  $\theta$ , parameters  $a_1$ ,  $a_2$  and  $a_3$  are relevant to axes  $[100]_\gamma$ ,  $[010]_\gamma$  and  $[001]_\gamma$ .

Another problem is the fact that no rotation can change the Bain deformation  $\mathbf{B}$  into **deformation with invariant plane**. Such situation would require existence of two parallel invariant lines. This implies that austenite cannot be transformed into martensite by means of a homogeneous deformation, which leaves one of the planes invariant. Nevertheless, experimental examination of products of the martensitic transformation proves that shape deformation leaves one interface plane between austenite and martensite invariant. Phenomenological theory of martensite crystallography deals with this problem in an elegant way: Bain deformation changes the structure of initial phase into the structure of martensite. Due to combination with a solid body rotation the homogeneous deformation ( $\mathbf{RB}$ ) corresponds to an invariant line deformation – steps a to c in Fig. 7.9. Nevertheless, the shape deformation observed matches the shape deformation with invariant plane  $\mathbf{P}_1$  (step a  $\rightarrow$  b in Fig. 7.9) but that produces an incorrect crystalline structure of martensite. In case the second homogeneous shear deformation  $\mathbf{P}_2$  is combined with the deformation  $\mathbf{P}_1$  (step b  $\rightarrow$  c), this will produce the correct structure and a wrong profile:

$$\mathbf{P}_1\mathbf{P}_2 = \mathbf{RB} \quad (7.5)$$

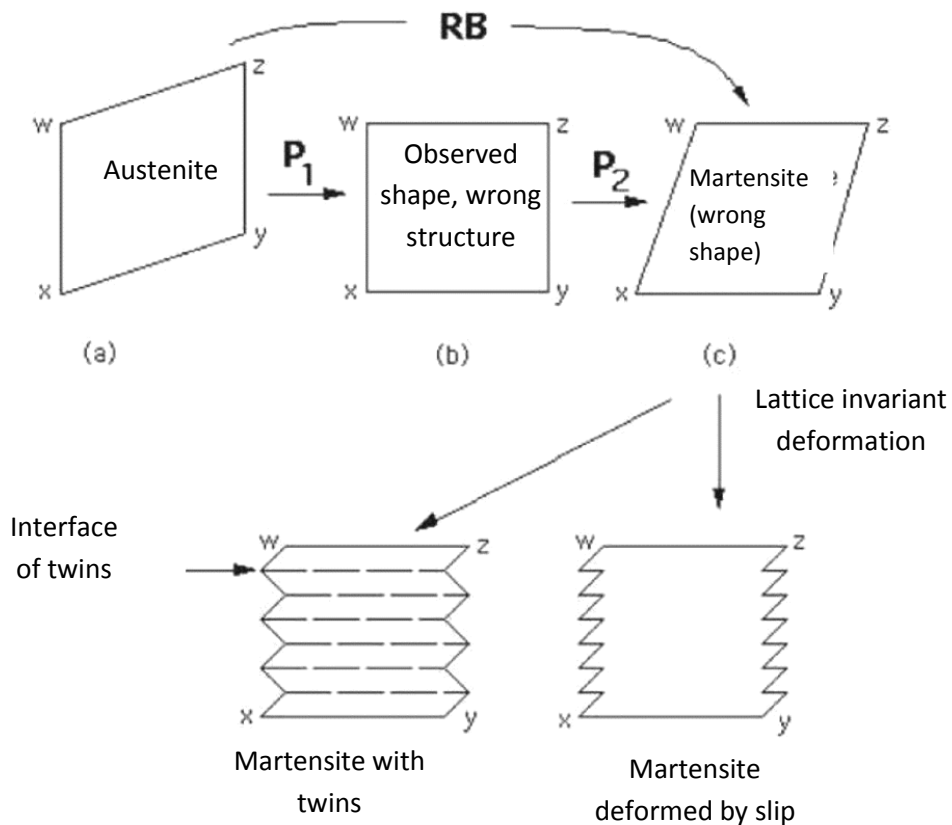


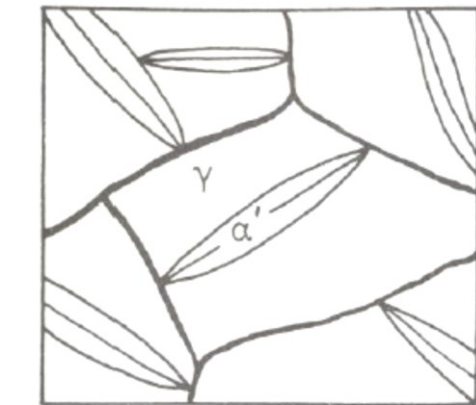
Fig. 7.9 Phenomenological theory of martensitic transformation

These problems are solved, if the impact of  $P_2$  on shape deformation is invalidated by the macroscopically inhomogeneous invariant deformation of lattice, which may occur either by slip or twinning, Fig. 7.9. The theory explains all characteristics of martensite crystallography observed. The orientation relationship is predicted when the Bain deformation is supplemented by rotation, which results in deformation with invariant line. The habit plane has no rational indices, as the magnitude of lattice invariant deformation is usually not rational. The theory predicts that substructure of martensite may include dislocations or twins. The martensitic transformation occurs to ensure a macroscopic match of the shape deformation and the invariant plane, as this enables reduction of the total strain energy.

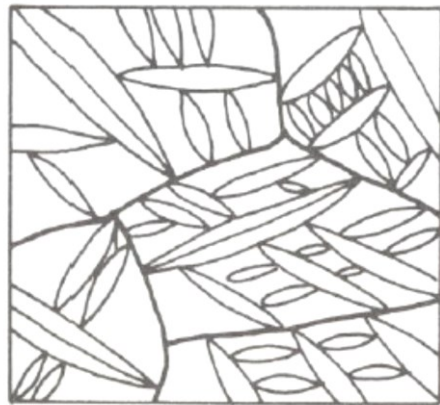
### 7.1.3 Morphology of Martensite in Iron Alloys

Martensitic crystals often adopt plate-like shapes and they are spread over the full width of the prior austenitic grain. It has been proven that *martensitic plates* grow at very high rate, which approximates the speed of sound in metals. Martensite can usually grow independent of thermal activation; this is called the *athermal growth*. Fig. 7.10 a,b documents that the volume fraction of martensite rises through gradual transformation of austenite, which is

preserved among the martensite plates already present. The first plates of martensite with a large free path to grow (depends on the size of the austenitic grain) may induce development of micro-defects due to their dynamic effects when impacting on prior austenite grain boundaries. The free path of further developing plates will be shorter, Fig. 7.10b.



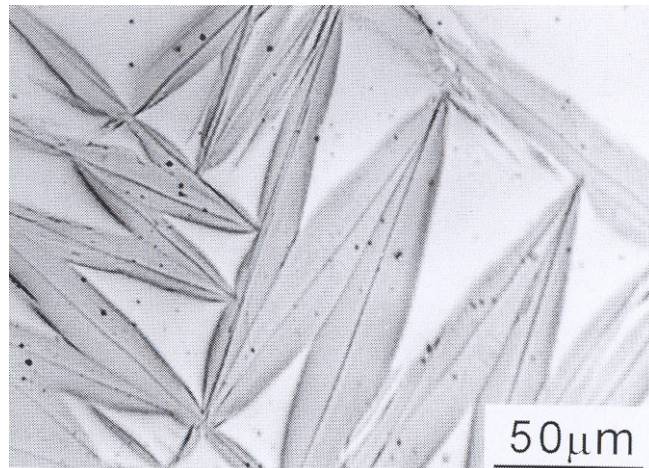
(a)



(b)

Fig. 7.10 a) and b) Growth of martensitic plates in high-carbon austenite below the temperature  $M_s$ ,  
c) morphology of plate-like martensite in alloy Fe-Ni-C,  
Remark: in plate centres are ribs, the so called "midribs"

(c)



Martensitic plates cannot grow beyond the prior austenite grain boundary, as austenitic grains are usually separated by high-angle boundaries and a transition into the adjacent grain would infringe the orientation relationship between the austenitic matrix and the martensitic plate. Martensitic transformation in high-carbon steels never runs until the very end, there is some retained austenite left among martensitic plates. Another feature of martensite in such steels is the autocatalytic effect ("burst") demonstrated by the process, when one martensite plate triggers nucleation of several other plates in its vicinity, probably because of local stress concentration, when the first martensite plate hits an obstacle, e.g. boundary of the prior austenite grain.

Martensitic plates in steels with carbon content exceeding approx. 0.6 wt. % usually adopt lenticular shape that is caused by restrictive effects of lattice, which prevents shape deformation accompanying the martensitic transformation. That complicates accurate

determination of the habit plane. The habit plane of plate-like martensite is irrational and it is close to planes type  $\{225\}_\gamma$  in medium-carbon steel, while it is near the planes type  $\{259\}_\gamma$  in high-carbon steels.

The progress of transmission electron microscopy enabled experiments to prove that martensite may contain both dislocations as well as transformation twins. Centres of martensite plates show the midribs in some alloys, every midrib is surrounded with high quantities of thin transformation twins. Twins on plate peripheries may be replaced with high density of dislocations, Fig. 7.11. The density of dislocations in iron-based martensite reaches the levels of  $10^{11} - 10^{12} \text{ cm}^{-2}$ , which is the value close to density of dislocations in metals subjected to intensive cold plastic deformation. The ratio comprising areas with twins or dislocations in particular martensite plates is a sensitive function of chemical composition of alloys.

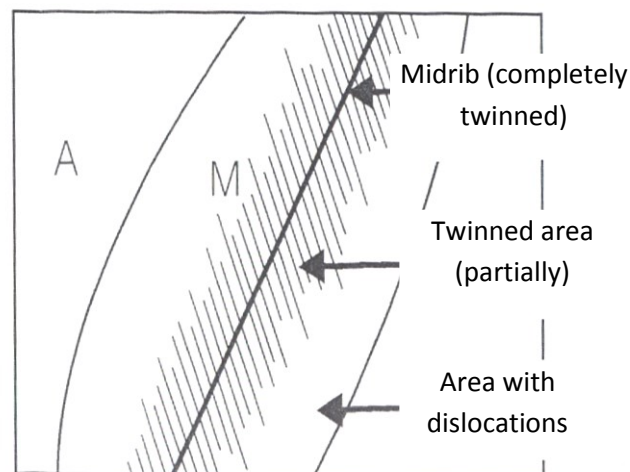


Fig. 7.11 Internal structure of martensitic plate (M) in a high-carbon steel

Low carbon steels develop the lath martensite-formed by long and approx.  $0.5 \mu\text{m}$  wide laths. Individual laths represent separated cases of nucleation, which is evidenced by thin films of retained austenite between laths. Groups of parallel laths form blocks, where individual laths are usually separated by low angle boundaries, Fig. 7.12. One prior austenite grain may include several packets formed by blocks that are usually separated by high angle boundaries. The habit plane of lath martensite approximates the planes type  $\{111\}_\gamma$  and that is why individual prior austenite grains contain max. 4 packets of martensitic laths. The volume fraction of retained austenite in lath martensite is usually very low ( $< 5 \text{ vol.}\%$ ). Inhomogeneous invariant deformation within martensitic laths occurs almost exclusively by means of slip mechanism.

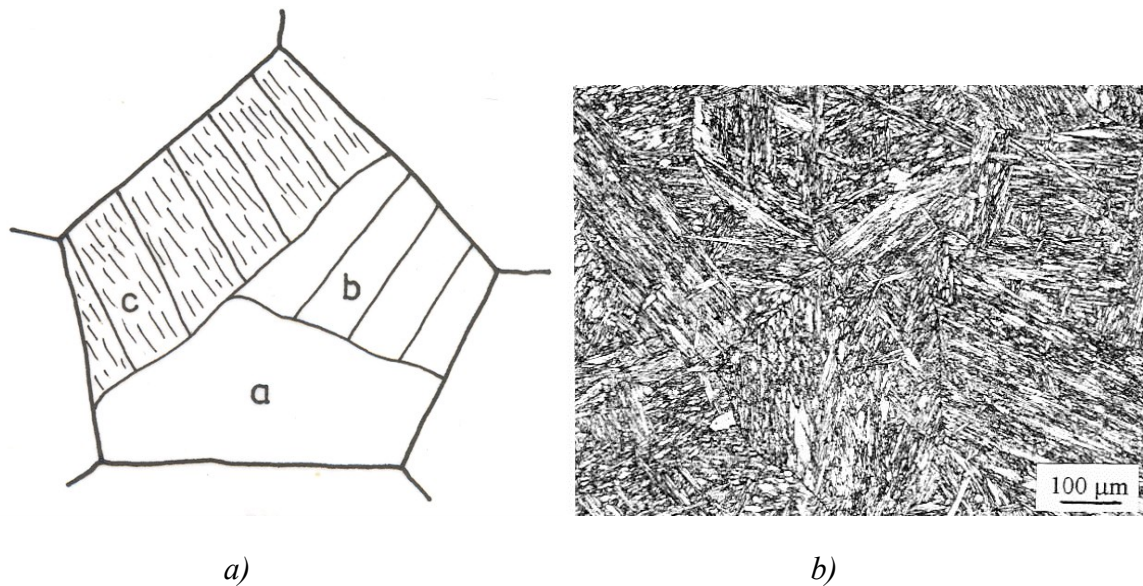


Fig. 7.12 a) Scheme of internal structure of lath (dislocation) martensite, a) Packets, b) Blocks, c) Martensitic laths, b) Lath martensite in a modified 9%CrMoV steel

#### 7.1.4 Nucleation and Martensite Growth

The driving force for start of martensitic transformation can be expressed as  $T_0 - M_s$ , where  $T_0$  is the temperature, at which the free energy of martensite and austenite is the same, Fig. 7.2. This figure also shows the temperature  $A_s$ , when martensite starts transforming back into austenite during annealing. Experimental examinations have shown that systems with significant shape deformation during the martensitic transformation involve a large driving force and the temperature interval  $M_s - M_f$  is broad. As far as iron based alloys are concerned, the difference between temperatures  $M_s$  and  $M_f$  amounts to approx. 200°C. The deformation energy following the development of a small martensitic plate likely plays an important role in the nucleation process. Athermal reaction may be handled with application of the classic theory of homogeneous nucleation, where:

- a) nuclei develop fast upon achievement of  $M_s$ ,
- b) subcritical nuclei exist in the initial lattice and these become supercritical upon achievement of  $M_s$  temperature.

The total change of free energy during nucleation comprises three terms:

- Change of the chemical free energy ( $\Delta G = G_{\alpha'} - G_{\gamma}$ ),
- Strain energy,
- Interfacial energy between austenite and martensite.

The following formula applies to a semicoherent nucleus of martensite of oblate shape with the radius  $r$  and half thickness  $c$ :

$$\Delta G = \frac{4}{3}\pi r^2 c \Delta G + \frac{4}{3}\pi r c^2 A + 2\pi r^2 \gamma \quad (7.6)$$

where A is the factor of strain energy,  $\gamma$  is the energy of  $\gamma/\alpha'$  interface per unit of area and  $\Delta G$  is the change of chemical free energy per unit of volume.

The critical size of nucleus is determined by the minimum of  $\Delta G$ :

$$c^* = -2\gamma/\Delta G, r^* = 4A\gamma/\Delta G^2 \quad (7.7)$$

and the critical barrier is defined as:

$$\Delta G^* = 32\pi A^2 \gamma^3 / 3\Delta G^4 \quad (7.8)$$

Substituting the equation (7.8) with rational values of  $\Delta G$ , A and  $\gamma$ , the calculated value of  $\Delta G^*$  is so high that the nucleation barrier is too large. However, it is very unlikely in this respect that nucleation of martensite could occur due to random fluctuations. Results obtained by these calculations indicate that nucleation of martensite must occur by heterogeneous nucleation on the already existing nuclei, which are assumed to lie beyond the maximum threshold on the curve of free energy. Nevertheless, there has been no experimental evidence submitted to prove the existence of such nuclei.

It has been assumed that the nuclei have a semicoherent dislocation interface with austenite in form of parallel dislocation loops, which link the nucleus with surrounding lattice, Fig. 7.13. The growth then occurs by nucleation of new dislocation loops that enlarge the original nucleus. The growth of particular martensitic plates occurs at an extremely high rate of the order of  $10^3 \text{ ms}^{-1}$ . It has been discovered that the growth rate is constant within a broad range of temperatures, which indicates that there is not strong thermal activation of the growth process. That complies with the fact that the transformation does not involve any diffusion. The assumption is that growth occurs by movement of the array of parallel dislocations with the same Burgers vector lying in the interface. When the  $\gamma/\alpha'$  interface moves into austenitic lattice, dislocations move by slip mechanism along the relevant slip planes (glissile interface). The movement of dislocations is associated with the movement of habit plane, the movement of interface occurs at the direction perpendicular to this plane.

There are generally three different types of kinetics for martensite formation, Fig. 7.14:

a) **athermal transformation**, where the fraction of austenite transformed depends on the transformation temperature only and the dependency of martensite fraction on the transformation temperature is of sigmoidal shape,

b) athermal transformation, which begins with a fast formation of a significant fraction of martensite ("burst") – this martensite fraction forms isothermally. Further formation of martensite upon temperature drop occurs athermally.

c) *isothermal transformation*, the martensite fraction at a particular temperature is proportional to transformation time. Transformations of this type occur in carbon free iron based alloys, e.g. Fe – Ni.

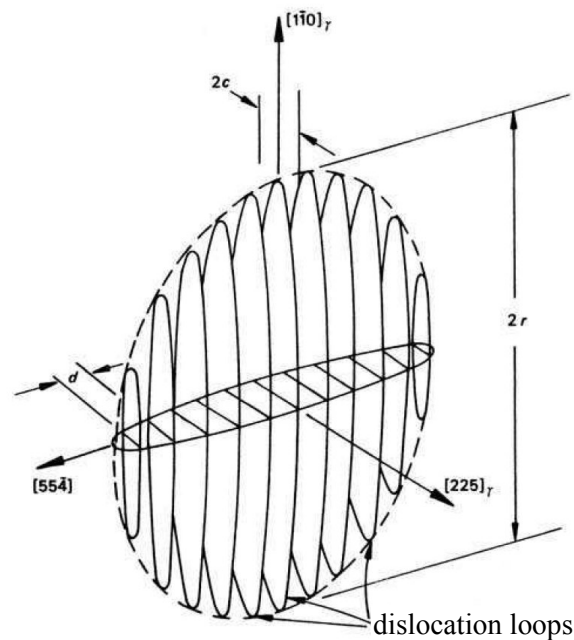


Fig. 7.13 Dislocation model of martensite nucleus

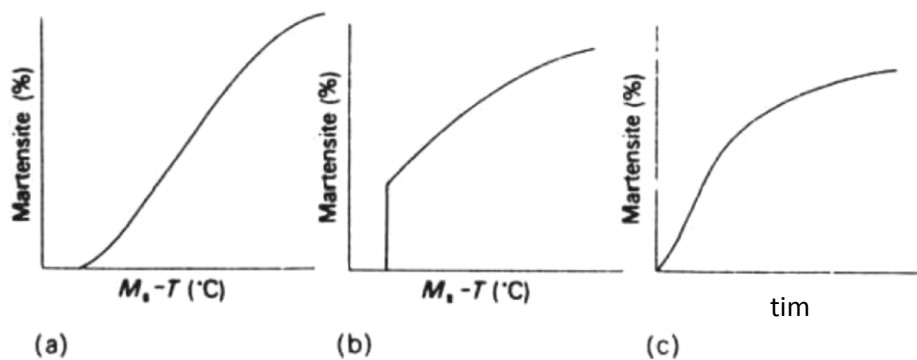


Fig. 7.14 Transformation curves of martensite, a) athermal transformation, b) athermal transformation with the autocatalytic ("burst") effect, c) isothermal transformation

## 7.2 Shape Memory Effect and Superelasticity

Martensitic transformation may be associated with special effects in some alloys. These effects include mainly *superelasticity* and *shape memory effect*. The Fig. 7.15 shows stress - temperature dependence with designated areas, where transformation superelasticity (SE) and

shape memory effect (SME) may occur. Both effects are applicable only to those levels of stress lying below the critical stress for slip, i.e. the mobility of  $\gamma/\alpha'$  interface must not be degraded by plastic deformation. **Transformation Superelasticity** is associated with the stress induced martensitic transformation in a high temperature phase ( $T > A_f$ ). Superelasticity can also develop at temperatures below  $M_f$ . Such case involves re-orientation of the martensitic variants present in the martensitic microstructure, that is why this is called the **re-alignment superelasticity**.

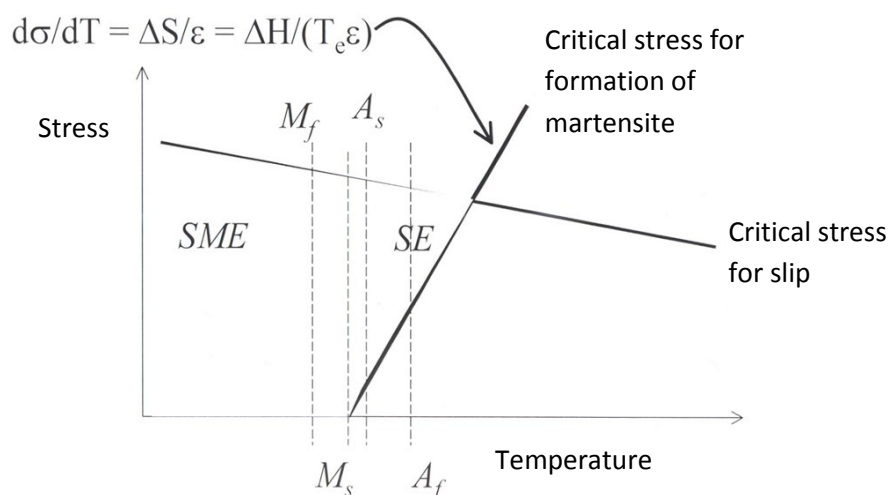


Fig. 7.15 Temperature-stress areas of existence of the transformation superelasticity (SE) and shape memory effect (SME)

Shape memory effect is closely related to the martensitic transformation, nevertheless this effect occurs in some systems only, where the martensitic transformation can occur. This issue requires identification of criteria that need to be met to ensure the system shows shape memory characteristics up to several per cent. The following criteria are important:

a) the first and the most important prerequisite is that the system involves occurrence of the **thermoelastic martensitic transformation**. This precondition basically implies that the magnitude of deformation during transformation is not sufficient to induce plastic deformation either in the parent phase or martensite. The thermoelastic martensitic transformation is characteristic for its  $\gamma/\alpha'$  interface being able to move in both directions easily in response to temperature changes, i.e. the fraction of martensite may increase or decrease.

b) martensitic plates in the resultant microstructure must create **self accommodating groups**. Minimising of the total deformation energy is associated with the formation of certain crystallographic variants of martensitic crystals.

c) adjacent plates should exhibit such interfaces that they can move in any direction without losing the memory of their positions. This criterion is met, if the majority of these interfaces complies with twinning orientation of adjacent crystals, Fig. 7.16.

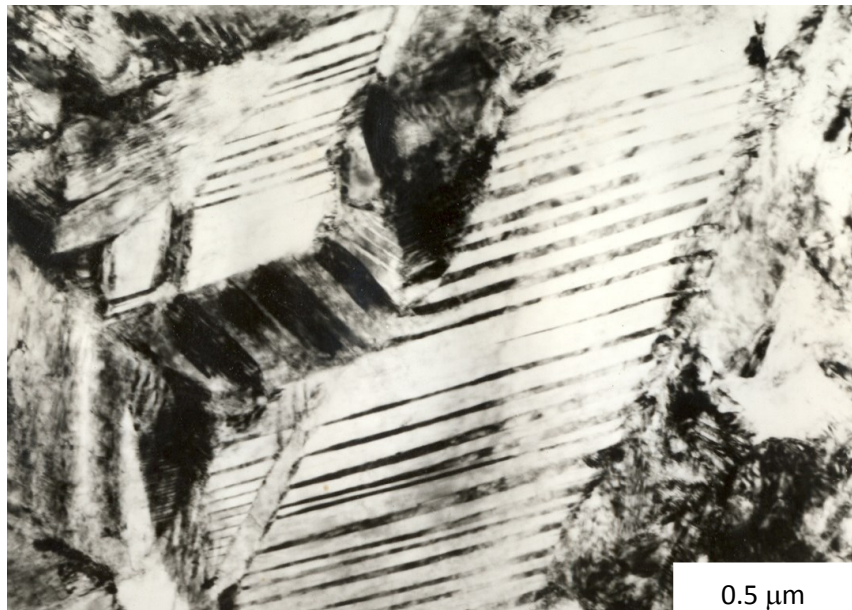


Fig. 7.16 Martensitic variants with twinning orientation in a NiTi alloy

d) Long range ordering of atoms, both in austenite and martensite, gives a preference to the shape memory effect, even though this is not a substantial requirement. The existence of atomic ordering limits the number of variants of martensitic crystals and increases the stress threshold for loss of thermoelastic reversibility due to the occurrence of plastic deformation in the vicinity of  $\gamma/\alpha'$  interface. For a long range ordered structure of a high temperature phase (type B2) in NiTi alloy see the Fig. 7.17.

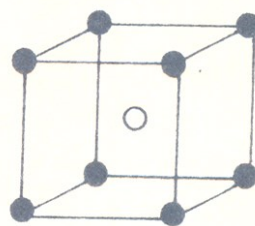


Fig. 7.17 Ordered structure of the high temperature phase (B2 type) in NiTi alloy, Ni – black atoms, Ti – white atom

The shape deformation introduced by martensitic transformation can be reversed by inverse transformation into the master phase. Let us assume that several variants of martensitic crystals develop during cooling of austenite, these crystals ensure mutual accommodation of the shape deformation and that is why there is no change of shape – this is called *self-accommodation martensite*, Fig. 7.18. Application of external stress causes growth of a

conveniently oriented variant of martensite, which results in shape change. Heating causes a shape change in the opposite direction, so the original shape is restored. This phenomenon is called the *shape memory effect*. Excessive deformation (greater than needed to create one variant of martensite) would result in a permanent plastic deformation and loss of the shape memory effect.

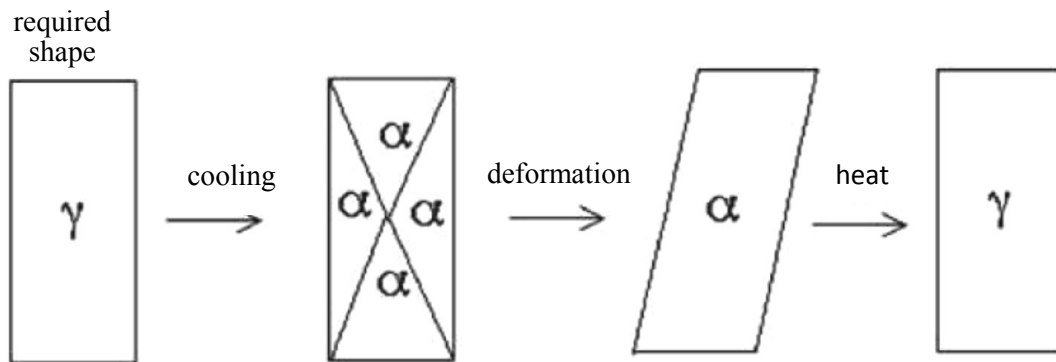


Fig. 7.18 General diagram of the shape memory effect

The shape-memory effect and superelastic deformation can be described using a series of diagrams showing stress/deformation curves obtained at various temperatures, Fig. 7.19. Assume a tensile test sample of alloy with the shape memory effect; deformation in the tensile machine is monitored with records of stress generated within the sample. For a tensile test performed at the temperature  $T_1 > M_d$  the stress - deformation records show elastic deformation up to a high level of stress, followed by a limited plastic deformation and completed with a brittle fracture. The master phase B2 is resistant to any phase transformation at temperature  $T_1$ . The behaviour described corresponds with expected characteristics of an intermetallic compound.

The phase B2 will be unstable at the test temperature  $T_2$  ( $M_d > T_2 > A_f$ ) with respect to the stress induced martensitic transformation, which occurs when the stress reaches its threshold level at point 1 in the stress - deformation diagram, Fig. 7.19. The area of plastic flow between points 1 and 2 is associated with an increasing volume fraction of martensite. That results in formation of such a variant of martensite which is most conveniently oriented with respect to the acting stress. Unloading of the sample is followed by drop of stress from point 2 to point 3, similarly to elastic unloading. At point 3 the reduction of the volume fraction of stress induced martensite starts and the stress - deformation dependency copies the trajectory  $3 \rightarrow 4$ . The closed stress - deformation hysteresis loop proves that the stress induced martensite fully transforms back into the master phase during unloading. The nonlinear part of

deformation, which is removable during alleviation, is defined as a *superelastic deformation*, Fig. 7.19.

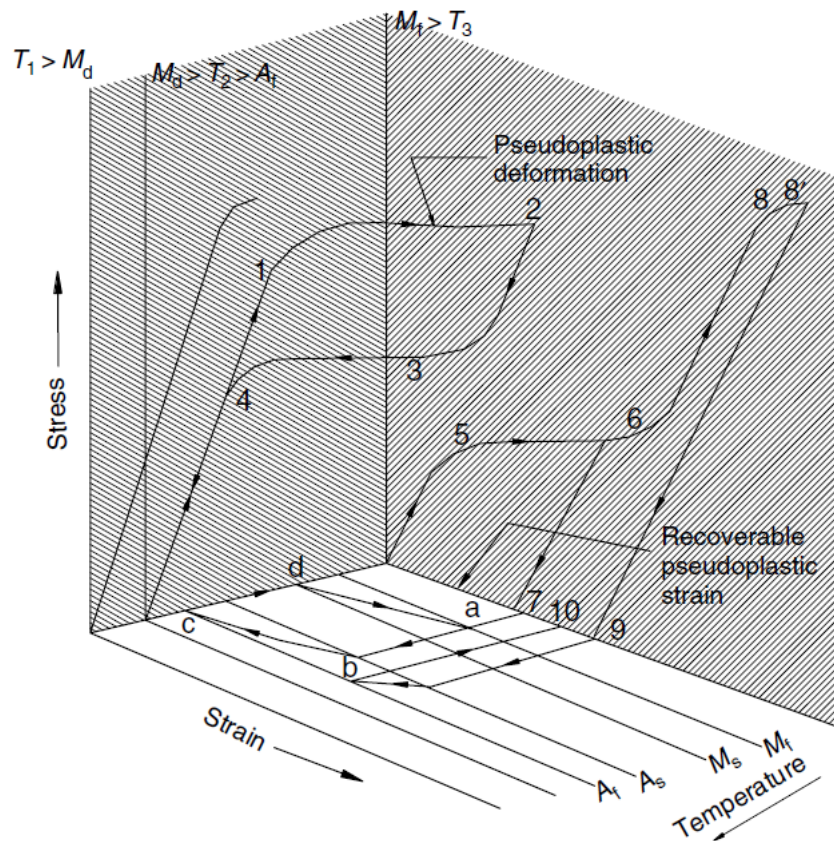


Fig. 7.19 Diagram illustrating superelastic (pseudoelastic) behaviour and shape memory effect in alloys exhibiting martensitic transformation [3]

The stress - deformation curve at temperature  $T_3$  ( $T_3 < M_f$ ) shows a deviation from the elastic behaviour at a relatively low stress, such deviation results in development of the plateau (5 → 6), Fig. 7.19. Alleviation from point 6 is associated with elastic alleviation into point 7. However, the plastic deformation at point 7 is removable by heating to a temperature exceeding  $A_f$ . This process for deformation restoring (shape restoration) of a material deformed by superelastic mechanism, when subject to the cycle of heating to the master phase, is called the shape memory effect.

If deformation occurring at the temperature  $T_3$  continues beyond point 6, the second stage of a linearly elastic deformation will appear. Stress is rising gradually up to the point 8, where the deviation from linearity occurs. Alleviation from the points 8 leads to linear elastic restoration

of deformation ( $8' \rightarrow 9$ ). Subsequent annealing above  $A_f$  ensures limited strain recovery ( $9 \rightarrow 10$ ).

When subject to repeated temperature and deformation cycles, parts made of some alloys show the *two way shape memory effect*. Under such circumstances, the parts (samples) remain in two states of deformation (or two shapes) at two temperatures, one of them exceeds  $A_f$  and the other one is below  $M_f$ . The two way shape memory effect can be characterised by means of the temperature-deformation cycle *abcd* in the Fig. 7.19.

Fig. 7.19 illustrates the ideal course of various effects with martensitic phase transformation: the superelastic deformation, the shape-memory effect and the two-way shape-memory effect. The physical processes associated with these effects are not identical for all alloys exhibiting shape memory. In spite of differences between individual systems, the processes responsible for the above mentioned effects can be simply described as follows: Temperatures between  $A_f$  and  $M_d$  may induce transformation of austenite into martensite if the chemical driving force for transformation is increased by means of applied mechanical stress. The deviation from linear elastic behaviour is observed at the level of stress adequate for initiation of stress induced martensitic transformation. Further rise of stress will lead to increase of the fraction of martensite; the mechanical work associated with the applied stress is used fully to create a metastable martensitic phase. Martensite developed under these conditions remains in thermoelastic equilibrium, that is why the transformation can be reversed (martensite can be transformed into austenite), if the level of applied stress is reduced. The path of unloading (curve 2 - 3 - 4) comprises the elastic unloading ( $2 \rightarrow 3$ ) followed by reverse transformation of martensite into austenite ( $3 \rightarrow 4$ ), Fig. 7.19. The loop therefore represents the stress - deformation dependency relevant to the stress induced martensitic transformation.

Deformation of fully martensitic structure at temperatures below  $M_f$  shows a pseudoplastic flow ( $5 \rightarrow 6$ ), which can be fully restored by means of a thermal cycle, as described above. That is contradictory to the usual plastic deformation of metals and alloys by means of dislocation slip with a shift of certain part of crystal above the slip plane into new positions with identical alignment of atoms around. As the slip process is irreversible, there is no tendency towards a reversed occurrence of the deformation path. The slip mechanism cannot explain a removable pseudoplastic deformation. The initial fully martensitic structure comprises several variants of martensitic crystals aligned in such manner that the deformation energy of crystal assembly is minimised (self-accommodation martensite). Experiments have proven that the nature of most interfaces between martensitic crystals corresponds to twinning

interfaces, Fig. 7.16. Application of external stress causes convenient orientation of certain variants towards growth, whereas the orientation of others remains inconvenient. Pseudoplastic flow may occur pursuant to such re-orientation process, which is irreversible during unloading. That interferes with the self accommodating effect in original martensite. The thermal cycle via austenitic phase restores the self accommodating assembly of martensite variants and this process removes the pseudoplastic deformation, Fig. 7.19.

When subject to cycles of pseudoplastic deformation and shape restoration, a component made of alloy with shape memory shows a two way memory effect. Such component then adopts two shapes given by two states corresponding to two temperatures, one of them below  $M_f$  and the other one exceeding  $A_f$ . Two way shape memory effect develops due to accumulation of residual plastic deformation in material during a repeated thermal cycling. The residual stress finally reaches such level, where it can control the pseudoplastic deformation without implementation of any external stress. Shape is restored via the heating cycle by usual means.

### **7.2.1 Transformation Sequence in NiTi Alloy**

As far as alloys with shape memory are concerned, the NiTi alloy is an exceptional material. Transformation temperatures and sequences of phase transformations in NiTi alloys are sensitive to chemical composition of alloys, thermal processing that induces the shape effect, previous cold forming and the externally applied stress. When fully annealed, the NiTi alloy comprising composition close to equiatomic shows a single peak only in the DSC (differential scanning calorimetry) record during continuous annealing or continuous cooling, Fig. 7.20. That proves the fact the martensitic transformation B2 (master phase, BCC long-range ordered, Fig. 7.17)  $\rightarrow$  B19' and the reverse transformation B19'  $\rightarrow$  B2 occur within a single step.

Subjecting the same alloy to cold forming with approx. 15 % width reduction, the transformation during cooling occurs in two stages: B2  $\rightarrow$  R and R  $\rightarrow$  B19', Fig. 7.20. Transformations during annealing occur within a single step producing a single endothermic peak. The difference in temperature between transformations B2  $\rightarrow$  R and R  $\rightarrow$  B19' increases with the rising level of the preceding cold deformation. TEM examination of thin foils made of the above mentioned alloy close the transition of B2  $\rightarrow$  R showed diffraction patterns with spots at such positions, which divide any reciprocal vector B2 into thirds precisely. A drop in sample temperature produces clearer plates of R phase, which undergo mutual arrangements within self-accommodation groups. In situ experiments have proven that

plates of the R-phase can nucleate at small centres of deformation, e.g. at dislocations. As these plates grow and fill in the space of B2 grain, the diffraction patterns will start showing sharp spots at  $1/3$  of the distance of individual diffraction vectors of the phase B2. Further cooling led to transformation of the R-phase into a martensitic phase of type B19 (orthorhombic cell). Six crystal variants of the phase B19 can be arranged into a self-accommodation group, which minimises the overall shape deformation, Fig. 7.21.

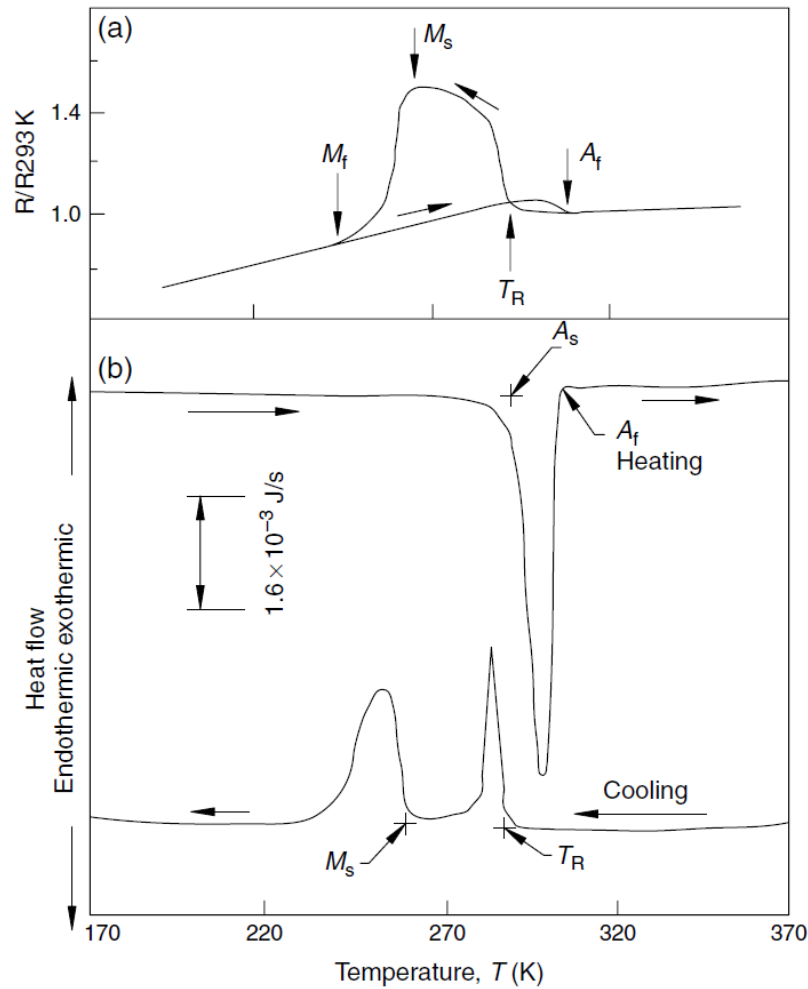


Fig. 7.20 DSC record showing temperatures of transformation and transformations sequences in the NiTi alloy [3]

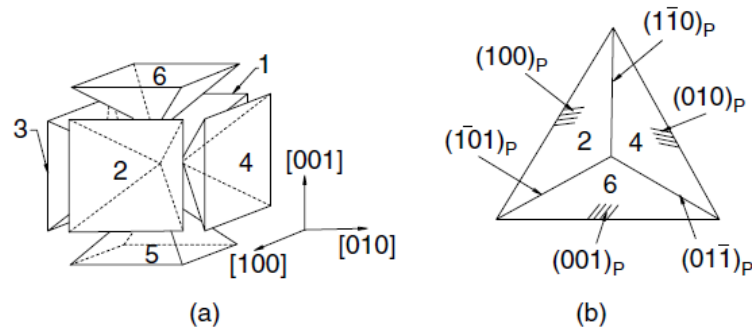


Fig. 7.21 Self-accommodation model of martensite B19, 6 variants of martensitic crystals[3]

The lattice shear in plane  $(100)_o$  and along the direction of  $[001]_o$  finally transforms the orthorhombic structure of B19 into the monoclinic structure of B19'. Each orthorhombic variant may produce 2 monoclinic variants, i. e. each grain of the phase B2 may include the total of 12 variants of the phase B19'.

### 7.2.2 Temperature-Actuated Switch

The shape of sample to be "stored in memory" must be created by means of plastic deformation first - either cold or hot deformation. However, this process should not be accompanied by formation of martensite. The material therefore needs to be in a specific state, which may require additional thermal processing. The Fig. 7.22 showing a temperature-actuated switch defines two different shape systems. The initial state can be achieved by hot extrusion or rod drawing and it may or may not be associated with any additional hot or cold deformation to obtain the shape required. The part in required shape must be heat treated in a mode including high-temperature annealing with subsequent hardening in water. Assuming the alloy composition, when the temperature  $M_f$  exceeds the ambient temperature level, the sample will be in martensitic condition after heat treatment. To induce the shape memory, samples in martensitic condition are either bent or straightened (see Fig. 7.22) and placed into a mechanical controller at ambient temperature. If the temperature of controller exceeds the temperature of reverse transformation of material with shape memory, the sample will be restored into the original shape ("stored in memory"). That results in disconnection or connection of electrical contacts.

Induction of a two-way shape memory effect requires application of special procedures when handling the shape-memory device. That can be explained once again, using a temperature-actuated electrical switch. If the sample in the shape "stored in memory" cools down to the ambient temperature again, it will not be expected to change its shape any more. Re-using of

samples after occurrence of the shape memory effect requires their repeated deformation (bent or straightened, Fig. 7.22). Further heating of such deformed samples to temperature levels exceeding  $A_f$  then induce the shape-memory effect. If this cycle, i.e. bending - heating - cooling, is repeated several times, this will set up the two-way memory. Cooling will bring the sample to a spontaneous change into the deformed shape, which will either connect or disconnect the electric contacts during cooling. This repeated cycling comprising deformation of material in martensitic state followed by the heating-cooling cycle is called "training". This cycling enables induction of the two-way memory effect.

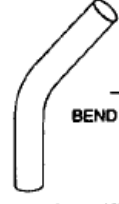
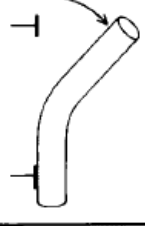
INITIAL SHAPE	ADDITIONAL COLD OR HOT SHAPING	SHAPE AFTER BETATIZING AND QUENCHING	POSITION AT ROOM TEMPERATURE	"REMEMBERED" POSITION (ABOVE $A_f$ )
	NONE	 → BEND TO CURVE		
		 → BEND STRAIGHT		

Fig. 7.22 Temperature-actuated switch designed to be activated or deactivated above a certain temperature level [4]



### Summary of terms in this chapter

**Diffusionless transformation:** a phase transformation associated with relocation of atoms over distances below one interatomic spacing. Products of diffusionless transformation are usually defined as martensite. Owing to the coordinated movement of atoms resembling a shear deformation, this transformation is often defined as a shear or military transformation.

**Shape deformation:** a diffusionless transformation induces a change in shape of crystals, which relates to a coordinated movement of atoms during transformation. Martensitic transformation is accompanied by the formation of a surface relief.

**Orientation relationship:** as the movement of atoms during diffusionless transformation is coordinated, there is a crystallographic relationship between the original phase and martensite. The orientation relationship is usually expressed by parallelism of atomic planes with low Miller indices of both phases as well as by parallelism of directions lying in such parallel planes.

**Habit plane:** a diffusionless transformation represents deformation with an invariant plane, i.e. the interface plane between the initial phase and martensite is undistorted and unrotated. This plane is called "the habit plane".

**Characteristic temperatures of martensitic transformation:**  $M_S$  – start temperature of transformation (martensite start),  $M_f$  – finish temperature of transformation (martensite finish),  $M_d$  – the maximum temperature to allow start of the martensitic transformation after plastic deformation of a high temperature phase (austenite).

**Superelasticity:** stress induced martensitic transformation in certain alloys results in significant change to the sample shape; the sample shape will be restored during unloading.

**Shape memory effect:** in alloys with thermoelastic martensitic transformation ( $\gamma/\alpha'$  interfaces may move in both directions at temperature changes) temperature – stress cycles may recover the shape of crystal (component).

**Self-accommodation martensite:** individual martensitic crystals (martensitic variants) create aggregates that enable minimising of the shape deformation.



### Questions addressing the content covered

1. What are the basic characteristics of diffusionless transformations?
2. What is the shape deformation?
3. How do you define an orientation relationship? What orientation relationships between austenite and martensite in iron-based alloys do you know?
4. Explain the term "deformation with an invariant plane".
5. What morphologies of martensite in iron based alloys do you know?
6. What are the temperatures essential for martensitic transformations?
7. Describe the effects of the transformation and re-orientation superelasticity.
8. What is the principle of the shape memory effect?
9. What are the criteria for occurrence of the two way memory effect?
10. What is the self-accommodation martensite?



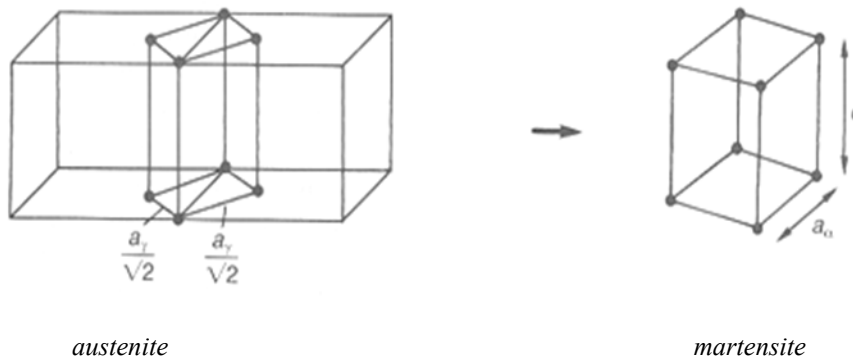
## Exercises

### Example 1

Draw a diagram illustrating the Bain model of homogeneous deformation during martensitic transformation of FCC  $\rightarrow$  BCC. Assuming that  $a_\gamma = 3.56 \text{ \AA}$ ,  $a_\alpha = 2.86 \text{ \AA}$  and the ratio of  $c/a$  parameters is equal to 1.1, calculate the maximum movements of atoms during the martensitic transformation.

*Solution:*

*Diagram for the Bain homogeneous deformation:*



*Movements of atoms can be calculated as follows:*

$$c/a = 1.1 \quad a_\alpha = 2.86 \text{ \AA} \quad c_\alpha = 3.15 \text{ \AA}$$

$$\frac{a_\gamma}{\sqrt{2}} = 2.52 \text{ \AA}$$

$$\text{Movement of atoms along vertical direction: } 3.56 - 3.15 = 0.41 \text{ \AA}$$

$$\text{Movement of atoms along horizontal direction: } 2.86 - 2.52 = 0.34 \text{ \AA}$$

$$\text{The maximum movement of atoms is defined by vector addition: } 0.53 \text{ \AA}.$$



### Literature for further studies

- [1] Haasen, P.: Physikalische Metallkunde, Ed. Springer – Verlag, 1984.
- [2] Honeycombe, R.W.K., Bhadeshia, H.K.D.H.: Steels Microstructure and Properties, Elsevier, 2006.
- [3] Banerjee, P., Mukhopadhyay, P.: Phase Transformations, Examples from Titanium and Zirconium Alloys, Elsevier, 2007.
- [3] Phase Transformations in Materials, G. Kostorz (Ed.), Wiley – VCH Verlag GmbH, Weinheim, 2001.